Systematic and Quantitative Analysis of the Early Embryonic Development of *Caenorhabditis elegans*

Angela Krüger

TESI DOCTORAL UPF / 2012

Thesis director: Dr. Ben Lehner

Department: EMBL-CRG Reasearch Unit in Systems Biology

Genetics Systems Laboratory

Center for Genomic Regulation (CRG)

UNIVERSITAT POMPEU FABRA

Für meine Eltern,
die immer für mich da sind.

Acknowledgements

I would like to dedicate this page to all the wonderful people I met during these five years in Barcelona - you are all very special to me and it has been great getting to know you! Every time had its people- and I went through very different ones... but because of you these years have been so beautiful and enriching!

To my close friends near and far – who I hope know who I mean - I want to say a particular THANK YOU ... for always being there for me and all the wonderful times we spent together! You are deep inside my heart and I am very grateful for your friendship!

Ein besonderes Dankeschoen an Marian, dass Du so bist wie Du bist, und immer da, denn das ist sehr viel!

A special thank you goes to all the people in the lab - it has been great working with you – I know that such a cool lab is really hard to find! Many thanks especially to Rob for providing the plots for the cell cycle analysis and developing the “Lineager“. Without this tool, we would not have been able to analyze the data in such an illustrative way and make all the nice pictures! I also would like to acknowledge Oleh Dzyubachyk and Erik Meijering for developing the cell tracking algorithm for us.

And of course, most of all, I want to thank my boss and supervisor Ben, whose support with the project was quite unique! Thank you for all your help, ideas and suggestions! It has always been very motivating and I really learned a lot during all those years! Thank you for giving me the opportunity to work on this project- it has been great having you as a supervisor!

Abstract

The embryo of *Caenorhabditis elegans* is a model system in which development can be studied at single cell resolution. In this thesis I describe the use of a semi-automatic nuclear tracking algorithm to analyze cellular movements in the early embryo, as well as how embryos respond to mechanical deformation and to genetic perturbation. During gastrulation cells were observed to not only ingress into the interior of the embryo, but also to egress onto the surface. Moreover, cell lineages were identified that undergo both directional movements, i.e. first internalize and then continue to move until finally reemerging on the surface, “transgressing” or “tunnelling” through the embryo. The previously described stereotypical early rotation movements in compressed embryos were found to be highly variable in uncompressed embryos, with this variable global rotation largely determining the final embryonic axes. In addition to constraining this early rotation, compression of the embryo was found to alter the relative positions of cell groups. A compensatory mechanism was identified consisting of a global rotation of cells initiating more than an hour after the four-cell stage that realigns the relative positions of cell groups and results in a further rotation of the embryonic axes. Possible mechanisms that drive these corrective cell movements are discussed. Inhibiting the expression of 20 general regulators of chromatin and analyzing the phenotypic consequences at single cell resolution revealed functions in chromosome segregation, mitotic cell cycle progression, cellular movements and lineage-specific

development, and suggested the existence of functionally diverse chromatin-modifying protein complexes in the embryo. Moreover, a global re-arrangement of nuclear architecture was observed upon the inhibition of zygotic gene expression. Taken together, these analyses illustrate the power of single cell resolution phenotyping, identify previously unrecognized cell behaviors during early development, and identify regulative cell movements as a mechanism that confers robustness to the effects of mechanical deformation.

Resumen

El nemátodo *Caernorhabditis elegans* ofrece la posibilidad de estudiar el desarrollo embrionario con una resolución celular. En esta tesis, describo el uso de un algoritmo semi-automático de seguimiento nuclear para analizar movimientos celulares en el embrión temprano, así como la manera en que el embrión responde a deformaciones mecánicas y a perturbaciones genéticas. Durante el proceso de gastrulación, observamos que ciertas células no solo ingresan al interior del embrión, pero también egresan hasta la superficie. Asimismo, identificamos linajes celulares que llevan a cabo ambos tipos de movimientos direccionales, esto es, primero internalizan y luego la continuan su movimiento hasta finalmente re-emerger en la superficie, “transgressing” o “tunneling” a través del embrión. Hemos descubierto que los movimientos estereotípicos de rotación en el embrión temprano, descritos previamente, son altamente variables en ausencia de compresión y esta variabilidad total en la rotación determina los ejes finales del embrión. Además de limitar esta rotación temprana, la compresión del embrión altera la posición relativa de grupos celulares. Hemos identificado un mecanismo compensatorio que consiste en la rotación global de células el cual tiene lugar mas de una hora después del estadio de cuatro células. Ese mecanismo re-alinea la posición relativa de los grupos celulares resultando en una rotación adicional de los ejes embrionarios. Posibles mecanismos responsables de estos movimientos correctivos son discutidos. La inhibición de la

expresión de 20 reguladores generales de la cromatina y el análisis de las consecuencias fenotípicas con resolución celular ha revelado funciones en la segregación de cromosomas, la progresión mitótica del ciclo celular, movimientos celulares y desarrollo linaje-especifico, sugiriendo la existencia de diversos complejos de proteínas modificadoras de la cromatina en el embrión. Además, hemos observado una re-organización global de la arquitectura nuclear al inhibir la expresión zigótica en el embrión. En conclusión, estos análisis han permitido ilustrar el poder de la fenotipificación con resolución celular, así como la identificación de comportamientos celulares previamente desconocidos durante el desarrollo temprano y movimientos celulares regulativos como un mecanismo que confiere robustez a los efectos de deformaciones mecánicas.

Preface

The invariant cell lineage and developmental pattern of *C. elegans* offers a powerful tool to study the genetic basis of animal development. Assays that detect changes in the cell lineage and patterning in mutants or RNAi knockdowns of gene function provide the opportunity to identify and decipher how developmental regulators act. To do this in a systematic and quantitative way, embryogenesis must be imaged with sufficient temporal and spatial resolution and images must be subjected to some kind of automated cell tracking.

For this aim, the objectives of this thesis were:

1. To implement methods for the extraction and imaging of early *C. elegans* embryos for the purpose of semi-automatic cell tracking and lineage curation.
2. To develop methods to quantify wild-type variability and RNAi phenotypes with a focus on the lineage, nuclear positions, movements, and division angles.
3. To study early wild-type *C. elegans* embryogenesis in a systematic and quantitative way to detect possible naturally occurring variability and robustness.
4. To dissect the effects of inhibiting genes encoding subunits of chromatin remodeling complexes.

With the methodology described in this study we could quantitatively analyze pleiotropic defects in chromatin factor depleted embryos, providing new insights into their functioning during *C. elegans* development and predicting the existence of multiple, functionally different chromatin remodeling complexes.

Results on wild-type embryogenesis provide the basis for a deeper understanding of the interplay between single cell and global movements during wild-type gastrulation in the pre-morphogenetic embryo. The described compensatory and regulative movements may form part of an intrinsic ‘design principle’ of *C. elegans* embryogenesis, conferring robustness to mechanical deformation.

Table of Contents

List of figures

List of tables

1. Introduction

1.1. Early *C. elegans* development

Fertilization marks the beginning of life in hermaphrodite worms. When a mature oocyte crosses the spermatheca and encounters a sperm cell, the sperm enters the egg from the side opposite to the oocyte nucleus. It confers posterior character to the site of entry and contributes with DNA and a pair of centrioles to the new embryo [1]. The centrioles assemble pericentriolar material to build up the centrosome, which serves as nucleation center for microtubules and is pivotal for polarity establishment [2]. The newly fertilized zygote then moves into the uterus. After approximately two hours of further development to the 30-cell stage, newly formed eggs are laid [3].

1.1.1. Generation of founder cells

The first five cell divisions, lead to the generation of the six founder cells: AB, MS, E, C, D and P4. Asymmetry of these divisions creates diversity as cells with different fates are generated. Descendants of founder cells each give rise to a specific subset of cell types (Figure 1).

The first asymmetric division of the one cell embryo produces a larger anterior blastomere, AB, and a smaller posterior blastomere P1. P1 then divides asymmetrical into EMS and P2. The third and forth asymmetric cleavages generate MS and E, and C and P3, respectively. P3 then further divides into D and P4 [3].

Descendants of the AB cell finally form the hypodermis, neurons, anterior pharynx and various other cell types. MS lineage cells generate the somatic gonad, musculature, the majority of the pharynx, neurons and gland cells. E cells are the foundation of the entire intestinal tract. Cells give rise to muscle, hypodermis and neurons, D to muscle, and the P4 cell is the precursor of the germ line [3].

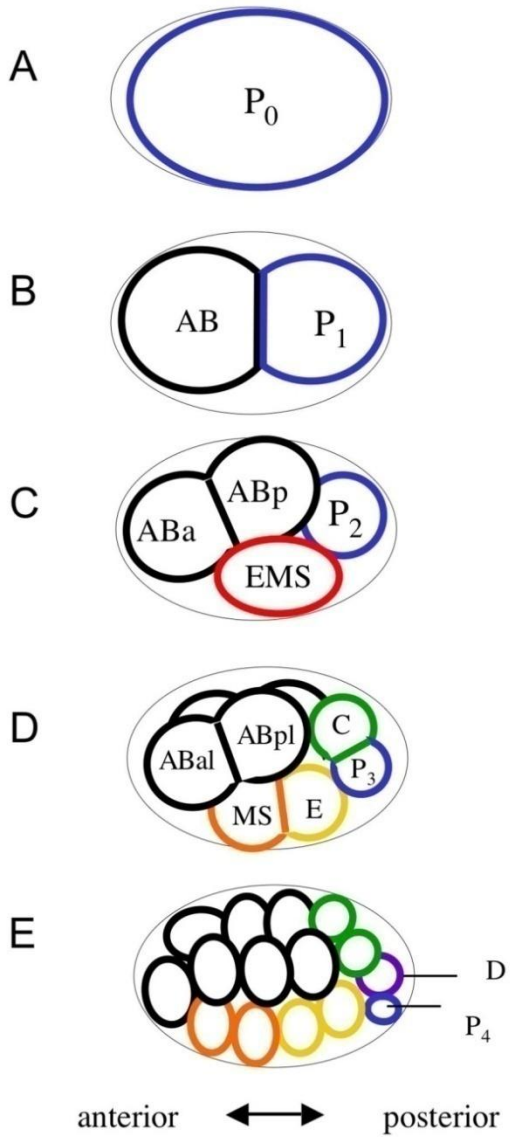

Figure 1: **Generation of founder cells in the early *C. elegans* embryo [4].**

1.1.1.1. Axis formation and establishment of polarity

Concomitantly with the generation of founder cells, the three principal axes of the *C. elegans* body plan are established during the early embryonic divisions.

1.1.1.1.1. Establishment of the anterior-posterior (AP) axis

The initial symmetry of the oocyte is broken as the sperm-derived centrosome initiates a sequence of events leading to the polarization of the embryo along the AP axis.

After fertilization, surface contractions lead to proper physical association of the centrosome to the posterior cortex. This is essential for correct AP polarity establishment [2, 5-8]. A dense cortical network of actomyosin first spans over the whole cortex but soon contracts and retracts from the posterior side. Surface contractions cease and a smoother cortical area expands from the posterior side.

Contractions and movements of the actomyosin network lead to the correct distribution of six PAR (partioning defective) polarity proteins [9-11]. PAR-3 and PAR-6, PDZ-containing proteins, form a complex with the atypical protein kinase C, PKC-3, and become localized at the anterior cortex. PAR-2, a Ring-finger protein, and PAR-1, a Ser/Thr kinase, constitute the posterior set of PAR proteins [7]. PAR-2 and PAR-6 are dynamically associated with the actomyosin network and as such might sense and transmit

network movement to localize to their respective area before division of the one cell embryo [7, 8, 12]. The remaining PAR proteins PAR-4, a Ser/Thr kinase, and PAR-5, a 14-3-3 protein, are distributed throughout the cortex and cytoplasm.

It is thought that *par-5*, *par-2*, *par-3* and *par-6* act upstream of *par-1*, whereas *par-4* may function in a separate pathway [10]. While actomyosin contractions establish the PAR-2 and PAR-6 domains, *par* genes as well as other factors such as the two partially redundant CCCH finger proteins MEX-5 and MEX-6, are in turn necessary for the generation of robust cortical flows [12].

Before division, the sperm-derived centrosome duplicates and nucleates a large number of microtubules. Together with the two pronuclei, the two centrosomes then move synchronously to the center of the cell [13].

Following pronuclear meeting, AP polarity is maintained by different centrosome independent mechanisms. PAR-2 is believed to restrict PAR-6 to the anterior [2, 7, 8]. The small G protein CDC-42 is also important for polarity maintenance, interacting physically with PAR-6 [14, 15], and most likely mediating the actomyosin network flows [16]. Downstream acting factors such as the two partially redundant CCCH finger proteins MEX-5 and MEX-6 are required for proper AP polarity establishment as well as for the unequal segregation of cell fate determinants [7, 12, 17]. PAR-1 restricts MEX-5 and MEX-6 to the anterior part of the one cell embryo where they prevent the presence of the PAR-3/PAR-6 complex as well as factors

destined specifically to the posterior born blastomere [7]. Other downstream factors, such as MEX-1, POS-1 [18-20], and the putative RAN binding proteins MEX-3 [21] and SPN-4 [22] are not essential for anterior-posterior polarity but only for the proper segregation of cell fate determinants. Thus, they rather act as polarity mediators than polarity proteins.

Unequal segregation of fate determinants in response to AP polarity is carried out by directed transport, localized degradation and translational control. For example, the P granules, large ribonucleoprotein complexes destined to the germ line, are transported to the posterior cortex by cytoplasmatic flows [1, 23, 24]. Additionally, localized degradation contributes to their removal from the anterior. The correct distribution of PAL-1, a fate determinant for posterior blastomeres [25], is controlled by translational repression instead. PAL-1 mRNA is present throughout the early embryo. PAL-1 protein, however, is only found in posterior [25], due to the activity of the KH domain protein MEX-3. MEX-3 in turn is controlled by PAR-1 [26].

Following the establishment of AP polarity, correct spindle positioning is essential for the asymmetric distribution of cell fate determinants. Polarity cues lead to the asymmetric distribution of members of a heterotrimeric G protein pathway. This in turn leads to the asymmetric generation of forces acting on the spindle poles causing asymmetric division. After the movement of the pronuclei and centrosomes to the center of the one cell embryo, cortically based pulling forces act on microtubules [27-30] and rotate the

unit and spindle by 90 degrees to align with the AP axis. This typically occurs before nuclear envelope breakdown [13, 31]. At metaphase, the spindle moves slightly towards the posterior [32, 33]. During division, larger net pulling forces act on the posterior spindle pole, giving rise to a smaller posterior and larger anterior blastomere [29, 32, 34]. The most important proteins required for nuclear rotation and spindle movements are G protein α subunits, GoLoco-motif proteins GPR-1/GPR-2, the DEP domain protein LET-99 and dynein [27-30].

1.1.1.1.2. Establishment of the dorsal-ventral (DV) axis

During the division of the two-cell embryo, the dorsal ventral axis becomes established. First, the AB blastomere divides symmetrical with its division axis perpendicular to the AP axis. Slightly delayed, the other blastomere, P1, divides asymmetrically in anterior-posterior direction.

In these divisions, establishment of polarity, spindle alignment and movement is controlled in a similar way as in the first division. PAR proteins control the correct orientation of the spindle. During the division of the AB blastomere, PAR-3 prevents the placement of the spindle onto the AP axis [35, 36]. Before division of P1, PAR-3 accumulates at the anterior side of the blastomere, whereas PAR-1 and -2 become constrained to the posterior cortex. Consequently, cell fate determinants are segregated asymmetrical so that the two P1 descendants, P2 and EMS

acquire different fates with EMS defining the ventral side of the embryo.

The 90° rotation of centrosomes and the associated nucleus before division of P1 [31] requires G protein α subunits, GPR-1/GPR-2, LET-99 and dynein as in the first embryonic cleavage [27, 28, 30, 37-40].

The position of the spindle together with the constraints of the eggshell, arrange blastomeres of the four cell embryo in such a way that specific cell to cell interactions induce different fates and consequently differentiate dorsal from ventral.

1.1.1.1.3. Formation of the left-right (LR) axis

Shortly after dorsal-ventral, the left-right axis is thought to be established by the division pattern of ABa and ABp.

The spindles of ABa and ABp are first orientated orthogonal to the AP and DV axes. However, during telophase they are skewed towards the anterior. Consequently, the left hand daughters of ABa and ABp are located further in anterior direction than their right hand counterparts. This allows for specific cell-to-cell contacts and as such differential fate inductions in the ABa/p daughters [3, 41]. Through Notch signaling between AB and MS descendants, distinct lineages arise on the left and right sides [42, 43], leading to the invariant left/right handedness of the worm [44]. Reversing the direction of the ABa/ABp spindle skew

experimentally, and by that reversing cell contacts creates worms that are mirror imaged [41].

Starting with the initial spindle skew, overall left/right asymmetry is maintained though development by complex morphogenetic movements. From the eight-cell stage onward, these movements establish an embryonic midline that is tilted from the AP axis towards the right. These so called chiral morphogenetic movements involve differential left/right protrusions of the ABpl cell and asymmetric actomyosin contractions as well as a chiral rearrangement of cells [45].

For the differential regulation of actomyosin contractility in the otherwise bilaterally equivalent ABpl and ABpr cells, noncanonical Wnt signals are necessary. The correct timing of protrusions is controlled by molecularly unknown signals from the cytokinetic furrow of EMS [45]. Yet, the most instructive signal in overall left-right patterning is the direction of the ABa/p spindle.

The only molecular component known to be involved in spindle positioning and skewing is the Gα subunit protein GPA-16 [36]. However, it is not known whether G protein signaling is the cue for the establishment of left/right handedness or if it acts downstream of earlier symmetry breaking events.

1.1.1.2. Early embryonic inductions

1.1.1.2.1. Early Notch inductions in the AB lineage

For the early specification of cell fates, Notch signaling plays an important role. Four characteristic inductions within cells of the AB lineage determine which AB sublineages finally constitute pharyngeal tissue, the bilaterally symmetrical head and the excretory cell. Maternally expressed Notch induces zygotic expression of the *ref-1* family of genes within roughly 25 minutes, corresponding to the birth of the ABp granddaughters. This gene family consists of *ref-1 hlh-25, hlh-26, hlh-27, hlh-28, and hlh-29*, with one or more of the genes being expressed after each of the four Notch interactions described below [43].

At the four-cell stage, ABa and ABp both express maternally provided GLP-1/Notch at their surfaces. However, due to the characteristic arrangement of cells, only ABp contacts the Notch ligand APX-1 expressing P2 cell and becomes activated (Figure 2). As such, the expression of two functionally redundant T-box transcription factors, TBX-37 and TBX-38 is repressed in ABp, preventing those cells from producing pharyngeal tissue [46]. TBX-37 and TBX-38 are thought to be direct targets of REF-1 mediated repression in ABp after the first interaction. However, some members of the *ref* family of genes are also expressed in EMS descendants [47]. Here, expression is Notch independent

and involves the maternal transcription factor SKN-1 as well as its targets MED-1 and MED-2, specifying EMS fate [48, 49].

At the 12-cell stage, maternal GLP-1/Notch expressing ABa daughters receive zygotic cell-to-cell signals from the P1 descendants MS and E [50-52] (Figure 2). The molecular identity of the signal is unknown, however, it depends on the activity of the transcription factor SKN-1 which is necessary for mesodermal fate specification [21, 53]. With all ABa descendants expressing TBX-37 and TBX-38, the second AB interaction specifies which of them will produce pharyngeal tissue. The key regulator of pharyngeal development is the forkhead transcription factor PHA-4 [54-56], and its expression depends on this second Notch signal [50, 54, 57-59].

In the third AB-Notch interaction left head precursors are made identical to right head precursors to form the bilateral symmetric head of the worm. The ABp descendant ABplaaa contributes to the left, the ABa descendant ABarpap to the right side of the head [3]. Both head precursors display identical differentiation and division patterns, although sisters and cousins have very different ones. The observation that Notch *lin-12 glp-1* double mutants exhibit the so called ‘twisted nose’ phenotype first showed that cell-cell interactions were necessary for proper head formation [60]. The left head precursor expresses LIN-12/Notch and receives signaling from the neighboring ABalapp cell that expresses the ligand LAG-2/Delta [61]. This third Notch interaction leads to the expression of *ref-1* in the precursors of the

left side of the head. However, for the formation of a bilateral symmetrical head, Notch independent REF-1 expression on the right side is also required [47, 62].

The fourth AB Notch interaction specifies which daughter of ABplpapp will become the excretory cell[3]. Notch *(LIN-12 and GLP-1)* signaling is activated in ABplpapp through LAG-2/Delta expressing MSap daughters [42, 60, 61] and leads to expression of *ref-1* family genes [47].

1.1.1.2.2. A combinatorial Notch code for AB specification

After completion of the first four Notch interactions, only two out of eight AB descendants at that stage (AB8) have not experienced Notch signaling: ABala and ABarp. These cells exhibit the primary fate for all AB descendants, with the Notch signals diversifying the rest [42, 50, 63]. In the absence of Notch signaling, all 8 AB cells express TBX-37 and TBX-38, and adopt one of the two fates according to their position: posterior cells adopt ABarp fates whereas anterior cells adopt ABala fate.

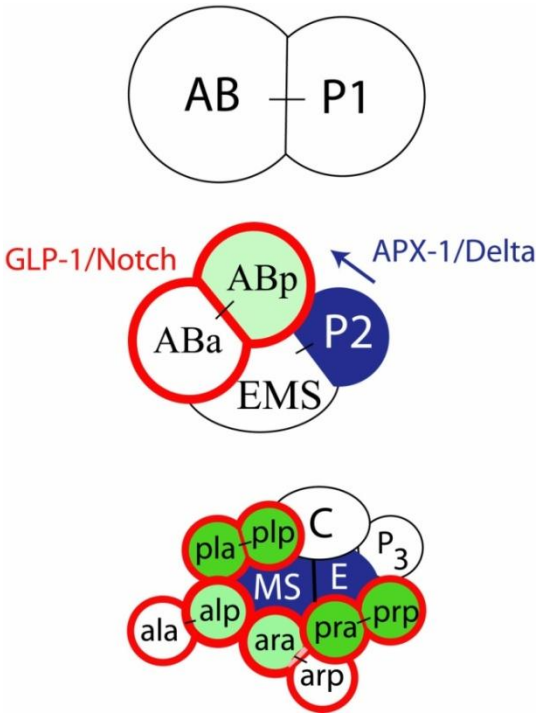

Figure 2: **Early blastomeres at the 2-cell, 4-cell, and 12-cell stages.** At the two-and four-cell stage, embryos are shown from the left side. The 12-cell embryo is a ventral view where AB descendants are splayed to better visualize cell contacts. For simplicity, AB descendants at the 12-cell stage such as ABala or ABarp are labeled "ala" and "arp". Cells expressing GLP-1/Notch are outlined in red, and Notch-activated cells are colored first in light green, then dark green at later time points **[4]**.

1.1.1.2.3. The POP-1 polarity pathway in the AB lineage

Independent of Notch signaling, cells throughout the embryo sense a common anterior-posterior axis of polarity, irrespective of their fate [19, 64]. The basis for this common a-p polarity of all

cells is the Tcf/Lef related transcription factor POP-1, whose activity is regulated by non-canonical Wnt signaling [52, 65, 66].
In the AB lineage, POP-1 asymmetry is first apparent at the AB8 stage, with eight AB descendants present, and is maintained in later divisions. For various a-p fate decisions at divisions, anterior fate requires high levels of POP-1 [66]. Consequently, to obtain the posterior fate, POP-1 has to be down regulated. This asymmetry is created by the control of nuclear uptake of POP-1 after division [67-69] and involves the ligand MOM-2/Wnt and a Nemo-like kinase LIT-1 [65, 67, 70, 71]. Later POP-1 asymmetries, after the AB8 stage, require high posterior levels of the transmembrane receptor MOM-5/Frizzled, a putative receptor for Wnt signaling [72, 73]. In mutants lacking MOM-2/Wnt, POP-1 asymmetry is visible after the AB8 stage [72, 74, 75]. Yet, cells do not show the normal a-p polarity of POP-1 expression [42, 73]. Therefore, early MOM-2 signaling might be needed to organize polarity of following asymmetric cell divisions.

1.1.1.2.4. Wnt-dependent maintenance of anterior-posterior polarity

Recently it has been suggested that the a-p polarity of AB descendants is not an autonomous feature established early in embryogenesis but rather is induced by P2 for the first time at the four-cell stage and constantly reinforced throughout development. Through MOM-2/Wnt signaling from P_2 and its descendants a

polar bias is introduced into the cleavages of AB-derived cells, causing a shift of the average division angle with respect to the a-p axis from 62 ° to 45°. During development, the MOM-2/Wnt signal is transduced from cell to cell by a relay mechanism. This constantly orients the polarity of the AB cells towards the P2-derived cells, even when signaling cells are moving. As lack of the MOM-2/Wnt signal also affects the cleavage orientations in P1 derived cells as significantly as in AB derived cells, cleavages of all cells might be oriented by the same mechanism. Thus, P2 and its descendants constitute a polarizing centre, which maintains polarity throughout development [76].

1.1.1.2.5. Wnt dependent POP-1 polarity specifies endodermal fate

One of the early fate inductions mediated by Wnt signaling is the polarization of the EMS cell at the four-cell stage. P2 derived non-canonical Wnt [70, 71] and SRC-1/MES-1 signaling [77] account for the orientation of the EMS spindle towards P2, assuring asymmetric division, and the regulation of endoderm specification [70, 77-79].

The Wnt pathway includes MOM-1/Porcupine, MOM-2/Wnt, MOM-2/MIG-14, MOM-5/Fz, DSH-2/Dsh, MIG-5/Dsh, KIN-19/CKI, GSK-3/GSK-3β, APR-1/APC, WRM-/β-*cat* and *POP1*/*TCF* [52, 67, 70, 71, 77, 79-83].

A parallel pathway, involving the kinases MOM-4/Tak1 and LIT-1/Nlk and the binding protein TAP-1/Tab1, interacts with the Wnt pathway to control E fate induction [67, 80, 82].

EMS divides into the anterior daughter MS, giving rise to mesodermal tissue and the posterior daughter E, producing endoderm. Due to Wnt dependent asymmetric division, MS contains higher nuclear levels of POP-1, and E contains low levels of nuclear POP-1 [52].

Wnt signaling activates both Wnt and TAK1/NLK pathways, leading to the formation of a WRM-1/LIT-1 complex that phosphorylates POP-1. Consequently, POP-1 is exported from the E nucleus and accumulates in the cytoplasm [67, 68, 80, 82, 84]. The endoderm specifying genes, END-1 and END-3, otherwise repressed by POP-1, become activated in the E cell by the activity of the transcription factors MED-1, MED-2 and the co-activator CBP-1.

The absence of the Wnt signal in the MS cell, in cooperation with UNC-37/Groucho and HDA-1/histone deacetylase, leads to the maintenance of POP-1 dependent repression of endoderm specifying genes [68, 85].

The parallel pathway involving the Src kinase SRC-1 and the inactive receptor tyrosine kinase MES-1 [77] as well as acetylation of POP-1 protein by histone acetylases [86] control the nuclear levels of POP-1 and as such endoderm specification.

Mutations in almost all of the Wnt and Src pathway genes lead to a Mom phenotype (more mesoderm) in which EMS gives birth to

two MS-like daughters. Consistently, *pop-1*/TCF mutations cause the opposite phenotype, two E-like daughters.

1.1.1.2.6. Notch signaling in P1 descendants

Although various P1 descendants express Notch receptors, interactions have only been described for the E lineage, which constitutes the entire intestine [87]. In the intestinal lineage, Notch signaling controls cellular behavior during morphogenesis, rather than determining cellular fate. At the E4 stage, with four E cells being present and expressing LIN-12/Notch, only two of the E cells contact LAG-2 Delta-expressing MS cells outside the intestinal primordium and become activated. REF-1 becomes expressed in the left E4 cells and leads to the down-regulation of LIN-12 in later left positioned daughters [43]. Thus, LIN-12 expression is maintained only in the right positioned E descendants. At the E16 stage, these cells become activated again by the ligand APX-1/Delta [87] resulting in a new wave of REF-1 expression on the right side [43].

This interaction at the E16 stage initiates asymmetrical movements of E lineage cells that eventually lead to a twist the developing intestine. The underlying mechanism is unknown.

1.1.1.2.7. Later Notch inductions

In addition to early AB Notch interactions, Notch signaling plays several other roles in late embryogenesis.

For example, Notch signaling seems to be required for proper development of the valve cell [88] and of the two ventral midline cells, G2 and W [89]. Moreover, the transcription factor PAL-1, which is required for rectal development, seems to be a direct target for Notch [60, 90]. MSapa and MSapp are the signaling cells for ABplpappp and ABplppppp, the grandparent of the anal depressor muscle and an intestinal muscle [90]. They express the ligand LAG-2/Delta while their bilateral symmetrical relatives do not [61]. The MS cells ingress to the center of the embryo during gastrulation, where they can contact those AB descendants that move towards the ventral midline. Thus, MS derived cells appear to be one of the main signaling centers in the embryo.

1.1.2. Gastrulation

1.1.2.1. Overview

The distribution and organization of embryonic cells into tissue areas comprising identical cell types is the prerequisite of a functional organism. This is usually achieved by changes in cell shape and movements during a process called morphogenesis.

Gastrulation is the earliest morphogenetic process in many organisms. During gastrulation, cells of the three germ layers, ectoderm, mesoderm and endoderm, become positioned. To do so, surface cells move to the interior of the embryo, leaving just the ectoderm at the outside.

Compared to other species, gastrulating cells in *C*. *elegans* move only small distances, generally in the range of single cell diameters. The blastocoel-space into which they move is relatively small.

C. elegans gastrulation starts early in development, at the 26-cell stage, soon after the first cell fates are acquired.

Before that stage is reached cells are surrounded by a vitelline envelope and eggshell and have acquired their specific positions within the embryo. Each cell can have up to three different membrane surfaces: an apical outer surface facing the vitelline envelope, lateral surfaces contacting adjacent cells, and a basal surface that faces cells on the envelope-opposing side. Gastrulation starts when surfaces of cells separate from one

another while lateral surfaces remain adherent, leading to the formation of the blastocoel space [91].

In many organisms gastrulation movements are driven by temporally and spatially precisely coordinated contraction of conserved actomyosin networks. The patterning mechanisms are varying and often organism specific [92, 93].

Recently, it has been shown that common cytoskeletal mechanisms underlie morphologically similar movements within the same organism. These mechanisms in turn are controlled by cell specific fate and polarity mechanisms to ensure spatially and timely proper internalization [92].

1.1.2.2. Initiation of gastrulation

The first cells to internalize in C. *elegans* gastrulation are the anterior and posterior endodermal precursor cells, Ea and Ep (referred to collectively as Ea/p). This takes place approximately 90 minutes after the first cell division.

Endodermal fate is necessary and sufficient for these two E precursor cells to ingress in time. Mutations in endoderm-specifying genes, such as the endodermal GATA factor genes *end-1* and *end-3*, result in gastrulation defects [94-96]. When endodermal cell fate is generated ectopically by fate transformation experiments, those cells also internalize [97].

After moving to the interior of the embryo, the gap left behind Ea/p on the ventral surface of the embryo is filled by a ring of six cells, composing three of the four MS cell granddaughters (MSpp,

MSpa, MSap, but not MSaa), two AB descendants (usually ABplpa and ABplpp), and the single germline precursor cell (P4) [98]. After internalization, Ea/p divide and eventually form the entire endoderm. (Figure 3)

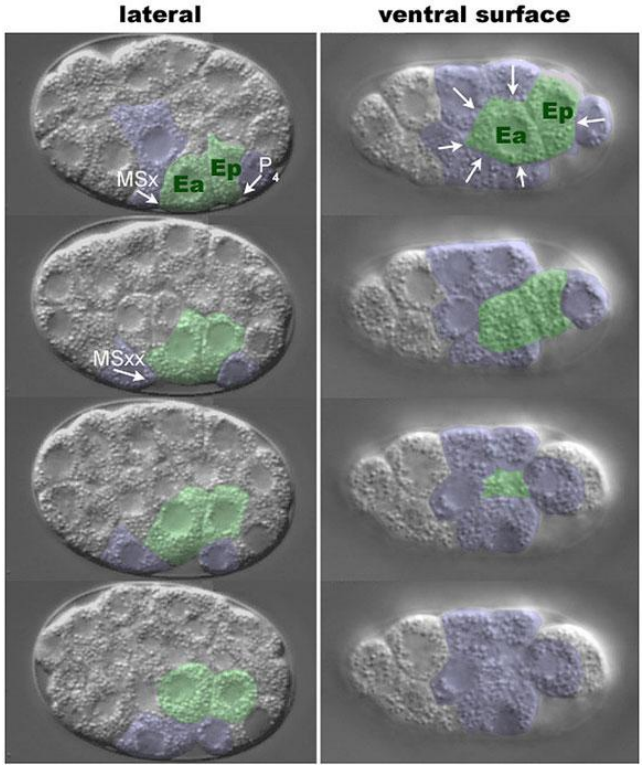

Figure 3: **Nomarski time-lapse images of initiation of *C. elegans* gastrulation.**
Ea and Ep are pseudocolored in green, and neighboring cells are in blue. Arrows indicate direction of neighboring cell movement. MSx divides between the first and second images. Embryos are oriented anterior to the left **[4]**.

The endodermal precursor cells move at least partially by apical constriction. Specifically localized PAR polarity proteins lead to the accumulation of non-muscle myosin II motor protein (NMY-2) on

the apical cortex of Ea/p [91]. PAR-3, PAR-6 and an atypical protein kinase C, localize to the apical surfaces of the Ea/p cells, whereas PAR-1 and PAR-2 locate basolaterally [91, 99-101].

Wnt-dependent phosphorylation of the regulatory light chains of myosin II at a conserved site activates the contraction of the actomyosin network at the apical surface of Ea/p. This in turn pulls the ring of neighboring cells underneath and hence drives the internalization of the E precursor cells [95] (Figure 4).

Recently however, it has been proposed that apical actomyosin contractions start before cell shape changes occur, contracting and generating cortical tensions without significant shrinking of apical surfaces. Connecting the already dynamic contractile apical cortex to apical cell-cell contact zones then triggers the actual apical constriction. This suggests a molecular clutch mechanism in which regulatable, molecular connections between actomyosin networks and contact zones transmit the forces created by actomyosin contractions to the contact zones. Possible components that might control the clutch are members of the cadherin-catenin complex or the Rac pathway [102].

In addition to apical constriction, it has been proposed that for the complete internalization of the endoderm, F-actin-rich extensions have to form. This takes place on the three MS derived cells, MSpp, MSpa, and MSap, forming part of the closing ring of cells that fill the gap left behind Ea/p [103]. The F-actin-structures form at the apical boundaries of MSxx with Ea/p and require the Arp2/3 complex *(C. elegans* homologue subunits are encoded by *arx-2*

and *-1,* respectively [104, 105], a major regulator of the actin cytoskeleton [106], as well as the apical protein PAR-3 [103].

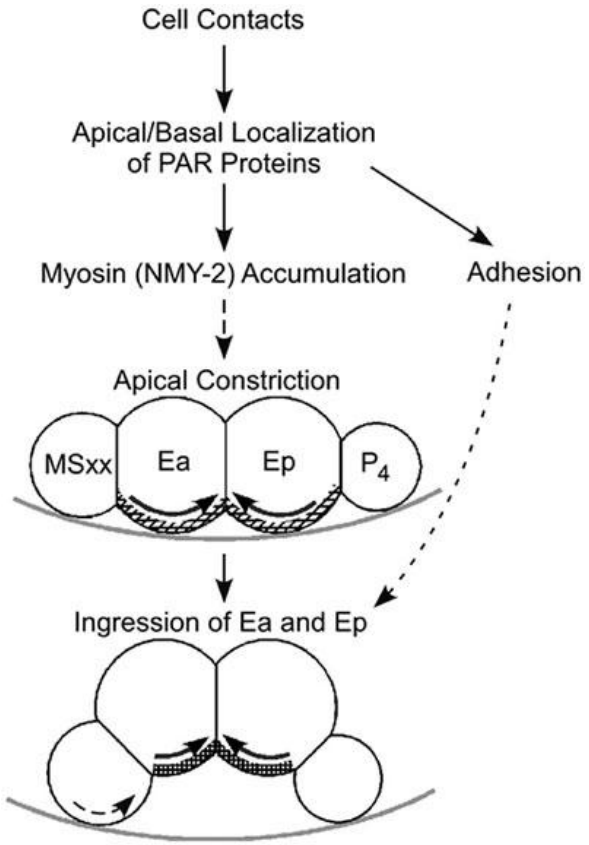

Figure 4: Model for *C. elegans* gastrulation [4]

1.1.2.3. Later gastrulation movements

After endodermal precursors have completed ingression, various other cells internalize before embryonic cell divisions are complete. This distinguishes gastrulation movements from the later occurring morphogenetic movements carried out by postmitotic cells.

With this definition, sixty-six cells have been identified to gastrulate during the following approximately 200 minutes after E cell ingression. Most of these cells give rise to neuronal and mesodermal tissue, as well as the germline [92].

Before internalization, cells position from anterior to posterior along the ventral midline, forming a coherent stripe in the embryo, from where they ingress [3, 91, 92].

The lineage specific positioning of cells during gastrulation correlates with their positions along anterior-posterior axis in the worm later on. Consequently, gastrulation has a major role in the overall positioning of cells and few large-scale movements along the anterior-posterior axis take place afterwards [92].

Although many cells ingress at different times during *C. elegans* gastrulation, the timely and positional origins are highly reproducible. This precise control of ingression timing requires cell fate regulators that are specific for each cell lineage [91, 92]. For example, the P4 cell fate regulator MES-1 is necessary for ingression of P4 descendants at the appropriate time, but not for ingression of cells of other lineages [92] Similarly, two groups of MS derived cells having different fates also ingress at different times: wishbone cells ingress earlier than central cells[3, 91]. Consistently, transforming the fate of central cells to those of wishbone cells induces their internalization at the time of their new fate [91].

Also, cell ingression control by polarity proteins is specific for each cell lineage. The apical PAR proteins, PAR-3 and PAR-6, that are required for early endoderm internalization, do not seem play an

important role in the control of ingression of MS and D lineage descendants [92].

However, it has not been demonstrated yet if an overlapping set of polarity regulators is used in different cells with only varying extend of redundancy levels.

In contrast to cell fate and cell polarity mechanisms, the cytoskeletal mechanisms used for internalization are the same in different lineages.

The myosin heavy chain protein NMY-2 becomes enriched apically within each ingressing cell (rather than in extensions from neighboring cells), and becomes activated there [92]. Thus, specific fate and polarity regulators might control the cytoskeletal force-producing mechanisms that underlie various cell movements.

1.1.3. Other pre-morphogenetic movements

Apart from gastrulation movements, other substantial and in part far-ranging cell migrations have been described [76, 107].

After the specification of the 12 founder cells, cells begin to migrate extensively with variable positioning and migration paths, to arrive at their terminal positions before morphogenesis starts [76, 107]. At this pre-morphogenetic state (~350 cells) cells of the same fate form coherent regions. Fate alterations lead to the positioning (‘sorting’) of the descendants according to their new fate, suggesting that fate determines their terminal positions [108].

To explain the extensive pre-morphogenetic ‘cell sorting’, the ‘cell focusing’ hypothesis has been proposed. Cells are supposed to

autonomously generate a positional value on their surface. Comparing these values, cells move relative to each other until they find their correct position as defined by their neighbors at the pre-morphogenetic stage [108].

Cells are able to obtain positional information from all other cells of the embryo and sort locally. As such they are guided by their neighbors. Directed cell migrations take the main part in this patterning process while mitotic divisions contribute rather little to cell displacement [108].

Also, direction of movement does not depend on cellular polarity but only on local cell-cell interactions [108].

The hypothesis is compatible with the general outline of embryogenesis of the worm. The stereotyped cleavages generated during early development establish the starting configuration [3], which enables a correct global patterning based on local cell sorting. Yet, there is some controversy about the variability and range of movements due to manipulation of embryos in the experimental setup (see chapter 1.3) [109].

1.1.4. Morphogenesis

In *C. elegans*, morphogenetic movements start around the 365-cell stage about 40 minutes after gastrulation is complete [3]. Morphogenesis is to a large extent controlled by the development of the epidermis (hypodermis), which surrounds the embryo as a single epithelial layer. During epidermal movement, cells interact with internal developing tissues including the nervous system and muscle cells, which act as movement substrates. Morphogenesis can be divided into different steps: specification of epidermal fate, closure of the depression on the ventral surface generated during ingression movements of gastrulation, enclosure of the embryo by a sheet of epidermal cells, and finally embryonic elongation (Figure 5).

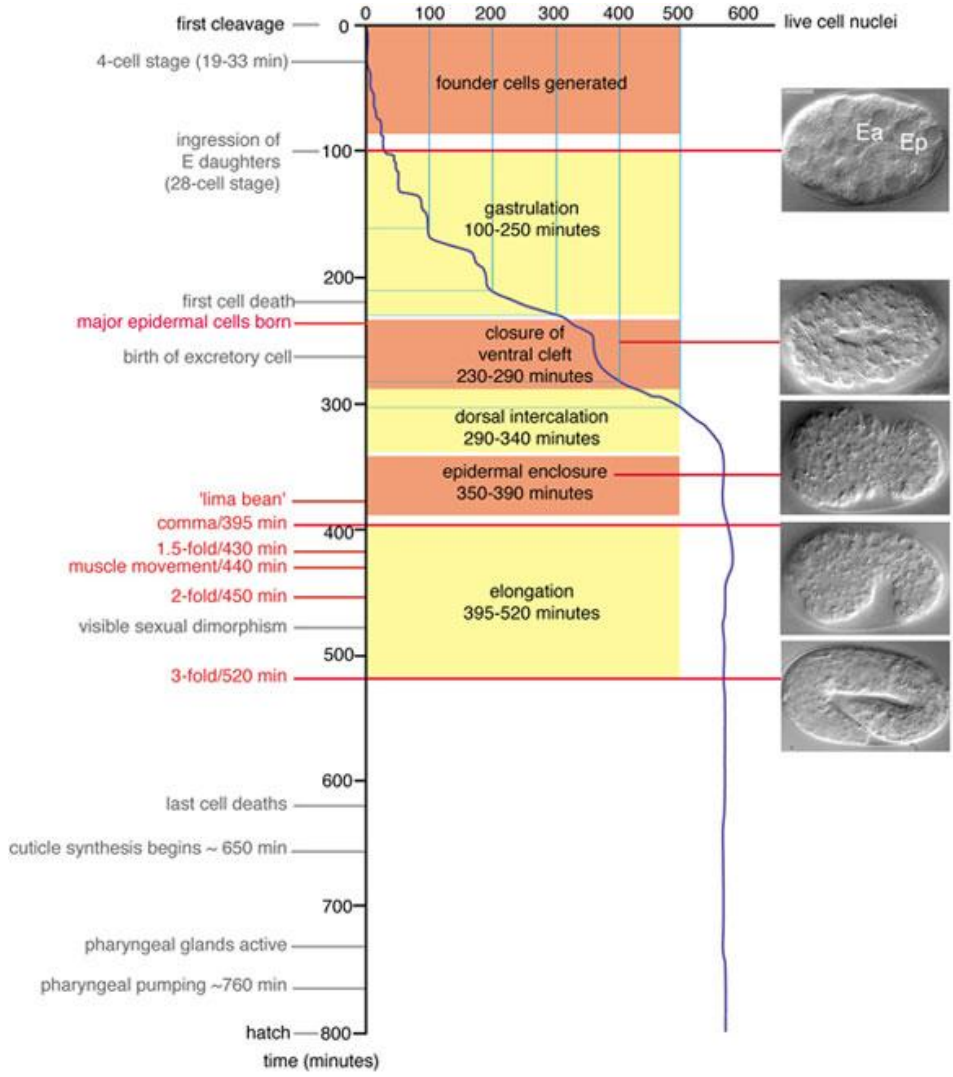

Figure 5: **Developmental timing of morphogenetic events.**
Nomarski Differential Interference Contrast images visualize developmental landmark stages. Times are relative to the first division, in minutes at 20°C [110].

1.1.4.1. Specification of epidermal fate

The so-called major epidermal cells constitute most of the epidermis. An additional 11 minor cells form epidermal syncytia at the tip of head and tail. Most epidermal cells fuse to generate multinucleate syncytia.

The major epidermal cells are descendants of four of the 12-cell stage blastomeres: ABarp, ABpla, ABpra, and C [74, 111].

They are born on the dorsal side of the embryo after the 9^{th} round of embryonic cell divisions, approximately 220-240 minutes after the first cleavage [112, 113].

Within the epidermal tissue, three different groups of cells can be distinguished: One group, the dorsal epidermal cells, forms two rows of ten cells, each overstretching the dorsal midline along the anterior-posterior axis [111].

These dorsal cells are flanked by two more lateral rows of seam epidermal cells. A third group of ventral epidermal cells is located at the extreme lateral edges of the epidermis and ultimately migrates to the ventral midline.

Shortly after their birth, approximately 250 minutes after the first division, major epidermal cells are specified. This initially requires the GATA family Zinc finger transcription factor ELT-1. Other factors believed to play a role in the expression of epidermal fates are LIN-26 and ELT-3. However, most likely a combinatorial interplay of multiple factors completes specification of epidermal fate [111].

1.1.4.2. Closure of the ventral cleft by neuronal precursors

After fate specification, epidermal cells rearrange in a process called dorsal intercalation. This process requires the previous movement of the ventral neuroblasts as these cells are destined to become the substrate for later epidermal movements. Inhibition or delay of neuroblast migration leads to defects in epidermal enclosure [114].

The depression on the ventral surface left behind by ingressing cells during gastrulation, the so-called ventral cleft, is surrounded by neuronal precursor cells. Between 230 and 290 minutes after the first cleavage, these cells begin to move from their more lateral positions towards the ventral midline, starting to close the cleft in posterior to anterior direction. Ventral closure is completed roughly one hour before the beginning of epidermal enclosure [3].

The exact timings and mechanisms of individual neuroblast movements are not known. However the presence of the ventral cleft is well defined and its duration can be quantified (M. L. Hudson and A.D.C., unpublished results) (Figure 6). Several cell signaling pathways, including the Eph receptor/ephrin system, seem to play a role [115-118]. Also, movements are thought to be actin-based [119]. Neuronal fate specification as well as correct fate of the movement-substrates such as the pharynx, are required, too [114] [54].

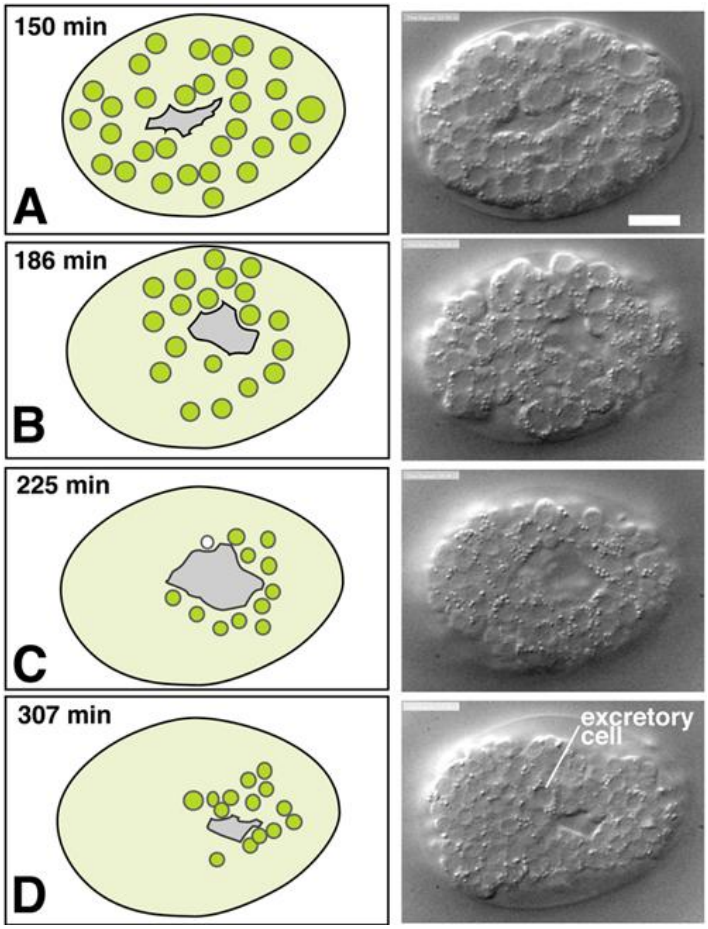

Figure 6: **Ventral cleft closure.**
In the left column schematics of embryos in ventral views are shown, with the migrating neuroblasts in green. The right column includes DIC images of embryos at the corresponding stage. Scale, 10 µm.

1.1.4.3. Dorsal intercalation of epidermal cells

Shortly after substrate neuroblast cells are positioned, dorsal intercalation of epidermal cells begins.

Dorsal cells become wedge-shaped, pointing towards the dorsal midline with their tips. They interlace with their contra-lateral neighbors and elongate until they contact with the seam cells on the opposite side of the embryo with their extending edge [3, 114]. Consequently, the two rows of dorsal epidermal cells engage to form a single row across the dorsal midline (Figure 7).

For these movements, actin microfilaments as well as microtubules are thought to be required [114]. Also, basolateral membrane protrusions in direction of the rearrangement have been observed. Interestingly, the cell shape changes required for intercalation are performed in a cell autonomous way [114, 120].

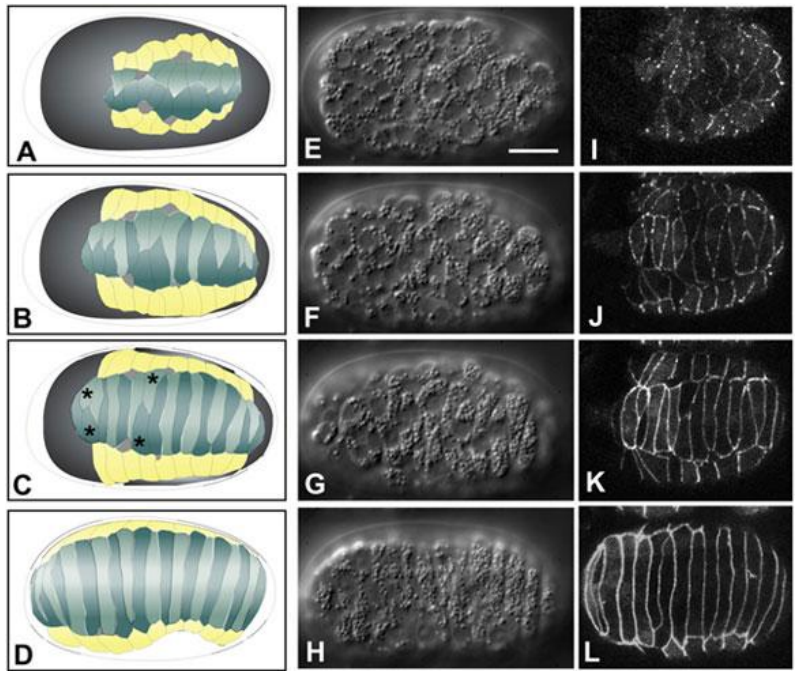

Figure 7: **Dorsal intercalation in the *C. elegans* embryo.**
Schematics of the process are seen in left column, A-D, Nomarski DIC images in the middle column, E-H, and **DLG-1**::GFP images highlighting epidermal cell boundaries (localizes at apical junctions of epithelial cells) in the right column, I-L. All views are from dorsal. Scale bar = 5 μm. In the left-hand column, dorsal cells are shown in teal, seam epidermal cells in yellow. Dorsal cells born on the right side of the embryo are displayed in a lighter color than those born on the left. For clarity, ventral epidermal cells and non-epidermal tissues are not shown. Asterisks indicate the last two pairs of dorsal epidermal cells to intercalate, which serve as fiduciary markers for the progress of intercalation [121, 122].

1.1.4.4. Ventral enclosure

Soon after intercalation of the dorsal epidermal cells begins, ventral epidermal cells also start to migrate towards the ventral midline to enclose underlying cells in an epithelial monolayer. This process is called ventral enclosure (Figure 8).

It begins with the migration of two pairs of anterior cells extending large protrusions towards the ventral midline. Their leading movement and protrusive activity is known to be essential for enclosure and continuing migration [121]. In the following, posterior cells become wedge-shaped and elongate towards direction of migration. By doing so, they fill the pocket around the ventral midline. Finally, ventral epidermal cells establish bilateral symmetric contacts [121]. To encase the embryo with a complete sheet of epidermis, the extreme anterior cells complete enclosure (Figure 8).

Both actin- and microtubule-cytoskeletal systems are essential for proper epidermal enclosure [121]. Onset of migration, initiated by the leading cells, requires *CED-10*/Rac dependent modulation [123, 124] of the actin cytoskeleton, probably acting through the Arp2/3 complex [104, 105]. This complex has also been found to be necessary during gastrulational movements [103]. *CED-10*/Rac [123] [125] localizes with its interacting proteins GEX-2/*Sra-1* and GEX-3/HEM2/NAP1/KETTE (Gex, *gut on the exterior*) to the periphery of epidermal cells near apical junctions, probably serving to maintain their shape and to build protrusions. Mutations in these proteins lead to disorganization of epidermal tissue that is unable

to undergo proper ventral migration [123]. Giving rise to a similar phenotype, GEX-1/WVE-1 is believed to act as a CED-10 effector in the same pathway, activating Arp2/3 [122].

For the essential protrusive activity of the leading anterior cells, the WASP family protein WSP-1 and Ena/VASP family protein UNC-34 are important [104, 119], as well as cell signaling by inositol triphosphate (IP3) [126].

As WASP and VASP proteins control the activation of the Arp2/3 complex, they are believed to act in regulating the polymerization of actin at the free edges of the enclosing epidermis [122].

Proper cell adhesion at the ventral midline requires the cadherin-catenin junctional complex (HMR-1A/cadherin, HMP-2/beta-catenin, HMP-1/a-catenin). Cytoplasmic HMP-1/cadherin accumulates at protrusions of leading cells and is rapidly recruited to nascent junctions as soon as they contact at the ventral midline [127]. In mutants of members of this complex, leading cell protrusions are still formed but are unable to establish stable adhesive contacts [127].

The mechanism of the final closure of the ventral pocket is less clear.

Among other prerequisites, proper control of protrusive contacts between adjacent pocket cells is necessary. Mutants of *mab-20/Ce-sema-2a*, encoding a secreted Semaphorin, display ectopic contacts during enclosure [128]. As in other contexts, semaphorins typically provide guidance information by mediating repulsive cues [129], MAB-20 might act by preventing ectopic protrusive activity

and thus limiting adhesion between adjacent pocket cells as they migrate [122].

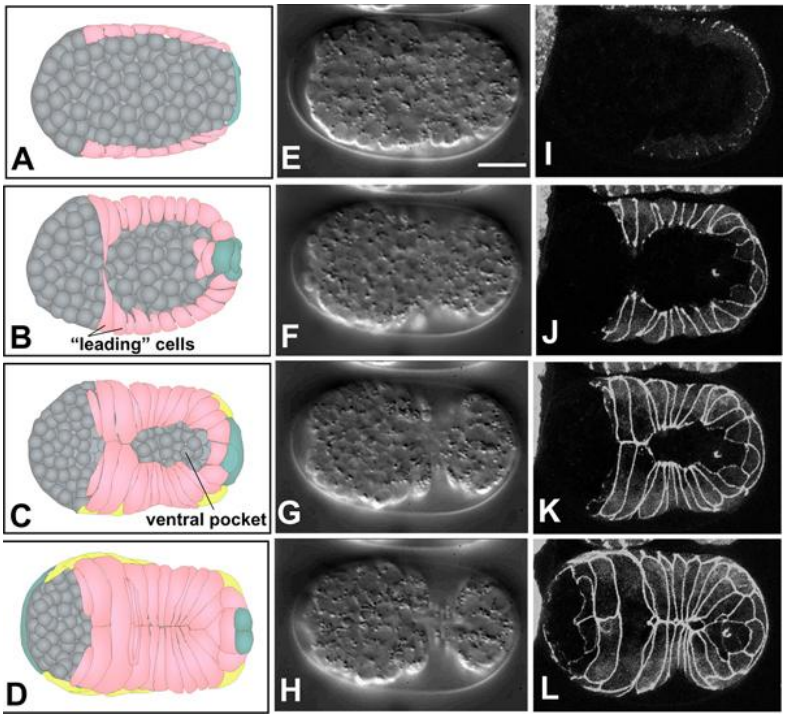

Figure 8: **Epidermal enclosure in the *C. elegans* embryo.**
Schematics of the process are seen in left column, A-D, Nomarski DIC images in the middle column, E-H, and **DLG-1**::GFP images highlighting epidermal cell boundaries (localizes at apical junctions of epithelial cells) in the right column, I-L. Scale bar = 5 µm. In the left-hand column ventral cells are depicted in pink, seam epidermal cells in yellow, and dorsal cells, which wrap around the tail, in teal. Neuroblasts and other internal cells are depicted in gray.

1.1.4.5. Embryonic elongation

Directly following epidermal enclosure, coordinated cell shape changes lead to embryonic elongation, converting the bean-shaped embryo to the elongated shape of the hatching worm [3, 130]. This process is mainly reflected by the anterior to posterior elongation of the epidermis, however internal body muscle cells play a role as well [131].

Epidermal elongation starts at around 350 minutes and is completed at roughly 600 minutes after the first cleavage. During this time, the circumference of the embryo is reduced by one third and length is increased by one fourth. After the 1.5 fold stage (430 minutes) the embryo elongates with a rate of about 50µm/hour until completion of elongation [132]. This rate is highly reproducible and allows stage determination of *C. elegans* embryos according to their extent of elongation [3].

For onset of elongation, both actin microfilaments and microtubules need to align in a highly organized, circumferential manner with the apical plasma membrane of epidermal cells [121, 131, 133, 134]. The formation of the circumferential actin filament bundles (CFBs) is essential for elongation. However this occurs transiently and only lasts during the time of elongation [121, 133].

As for gastrulation movements, actomyosin based contraction of elongating epidermal cells is driving the process. Hereby, it is thought that lateral seam cells transmit contractile forces to not actively contracting dorsal and ventral epidermal cells via CFBs and cadherin-catenin junctions [135].

Proteins of the cadherin-catenin complex such as HMP-1, -2 and HMR-1, are essential for proper attachment of CFPs to adherent junctions and as such for elongation. Absence of HMR proteins leads to failure of epidermal enclosure (Hammerhead phenotype), whereas zygotic hmp-1 and -2 mutant embryos enclose properly but CFPs detach from adherent junctions and elongation is impaired (Humpback phenotype) [134].

Other proteins associated with adherent junctions, such as the claudin-like VAB-9 transmembrane protein [136], and a-and b-spectrins (SPC-1, UNC-70, SMA-1) [132, 137-139] were also found to play a role in proper elongation.

As being involved in actomyosin contraction, the Rho-binding kinase LET-502, the myosin regulatory light chain MLC-4 as well as the myosin phosphatase MEL-11 have important, however antagonistic functions in elongation [135, 140]. A redundant parallel pathway for contraction includes the phosphatase FEM-2 [135, 141, 142].

The two non-muscle myosin heavy chains, NMY-1 and NMY-2, are thought to act partially redundantly in elongation and might be regulated by MLC-4 [143].

After the two-fold stage, elongation is mediated by different mechanisms. Hemidesmosome-containing trans-epidermal attachment structures are induced and localized through unknown mechanisms by muscle cells [144, 145]. The forces of muscle contraction are then transmitted to the cuticular exoskeleton via these attachments. Consequently, loss of muscle function, as caused by mutations in the *pat-1* gene (pat, *paralyzed arrest at*

two-fold), result in elongation failure after the two-fold stage [145]. Less severe phenotypes at late elongation are observed in mutants of attachment structure proteins such as Myoactin/LET-805 [146], Plectin/VAB-10A [147], intermediate filament proteins IFB-1 and IFA-3 [148]. Equally important for elongation as muscle function is the epidermal secretion of the extracellular matrix basement membrane. However, the importance of basement membrane components varies with plectin being the most important factor [145, 149, 150].

The elongating epidermal shape is actively regulated by the actin cytoskeleton of these cells.

The final shape is maintained by the collagenous exoskeleton, secreted by the apical surface of the epidermis.

After elongation is terminated, the epidermis secretes the cuticle of the first stage larva, which then takes over the role of holding the epidermal cells in place [122].

1.2. Cell lineage tracing in *Caenorhabditis elegans*

Due to its invariant cell lineage [3], fast development, small cell number, and transparency, the nematode *C. elegans* is a widely used model system to study embryonic development. Large number of available mutant alleles and transgenic reporter strains as well as a publically available RNAi library make *C. elegans* ideal for genomic and systems biology studies.

The seminal work of Sulston and colleagues [3] set the basis for developmental studies in the worm. They reconstructed the complete embryonic lineage following single cell divisions over the entire embryonic development. With a dissection microscope only single cells could be followed at a time. Thus a consensus of hundreds of embryos had to be studied and divisions had to be drawn manually in order to deduce the lineage. This time-consuming and labor-intensive approach, could not feasibly be extended to study mutant development.

To facilitate image recording and lineage analysis for a wider range analysis of wild type and mutant embryonic development, several methods have been developed afterwards.

A big step forward came with the development of four dimensional (4D) microscopy allowing observation and documentation of all cells of a single embryo in space and time [107, 109, 151-153]. In the following, improvements were made especially in documentation and analysis of the image output. In 1997, Schnabel et al. [107] described the use of ‘Biocell’, a programme documenting cell positions at different times and consequently

allowing analysis of cell migrations, cleavages, and terminal fates in further detail. This allowed for the manual curation of the embryonic lineage up to the 350cell stage within one week.

In 2005, Hamahashi et al. reported the first automated algorithm to identify and track nuclei using 4D differential interference contrast imaging (DIC) [154]. DIC image analysis relies on the detection of the variation of texture between nuclei and cytoplasm. However, as cells divide and become smaller, the detection of texture variation becomes increasingly difficult. Furthermore, in DIC images, nuclei disappear during mitosis when the nuclear envelope dissolves. As such, assigning newborn cells to mother cells, especially when neighboring cells go through synchronized divisions, becomes increasingly difficult over time. Consequently, correct automatic tracking could only be performed until the 24-cell stage.

More recently, 4D recordings of histone proteins tagged with fluorescent proteins have been used to semi-automatically follow cell divisions and track cells over time to determine the lineage [155, 156]. Using confocal imaging, a semi-automatic cell-tracking (StarryNite) and a lineage extraction programme (AceTree) have been developed. They allow generation of the *C. elegans* embryonic lineage up to the 350-cell stage in a semi-automatic manner within a day [155, 157, 158].

Approaches to improve robustness of the tracking algorithm and to extend the time frame and automation of lineage generation have been made subsequently.

Most important limiting factors for automatic tracking, especially at late stages of embryogenesis, are the large number and the small size of nuclei that might overlap and often divide simultaneously. Also, auto-fluorescence effects, low and uneven contrast throughout the image set, and light scattering at lower planes complicate tracking.

Great potential over previous algorithmic approaches appears to lie in a method using a model evolution framework for cell identification and multi-object tracking scheme based on energy minimization via graph cuts [159].

1.3. Variability in the embryo

With the development of 4D time-lapse recordings, better data storage and analysis methods, there is now conflicting evidence with respect to the extent of invariability of embryonic development. While early work [3, 160, 161] showed only little variability in division timing, cell positions, movements and contacts, newer studies reported substantial variability, large migration of cells and rotation of the embryo [107, 108].

To examine these discrepancies, Hensch et al. analyzed six different embryos and compared cellular variability to other datasets. To minimize interference with development, they employed a mounting method not compressing embryos in size [109]. These embryos are comparable in appearance on agar plates and correspond well with the standard size given in literature [162]. Consistently with the remarkable differences in size and shape (e.g. z-axis: 36µm in uncompressed vs. 18.4µm in compressed embryos) uncompressed embryos also displayed much lower variance regarding cell positions and movements. No apparent migration of single cells or small groups of cells relative to others could be observed. The major global cell movement observed was found to be gastrulation-associated, while other cell displacements were attributed to divisions.

As previously reported [76, 107, 163], around the 350-cell stage, cells with the same fate cluster in regions before morphogenesis starts. This also occurs in uncompressed embryos. However, it

could not be observed that cells migrate far from their position and later return to their kindred cell group.

Rotation of embryos around their a-p axis, equal to the change in cellular positions relative to the eggshell, was also observed. However, this appeared to be less pronounced in uncompressed than in compressed embryos. The trend noticed seems associated with clockwise rotation (from the embryo perspective) and the average rotation angle measured was 27.2° [109].

Using Vronoi decomposition, a list of all predicted cell contacts during early embryogenesis was generated and contacts were calculated up to the ~ 150-cell stage. Comparison of the uncompressed 4D model with a compressed embryo showed that up to 40% of cell contacts can be different. However, inductive early contacts seemed to be conserved [109].

Consequently, there seems to be a large degree of robustness in cell positions and movements during embryonic development. This allows adaptation to space restrictions and probably accounts for most of the variability observed in compressed embryos.

1.4. Cell division in *C. elegans*

Mitotic divisions in *C. elegans* are fast and highly stereotypical. The time span from the onset of DNA condensation to the completion of furrow ingression at cytokinesis is approximately 14 minutes.

Minor effects of DNA damage and spindle check points enable analysis of the depletion of essential cell division proteins [164, 165]. The embryo can proceed through the cell cycle despite dramatic defects in e.g. nuclear structure, spindle assembly, chromosome segregation and centrosome function.

Technically easily achievable depletion of target proteins by RNAi has permitted several genome wide screens that identified 2100 genes to be essential for embryogenesis [166-174]. Time-lapse recordings of embryos depleted of each of these 2100 genes showed 660 of them to be required for the first two rounds of cell division [170, 172, 173, 175]. Approximately half of them are specifically required for cell division processes such as chromosome segregation or cytokinesis, whereas the other half contributes to cell maintenance, via roles in processes such as translation and mitochondrial function [173].

Being most intensively studied, the first embryonic division following fertilization is taken to illustrate the division process in the following.

During mitotic prophase, the male and female pronuclei migrate towards each other, coinciding with the condensation of chromosomes. After the pronuclei meet, the nuclear-centrosome

complex moves to the center of the embryo and rotates to align with the anterior-posterior axis of the embryo [13, 31]. This coincides with the breakdown of the nuclear envelope (NEBD) [176, 177]. Condensed chromosomes now interact with spindle microtubules to align and segregate (Figure 9).

For accurate chromosome segregation, proper condensation of interphase chromatin, chromosome congression to the metaphase plate, sister chromatid separation and cytokinesis is essential.

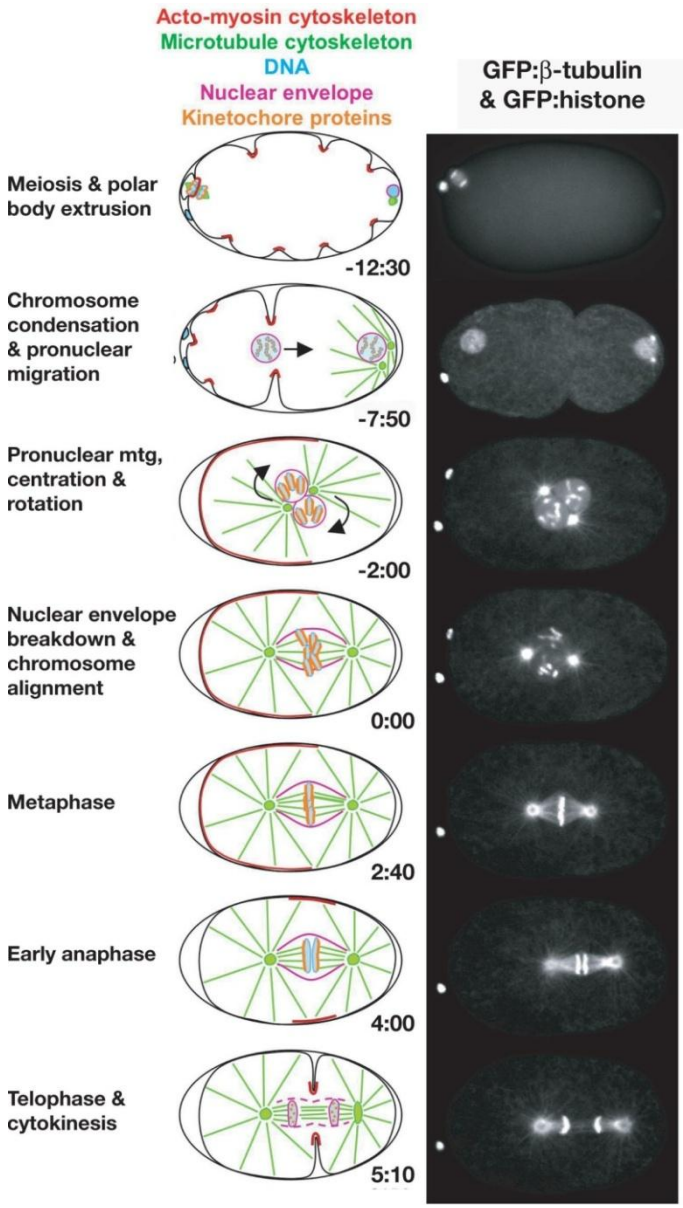

Figure 9: **The first division in the *C. elegans* embryo.**
The left column includes schematics illustrating major features of the first division. Approximate times are in minutes:seconds after nuclear envelope breakdown. In the right column images of each stage in a strain expressing GFP: beta-tubulin and GFP: histone are shown to simultaneously visualize the microtubule cytoskeleton and DNA [178].

1.4.1. Formation of mitotic chromosomes and condensation

Mitotic chromosomes are formed during DNA replication in S phase when cohesin is loaded and the cohesion between sister chromatids is established. Cohesin is a member of the SMC (structural maintenance of chromosomes) family of protein complexes, all consisting of five domains [179]. Mitotic cohesin contains a heterodimer of SMC-1 (HIM-1) and SMC-3, the non-SMC subunit sister chromatid cohesion 3 (SCC-3) and the α-kleisin subunit SCC-1 [180-183]. Sister chromatids are held together by SCC continuously from the time of their formation until their separation during mitotic anaphase. Proteolytic cleavage of the kleisin subunits carried out by separase removes the linkage between sister chromatids and allows their segregation [184]. Depletion of any of the cohesion subunits leads to defects in chromosome segregation and in pairing of homologous chromosomes during meiosis [180, 181, 183].

Similar to cohesin, condensin complexes are essential for the formation, compaction and segregation of mitotic and meiotic chromosomes [179, 185]. Like cohesin, condensin complexes contain a pair of SMC subunits and ancillary non-SMC subunits. The heterodimeric SMC subunits form the enzymatic core of the complex, exhibiting ATPase activity. The non-SMC subunits consist of three regulatory CAP (Chromosomes-associated-polypetide) proteins.

C. elegans contains two condensin complexes, condensin I and II, and an additional third condensin I^{DC}, which plays a role in the

hermaphrodite and X-chromosome-specific process of dosage compensation [186, 187]. Whereas condensin I and II bind to all chromosomes, condensin I^{DC} only associates with X chromosomes in hermaphrodites to halve gene expression, equalizing X-linked product in XX hermaphrodites and XO males [186]. The two mitotic complexes I and II have identical SMC subunits, SMC-4 and SMC-2, and a unique set of CAP subunits: CAP-D2, CAP-G, and CAP-H in condensin I, and CAP-D3, CAP-G2 and CAP-H2 in condensin II [188-190]. Condensin I and condensin I^{DC} only differ in their SMC-4 subunit. In condensin I^{DC}, the SMC-2 orthologue MIX-1 forms a heterodimer with the DC-specific SMC-4 orthologue DPY-2 [191]. Condensin I and II localize to distinct chromosome regions and contribute differently to chromosome segregation. Condensin II is nuclear, concentrates on chromosomes when condensation initiates at prophase and is required for proper kinetics of chromosome condensation. In contrast, condensin I appears to stabilize chromosome rigidity [188, 189, 192-197]. Depletion of each complex individually leads to distinct and characteristic defects in chromosome morphology and simultaneous depletion of both leads of more severe defects [189, 192-194]. However, both complexes are required for sister-chromatid segregation and chromosome bridging at anaphase is observed after depletion of either complex. Sister chromatid pairs that are structurally defective cannot be properly separated by the mitotic spindle [190, 194, 196]. Kinetically, chromosome condensation is temporally biphasic in *C. elegans*, suggesting that compaction occurs in at least two discrete steps. Primary

condensation converts diffuse chromatin into discrete linear chromosomes, and secondary condensation further compacts these chromosomes to shorter bar-shaped structures. In condensin depleted embryos, primary condensation fails, and discrete chromosomes of normal structure have not been observed [197]. However, as some kind of condensation is ultimately achieved, condensin-independent mechanisms must exist that are able to compact mitotic chromatin.

Concurrent with, but to a large extend independent of condensation, kinetochores assemble on centromeric chromatin to provide a chromosomal attachment site for spindle microtubules. Interestingly, CENP-A, the centromeric H3 histone variant constituting the kinetochore attachment site in chromatin, colocalizes with condensin II and is needed for its recruitment during metaphase [188, 190].

In addition, the chromosomal passenger complex (CPC, including the aurora B kinase AIR-2, BIR-1/Survivin, ICP-1/INCENP and CSC-1) is recruited to mitotic chromosomes as they form. The CPC is essential for proper segregation of mitotic chromosomes [33, 196, 198-201]. Recent studies reported Air-2 to be required for mitotic recruitment of condensin I but not II [202], consistent with its distribution on mitotic chromosomes that resembles the pattern of condensin I (but not II) [203]. Condensin II complexes associate with chromosomes at prophase and facilitate condensation-independent of AIR-2. However, after prometaphase, condensin I complexes assemble to chromosomes at least in part dependent on AIR-2 [196, 202].

1.4.2. Nuclear envelope breakdown (NEBD)

In contrast to mammalian cells in which the NEBD marks entry into prometaphase, in *C. elegans*, nuclear core complexes break down in prometaphase, but the nuclear envelope does not fully disassemble until anaphase [176].

Structurally and molecularly the *C. elegans* nuclear envelope is similar to that of vertebrates. It consists of an outer and inner membrane, enclosing a luminal space, nuclear pore complexes mediating bidirectional transport between cytoplasm and nucleus, and an underlying laminar network [204] (Figure 10).

C. elegans possesses a single B-type lamin, LMN-1 [177, 205] that builds a meshwork of intermediate filaments beneath the inner nuclear membrane. It also contains the LEM domain proteins, Ce-emerin, CeMan-1 and CeLem2, sharing a defining 40 amino acid motif typical for a family of nuclear envelope proteins [176, 206, 207]. LEM family proteins all bind to lamins [208] and to the small protein BAF that is associated with the inner nuclear membrane [209, 210]. Depletion of LMN-1, Ce-BAF, or simultaneous depletion of the LEM family proteins Ce-Emerin and Ce-MAN-1, results in defects in nuclear structure, chromosome condensation, and chromosome segregation [177, 207, 210, 211] (Figure 10).

During pro-metaphase, LMN-1 leaves the nuclear envelope [176]. However, inner nuclear membranes, containing Ce-emerin and Ce-MAN-1, remain largely intact during metaphase and early anaphase. They surround the mitotic spindle everywhere except near spindle poles until their complete disassembly during mid to

late anaphase [207, 212]. The remnants of the old nuclear envelopes disperse, and new nuclear envelopes form around the segregated chromatin about one minute after anaphase onset (Figure 10).

Nuclear pore complexes (NPCs) of *C. elegans* are also similar to NPCs in vertebrates. *C. elegans* has orthologues to at least one component of each vertebrate NPC sub-complex [213]. 17 genes encode 19 nucleoporins and all are essential for embryonic viability. Depletion of 14 of these proteins results in defects in nuclear morphology and, in some cases, to reduced nuclear size consistent with defects in nucleo-cytoplasmic transport [213]. For proper nuclear envelope assembly the small GTPase, Ran and the nuclear transport receptor importin-γ IMB-1 are important as well [214-216]. RanGTP associated with chromatin is believed to aid in the dissociation of importin-γ from nucleoporins to trigger NPC assembly on the chromatin surface.

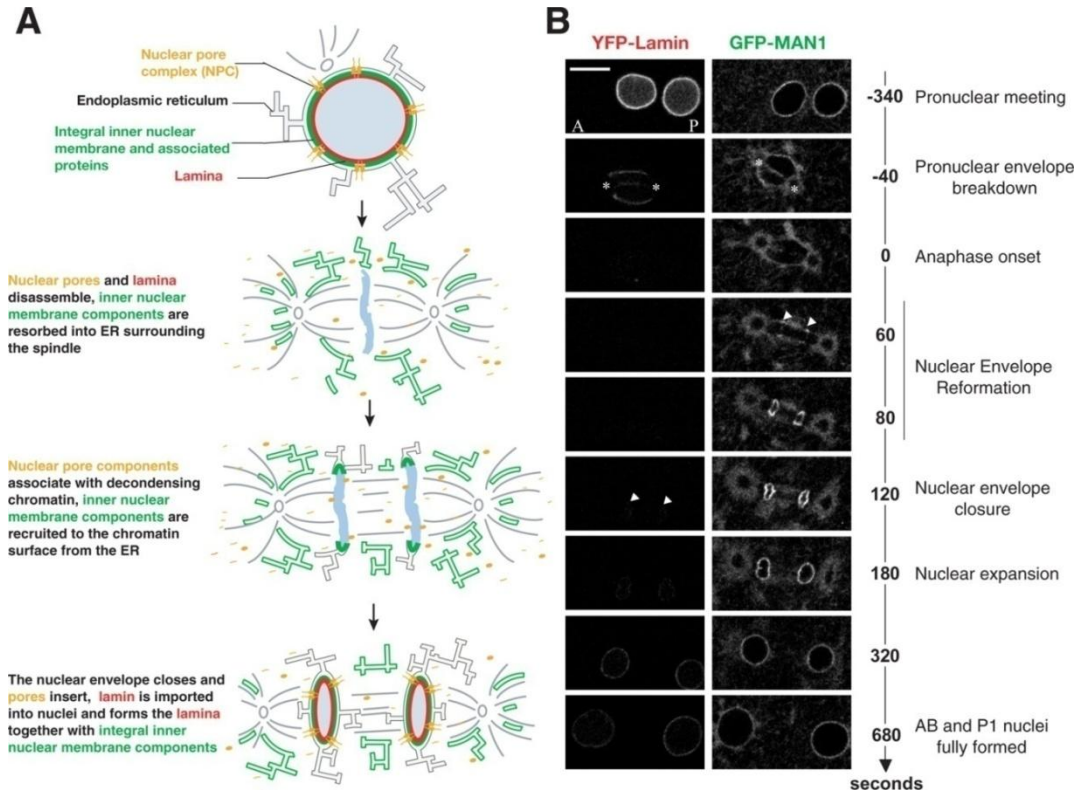

Figure 10: Nuclear envelope dynamics in the *C. elegans* wild-type embryo.
(A) Schematics of nuclear envelope breakdown and reassembly.
(B) Still images of the first mitotic division of embryos expressing YFP-Lamin (left) and GFP-MAN1 (right). Times are relative to first metaphase to anaphase transition. Arrowheads indicate the reappearance of GFP-MAN1 around the chromatin at t=60 sec and YFP-Lamin at t=120 sec. White stars mark the positions of the centrosomes. Scale bar = 10µm [178]

1.4.3. Kinetochore and spindle assembly

Simultaneously with the breakdown of the nuclear envelope, centrosomal proteins enter the nuclear space and start to interact with mitotic chromosomes. Within the next approximately 2.5

minutes spindle assembly is completed before the onset of anaphase. In *C. elegans,* mitotic spindles consist mainly of microtubules connecting centrosomes to kinetochores.

The mechanism of spindle assembly in *C. elegans* utilizes centrosomal microtubule asters to reinforce spindle bipolarity and position the spindle within the cell. Functional centrosomes are essential for spindle assembly [217-219] and most proteins necessary are known centrosome components [173].

For the proper assembly of the mitotic spindle, kinetochores that are capable to form stable bipolar microtubule attachments are indispensable. In the absence of functional kinetochores, the two spindle poles are abruptly pulled apart [33]. The same is seen after damaging the spindle with an UV microbeam, confirming the importance of kinetochores for integrity of the mitotic spindle [34].

Among eukaryotes two distinct chromosome architectures are prevalent: monocentric (e.g. vertebrates), in which kinetochore assembly is restricted to a localized region of each chromatid, and holocentric (e.g. *C. elegans*), in which diffuse kinetochores assemble along the entire chromatid length [220] (Figure 11 A). Both monocentric and holocentric organisms assemble kinetochores on chromatin containing nucleosomes with the histone H3 variant CENP-A [33, 221-224].

C. elegans embryos depleted of CENP-A fail to assemble functional kinetochores, capable to interact with spindle microtubules. Consequently chromosomes fail to distribute over the spindle midzone and to segregate properly, giving the characteristic “kinetochore-null” phenotype [33] (Figure 11 B). The

only other proteins, apart from CENP-A, that exhibit the kinetochore-null defect are CENP-CHCP-4, KNL-3 and KNL-1 [33, 225-227]. KNL-3 and KNL-1 form part of a 10-protein complex being essential for the establishment of the outer domains of the kinetochore that interact with spindle microtubules [226, 227]. Less severe chromosome segregation defects are observed after depletion of proteins further downstream in kinetochore assembly [228, 229] (Figure 11 B). The hierarchy of proteins forming the mitotic kinetochore complex and their timing can be seen in Figure 11 B+C [227].

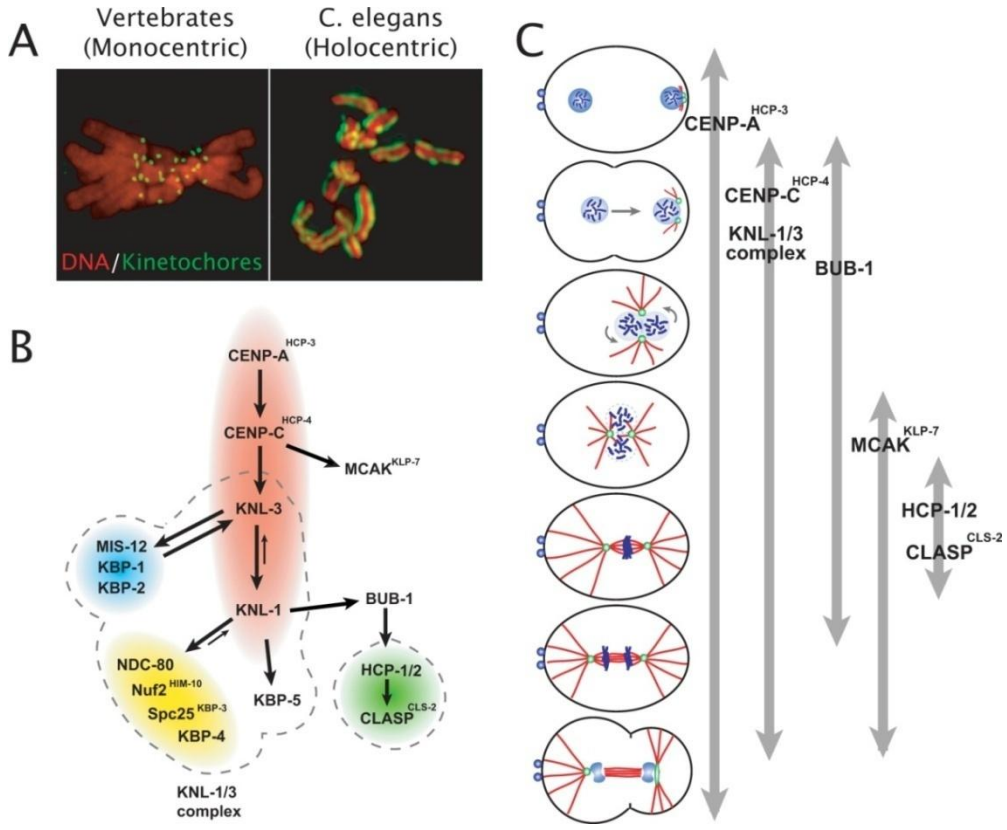

Figure 11: Mitotic kinetochores in the *C. elegans* embryo.
(A) Comparison of the localized kinetochores from a vertebrate tissue culture cell with monocentric chromosomes to diffuse kinetochores in *C. elegans* with holocentric chromosomes.
(B) Schematic illustrating the hierarchy for mitotic kinetochore assembly. Dotted lines are drawn around groups of proteins that co-purify in immunoprecipitations and tagged protein isolations from *C. elegans* embryonic extracts. The colored ovals indicate groups of proteins whose individual depletions result in a similar phenotype. Red: “Kinetochore Null”/KNL proteins. Blue: “MIS” proteins whose depletion leads to relatively subtle chromosome segregation defects. Yellow: “NDC” proteins whose depletion results in intermediately severe chromosome alignment and segregation defects, relative to the KNL and MIS classes. In NDC embryos, attachments that can sustain tension fail to form, leading to premature spindle poles separation. Green: HCP/CLASP proteins, whose depletion causes sister chromatids to co-segregate to the same spindle pole.
(C) Schematic displaying the temporal localization of kinetochore proteins[178].

The next protein downstream of CENP-A/HCP-3 is CENP-C/HCP-4, thus playing a major role in directing kinetochore assembly. Additionally, CENP-C/HCP-4 seems to be important for resolving kinetochores of sister chromatids from each other to position them on opposite sides of the mitotic chromosome [225].

Apart from proteins localized at the kinetochore, KLP-19, a chromokinesin that positions to chromatin between the diffuse kinetochores, is also required for proper segregation of chromosomes. KLP-19 interacts with spindle microtubules to generate pushing forces that rotate chromosomes in order to orient sister kinetochores to face opposite spindle poles [230]. As such, KNL-19 aids to prevent incorrect attachment of a single kinetochore to microtubules from both spindle poles (mereotelic attachment) [230].

1.4.4. Chromosome segregation and cytokinesis

The first step of chromosome segregation at anaphase consists of the movement of chromosomes towards the spindle poles. Secondly, spindle poles separate from each other with the chromosomes in tow, contributing the largest part of chromosome movement in *C. elegans* [33]. This movement derives from a combination of pulling forces from the cortex and pushing forces from the central spindle that forms between the separating chromosomes. Both act on the centrosomal microtubule asters to segregate them. The central spindle is thought to limit the rate of pole separation [34], as well as G protein signaling [30].

During cytokinesis, signals from the anaphase spindle lead to the assembly of an equatorial cortical contractile ring, mainly consisting of actin and myosin II. Constriction of the contractile ring triggers cell shape changes and consequently enables division (reviewed in [231]). Proteins associated with the acto-myosin cytoskeleton and which are necessary for cortical contractility, include the small GTPase RHO-1 [232] and its activating Guanosin-exchange-factor (GEF) LET-21 [233]. Downstream of RHO-1 signaling acts the formin CYK-1 [105] [234], which regulates the assembly of actin filaments in the contractile ring. Motor of contractility is the non-muscle myosin II NMY-2 [235]. Upon phosphorylation of its regulatory light chain, MLC-4 [140], myosin II becomes activated and triggers the formation of bi-polar filaments that can interact with actin to generate cortical ingression [236]. MLC-4 phosphorylation is in turn regulated by the Rho kinase homolog LET-502, one of the RHO-1 effectors [237].

Equally important for cytokinesis are proteins that lead to the formation of the spindle midzone, an array of microtubule bundles that is generated between separating chromosomes [231]. These include a protein complex called centralspindlin, formed by kinesin ZEN-4 and a GAP for Rho family GTPases, CYK-4, [199, 232, 238-240]. In addition, the chromosomal passenger protein complex containing the *C. elegans* homologue of aurora B kinase, AIR-2, is essential for the formation of the central spindle [33, 200, 203, 241-244].

During the progression of cytokinesis, microtubule bundles in the central spindle compact to build a single structure, the midbody.

Around the midbody, the cleavage furrow constricts. This promotes membrane fusion and completion of division. In embryos depleted of spindle midzone assembly proteins, the cytokinetic furrow initiates to form, but soon regresses due to the absence of the midbody. Spindle midzone microtubules also function earlier in cytokinesis, signaling to the cortex to assemble the contractile ring. Midzone disruption however does not inhibit the formation of the furrow, as the midzone-based signal is redundant with signals from microtubule asters [233].

1.5. Chromatin modifying and remodeling complexes in *C. elegans*

Chromosomes go through various dynamic processes including transcription, replication, repair and packaging. Recruitment and assembly of not only RNA Polymerase II and transcription factors, but also proteins involved in chromatin regulation, are crucial for these activities. ATP-dependent chromatin remodeling complexes regulate the accessibility of nuclear proteins to DNA. Thus, they play pivotal roles in various cellular processes by reshaping the epigenetic landscape. Epigenetics comprises all inheritable changes that are able to modulate gene expression but are not encoded by the DNA sequence itself. These changes comprise modifications at the chromatin level, which can be mainly achieved by four processes: DNA methylation, histone modifications, ATP-dependent chromatin remodeling and incorporation of histone variants.

In eukaryotes, genomic DNA is packaged with histone proteins into chromatin. The four existing core histones, H2A, H2B, H3 and H4, all have flexible amino-terminal ‘tails’ of 25 to 40 residues, which are highly conserved. However, in crystals of mononucleosomes, the tails of histones did not display a defined structure [245]. The target sites of important posttranslational modifications of histone tails are highly conserved. These modifications include acetylation and methylation of lysines, and arginines, phosphorylation of serines and threonines, ubiquitylation and sumoylation of lysines, as well as ribosylation. Modifications

are carried out by various chromatin modifying complexes, such as, for example, COMPASS (for histone methylation), NuA4/Tip60 (for Histone H4 acetylation), NuA3 (for Histone H3 acetylation) complexes [246-249]. All chromatin modifying complexes contain histone modification enzymes, such as histone acetyltransferases (HAT), histone deacetylases (HDAC), histone methyltransferases (HMT) and histone kinases (reviewed in [248, 249]). Chromatin modification complexes work together with ATP-dependent chromatin-remodeling complexes, which recognize specific histone modifications to restructure and mobilize nucleosomes (reviewed in [250, 251]). Also, histone variants can be incorporated into chromatin at specific regions, e.g. by the SWR1/SRCAP complex, thus adding an extra layer of regulation of chromatin remodeling [252-255].

Chromatin remodeling complexes show a surprising complexity in their composition and function. Based on sequence and structure, the ATPase subunits of these complexes can be divided into four families: the SWI/SNF (switching defective/sucrose nonfermenting), ISW (imitation switch), INO80 (inositol requiring 80), and NuRD/Mi-2/CHD (chromodomain, helicase, DNA binding) families.

As *C. elegans* core histones are highly conserved in structure, it is reasonable to assume that homologues of mammalian histone modification enzymes are present as well. *C. elegans* histones are at least 80% identical in amino acid sequence compared to human histones [256-260]. Also, some post-translational modifications

were shown to be identical to those in humans [258, 259, 261-263].

In addition, *C. elegans* possesses homologues of many other mammalian chromatin factors (i.e. chromatin modifying and remodeling complexes), for many of which important cellular and developmental roles have already been established. There is substantial evidence that most, if not all developmental transitions require chromatin regulation and that such regulation is more specific than previously thought [264]. Most chromatin regulation complexes contain various different subunits, some of which have multiple isoforms. The different subunits and their combinations enable multiple varieties of one complex to exist both within a given cell and across cell types.

C. elegans chromatin factors have been found to play essential roles in a variety of cellular and developmental processes, including vulval development, germline development, germline-soma distinction, repetitive transgene silencing, RNAi, somatic gonad development, and larval development [261, 265-273]. However, they appear to be involved in many other biological processes [274, 275]. Identification of more genes or chromosomal regions that are direct targets of chromatin factors is the key for further understanding chromatin regulation in response to specific developmental signals.

1.5.1. Chromatin factors in vulva development

The differentiation of the *C. elegans* vulva is one of the most intensively studied systems for gaining insights into cell signaling and developmental pattern formation. Various signaling pathways including the RTK/Ras/MAP kinase pathway, the LIN12/Notch pathway and the Wnt pathway lead to the differentiation of different vulval cell types from hypodermal precursors. Most intriguing in vulva differentiation, however, are the so-called synthetic Multivulva (SynMuv) genes that act redundantly to repress vulval fate [276, 277]. Based on their genetic properties, SynMuv genes are categorized into three classes, A, B, and C. Combination of two mutations in two of the three classes generates a Multivulva phenotype, whereas mutations in only one of the SynMuv genes does not [276, 278].

Most SynMuv genes have been identified through positional cloning. Many encode for chromatin factors involved in gene repression. These chromatin regulators include histone deacetylases (e.g. *hda-1*, [279, 280]), histone lysine methyltransferases (KMT) (e.g. *met-2*, a homologue of the mammalian SETDB1, a histone H3 lysine 9 (H3K9) KMT, as well as nucleosome remodeling factors and members of the sumoylation pathway. *Smo-1*/SUMO, *uba-2 (SUMO activating enzyme subunit 2),* and *ubc-9 (SUMO-1 conjugating enzyme),* possess genetic properties similar to SynMuv. Histone sumoylation is known to be involved in transcription repression in *S. cerevisiae* [281]. Furthermore, the SynMuv B genes *lin-53*, *let-418* and *mep-*

1, encode members of the NuRD complex [282-284] which is thought to act mainly in transcriptional repression [285].

In contrast to SynMuv B genes, members of the SynMuv class C encode for chromatin modifiers that are involved in transcriptional activation. They encode e.g. potential components of the NuA4/Tip60 complex, which is known to act in histone H4 acetylation, a mark of gene activation [249, 278]. As such, genes encoding for members of these two SynMuv classes most likely act on different target genes giving rise to the SynMuv phenotype in class B and C synthetic mutants.

Furthermore, several genes have been found to suppress the synMuv mutant phenotype. These SynMuv suppressor genes are thought to positively regulate vulval development, and indeed, many of the SynMuv suppressors encode chromatin factors that are transcriptional activators [265, 273, 286]. For example, homologues of the NuA3 histone acetylation complex, the histone H3 methylation complex COMPASS/MLL, the histone exchange complex SWR1/SRCAP, and the ATP-dependent chromatin remodeling complex ISW1/NURF are thought to be SynMuv repressor genes [247, 255, 265, 273, 286-289]. These complexes are generally linked to active transcription in yeast and mammals (reviewed in [249-251]).

1.5.2. Chromatin factors involved in asymmetric cell divisions

The mechanism of asymmetric cell divisions involves the interaction of various signaling pathways and extensive

reprogramming of gene expression [290, 291]. Thus, general chromatin modifiers are believed to be indispensable in the process. For the asymmetric cell division of the T blast cells in *C. elegans*, components of the SWI/SNF and the NuRD chromatin remodeling complexes are essential [269, 292, 293]. In a genetic screen for the phasmid socket absent (psa) phenotype, the genes *psa-1* and *psa-4* were identified, encoding components of the SWI/SNF complex [293]. Phasmid socket absence is the result of defects in the asymmetric division of the T cell [294]. Other components of the SWI/SNF complex in *C. elegans* also play important roles in asymmetric T cell division [293]. It is thought that either Wnt signaling directly controls SWI/SNF complex activity or that it regulates transcription factors acting in parallel [295, 296]. Most likely, chromatin factors are also important for other asymmetric cell divisions during embryonic development in *C. elegans*, although this has yet to be demonstrated.

2. Results

2.1. A systematic and quantitative method to study early *C. elegans* embryogenesis

To dissect early *C. elegans* embryogenesis and to get further insights into its underlying molecular mechanisms, we developed procedures for imaging and semi-automatic extraction of the cell lineage, nuclear positions, movements, division angles, shapes and fluorescence intensities from *C. elegans* embryos in combination with RNAi knockdown of specific factors.

A protocol based on methods described by Bao *et al.* was designed, providing 4D images of embryos expressing a histone-GFP fusion protein [297]. This permits imaging with high spatio-temporal resolution without apparent changes in embryonic development. In the group of Erik Meijering, a set of algorithms to automatically identify nuclei and trace the lineage through 350 cells was developed. A software, termed “Lineager”, designed in our lab, links the images and annotations obtained by automatic cell tracking using tree representations of the lineage. This enables image viewing and manual editing of the tracking output to generate the lineage. The visualization tools of the software are then used to examine nuclear behavior in 4D.

2.1.1. Imaging

By careful adjustment of the microscope settings, our imaging strategy minimizes exposure of the embryo to excitation light with optimized distinction of GFP signal over background noise. This becomes increasingly difficult over time as cells divide, become smaller, and overlap due to the increase in cell number and resolution limitations of the microscope. By increasing the excitation intensity throughout the depth of the embryo we reduced the decline in image quality in deeper sections of the sample. Other parameters, such as pinhole size, zoom, y-axis resolution, and line averaging were adjusted to further enhance the signal-to-noise ratio (see Methods for details). Minimizing exposure of the embryo to laser excitation is crucial as small increases in exposure, such as by addition of extra planes to the image stack, may result in hatching failure of some of the embryos.

To obtain reasonable correct lineage output from the automatic tracking, nuclei must be captured with sufficient spatial and temporal resolution. Stacks of images were collected every minute, which allows the recording of cell divisions with high resolution. Mitosis takes place over approximately four minutes, giving multiple time points at which condensed mitotic chromosomes are observable.

With similarly high resolution, images from 28 focal planes were collected every minute, each one with a distance of one micrometer apart. As nuclear diameters range from 11µm in the

early embryo to 3µm in later stages, each nucleus is detected in at least three planes.

With these settings and parameters, developmental events are not perturbed. The embryo hatches with normal morphology and movement, and the resulting lineages are comparable to published wild-type data [3, 155]. Moreover, variability of division timings (SD 1-3 minutes, ~ 7% of cell cycle length, n=3) and cell positions (SD 1.1µm, 6.8% of distances between cell pairs) is small between embryos imaged under the described conditions (Figure 13 and Figure 14). The observed variability across embryos corresponds to previously reported data [298]. This allows for comparison of wild-type to RNAi-disturbed development.

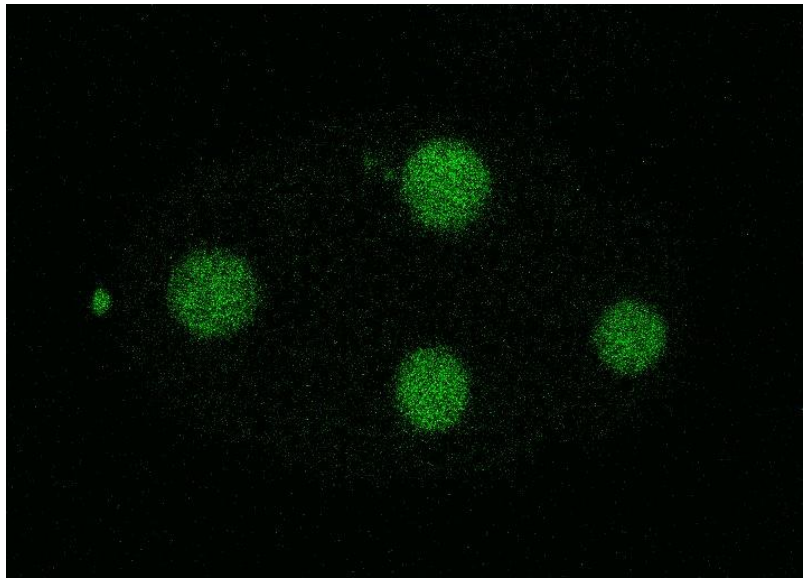

Figure 12: Representative raw 2D image of a four-cell embryo with GFP-histone-labeled nuclei, imaged with the protocol described. The embryo is aligned with anterior to the left, posterior to the right, dorsal up and ventral down. The green dot at the left corresponds to the polar body, a remnant of the meiotic divisions.

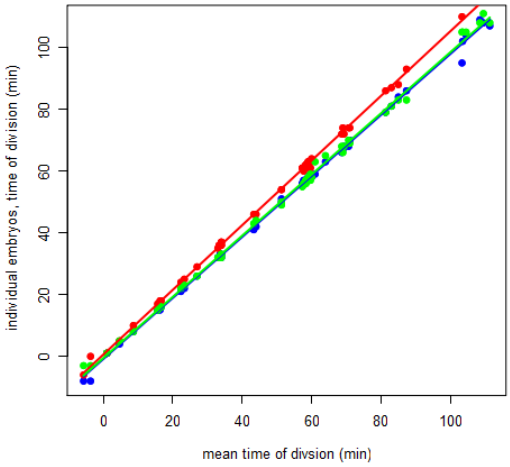

Figure 13: **Little variability in division times is observed between embryos imaged with the designed protocol.**
Different colors represent different embryos. Each dot represents the time of division of one cell.

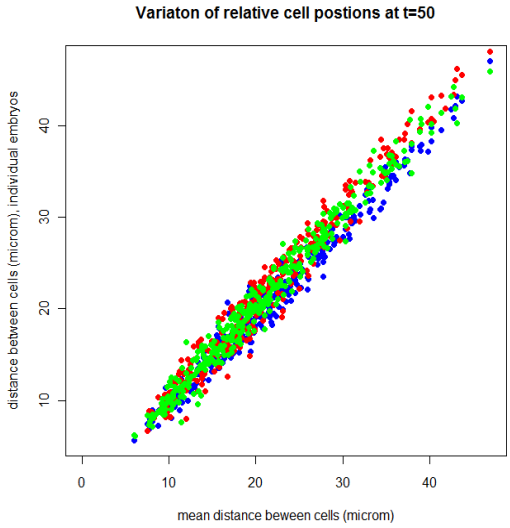

Figure 14: **Little variability in cell positions between wild-type embryos, imaged with the same protocol.**
Different colors represent different embryos. Each dot represents the distance of one particular cell to another (distances of cell pairs are compared between embryos, indicating the relative position of a cell within the embryo).

2.1.2. Generation of the embryonic lineage

Images from the time-lapse recordings were processed and submitted to automated nuclear tracking (Figure 15 see Material and Methods for details). The resulting lineages were then corrected and cells were named using the Lineager software.

There are three possible sources for errors in lineaging: failure to identify a nucleus (false negatives), identification of a non-existing nucleus (false positives), and incorrect matches in tracking. In addition, there can be missed division and false true divisions. Table 1 shows the rate for each type of error at the different stages of embryogenesis. From the four-cell to 100-cell stage, the overall accuracy is >98% and editing is accomplished in less than one hour. The accuracy of cell division tracking is 95%. As the embryo proceeds through further divisions, error frequency increases rapidly. Editing is still feasible up to 150 minutes and takes approximately three to five hours. In general, the error rate after 200 minutes after the four-cell stage increases drastically so that only particularly interesting cases were analyzed further.

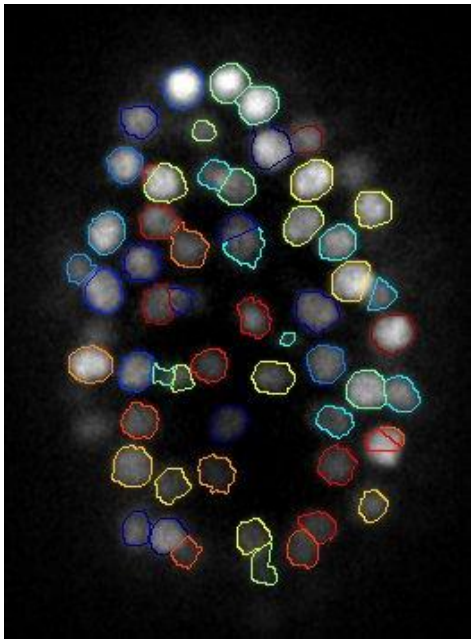

Figure 15: Representative, processed 2D image of an embryo with GFP-histone-labeled nuclei.
The nuclei are annotated as determined by the nuclear tracking output. Circles represent the spherical models of identified nuclei, i.e. the intersections at the given plane.

Number of cells	Last time-point	Number of nuclei	False negative/ 1000 nuclei	Divisions	Error/division	Tracking errors
4-51	82	2039	0.98	47	0	0
51-102	115	2846	0	51	0	1
102-194	155	6801	11.32	92	0.17	4
194-350	184	8140	77.76	156	0.5	33

Table 1: Benchmarks of the tracking algorithm, performed on wild-type dataset (100809).
Error rates for false negatives during nuclear identification, number of errors that occur due to division, and mismatches during nuclear tracking are shown. A correctly tracked division is defined by correct identification and match of mother and two daughter cells. Data from Rob Jelier.

2.2. Novel insights into wild-type *C. elegans* development

2.2.1. Gastrulation movements are not restricted to movements into the interior - cells tunnel and egress to the surface

Using the semi-automatic cell tracking and lineaging approach described in the previous chapter, we followed specific embryonic cell lineages in order to study their movements.

Hereby we noted that gastrulation movements are not limited to be directed from the surface into the interior of the embryo, but can also be observed from the inside to the outside (egressions). Additionally, by following cells systematically during embryogenesis, we identified several cells that previously have not been reported to gastrulate.

The identity of many cells that ingress during embryogenesis has been known for long [91, 299]. These include cells from the AB, E, MS, C, and D lineage, as well as the germline precursors Z2 and Z3. However, there remained ambiguities about their time of ingression. Also, the list of cells was not complete. Especially the exact identities of ingressing ABa and ABp descendants were not clear. Only recently the full lineage of gastrulating cells has been published, reporting 66 cells in total to internalize in *C. elegans* [92].

From our study, we could confirm the ingression of most of these cells. Apart from the previously known AB derived pharyngeal and buccal cavity precursors, we confirmed the internalization of many

cells of the AB derived nervous system [92]. We observed seven of the eight reported precursor cells (that give rise to 60 neurons) to gastrulate. ABprpaap descendants however, were not found to internalize. Also, we observed many of the reported ingressing cell lineages to reemerge on the surface, thus to egress (Table 2, Figure 16, Figure 17, Figure 18 A). We called these movements “transgression” movements, in which cells internalize, “tunnel” through the embryo and egress afterwards. This was observed for several anterior cell lineages. In addition, we identified several cells that end up in the interior of the embryo because of an oriented cell division, not an ingression movement (Table 3, Figure 18, Figure 19, Figure 20).

Ingressing cell	Precursor of	Notes on ingression/egression
ABalaap	Ring ganglion	ABalapp born internal, daughters tunnel between ABara and ABarp lineages to egress
ABalapp	Ring ganglion, lateral CANR neuron	
ABalpppa	Ring ganglion	Egression of daughters amongst ABpl, granddaughters ingress again
ABalpppp	Ring ganglion	
ABarappp	Ring+ ventral ganglion	Ingresses as pair with ABarappa (Table 2), egression right after division, movements are associated with overall embryonic rotation
ABplppap	retrovesicular ganglion, central cord	Ingresses from the lateral left surface along with the ventral directed ABpl movement. Granddaughters egress on the right surface, but ingress later again

Table 2: **Early ingressing cells that tunnel and reemerge on the surface again (egress).**
CANR neuron: process runs along excretory canal, no synapse seen, essential for survival [299]

Ingressing cell	Precursor of	Notes on ingression/egression
ABarappa	Ring + ventral ganglion, hyp 1	Ingresses as pair with ABarappp (Table1)
ABarpppp	V6R, V4R, V2R, V1R	Mother ingresses, internal by division, egresses immediately after birth
ABalpaap	Pharynx, arc post DL, arc ant DL, arc post VL, hyp1 +2	Internal by division angle (mother on ventral surface)
ABarpapa	Ring ganglion, hyp 1+6	Mother ingresses, internal by division, egresses immediately after birth
ABarpapp	Hyp5, H0R, H1R	
ABprppap	ventral ganglion and central cord	Ingress from the posterior
ABpraaapp a/p	Ring ganglion	Ingress from the anterior-dorsal surface
ABpraaapa a/p	Ring ganglion	Ingress, ABpraaapap daughters egress

Table 3: **Newly identified ingressing/egressing cells that previously have not been reported to gastrulate.**
Cell identities were identified from the lineage tree [3].
Hyp 1,2,5,6: cylindrical hypodermal syncytia
V1R, V2R, V4R, V6R: seam hypodermal cell, postembryonic blast cell
H0R: seam hypodermal cell
H1R: seam hypodermal cell, postembryonic blast cell
Arc ant DL/post VL: arcade cell, anterior-dorsal-left/posterior, ventral-left; both form the interface between pharynx and hypodermis, form anterior part of buccal cavity (alimentary tract)

A nice example for transgression is shown in Figure 16. ABalaap and ABalapp ingress from the left side of the embryo and move towards the right. Both cells then divide at the same time in the interior of the embryo. Their descendants egress amongst ABara

and ABarp. Interestingly, their egression goes along with the ingression of MS cells (Figure 16 C). Thus, the egression movement might be driven by ingression of MS descendants, pushing ABalaap cells to the dorsal surface of the embryo.

A similar observation could be made for ABalppa and ABalpppp. Both cells are born interiorly and immediately start to egress among ABpl lineage. This movement goes along with the ingression of MS descendants, likely to push them out of the way (Figure 17).

Figure 18 A shows the ingression of ABarappa, which has not been reported to internalize before. ABarappa ingresses as pair with its sister ABarappp, and both cells divide in the interior of the embryo. After division, descendants immediately egress. Curiously, ingression and egression movements go along with the overall embryonic rotation that occurs in compressed embryos approximately 80-120 minutes after the four-cell stage.

ABplppap is another cell observed to tunnel through the embryo. It ingresses from the lateral left surface as ABpl cells move ventral during the embryonic rotation (Figure 18 B).

Figure 19 shows newly identified interior cells. ABarppp has not been reported to internalize before. After division in the interior, the daughters move further ventral and granddaughters egress again on the lateral left surface (Figure 19 A).

In addition, the internal localization of ABalpaap has not been reported before. It is found internal due to displacement at division. Shortly afterwards, ABalpaap moves towards the anterior side and egresses again (Figure 19 B).

Ingression of ABarpap has also not been described before. Right after division of ABarpap, its daughters egress again to the right dorsal surface (Figure 19 C).

Newly identified interior cells of the ABpr lineage are shown in Figure 20. These include ABprppap (Figure 20 A), ABpraaapp (Figure 20 B), and ABpraaapa (Figure 20 C).

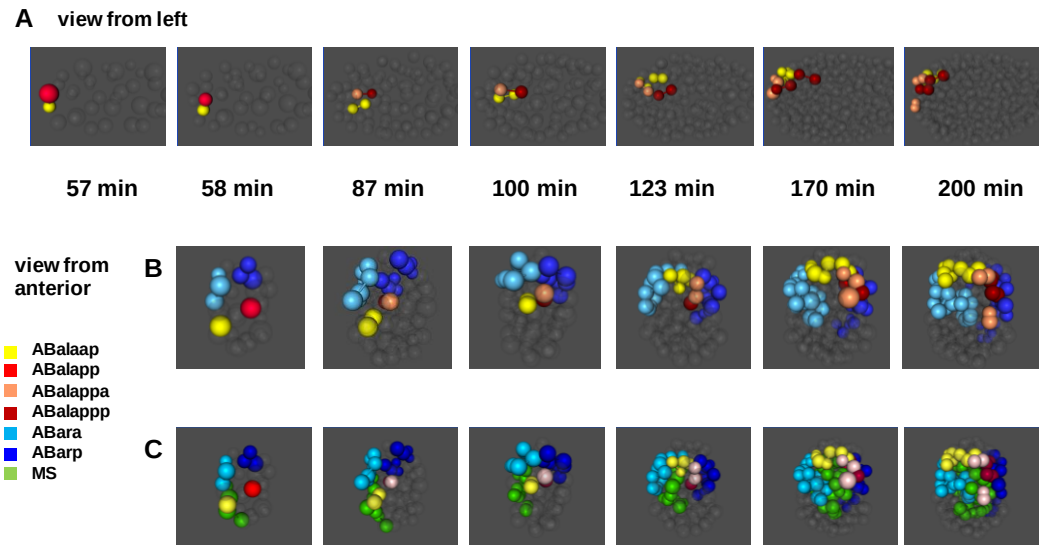

Figure 16: **ABalaap and ABalapp transgress through the embryo.** Transgressing (tunneling) nuclei and surrounding cells are represented as balls in different colors as indicated. Other nuclei of the embryo are shown in gray in the background. Time is displayed in minutes after the ABa division. **(A)** ABaraap and ABarapp ingress, move to the right and divide at the same time in the interior of the embryo (87 min). Two out of four ABalapp granddaughters and five out of eight ABalapp granddaughters egress at the right dorsal surface. **(B)** ABalaap and ABalapp tunnel amongst ABara and ABarp to egress (123-200 min). **(C)** MS descendants move amongst ABara and ABarp and seem to push ABalaap to the surface (123-200 min).

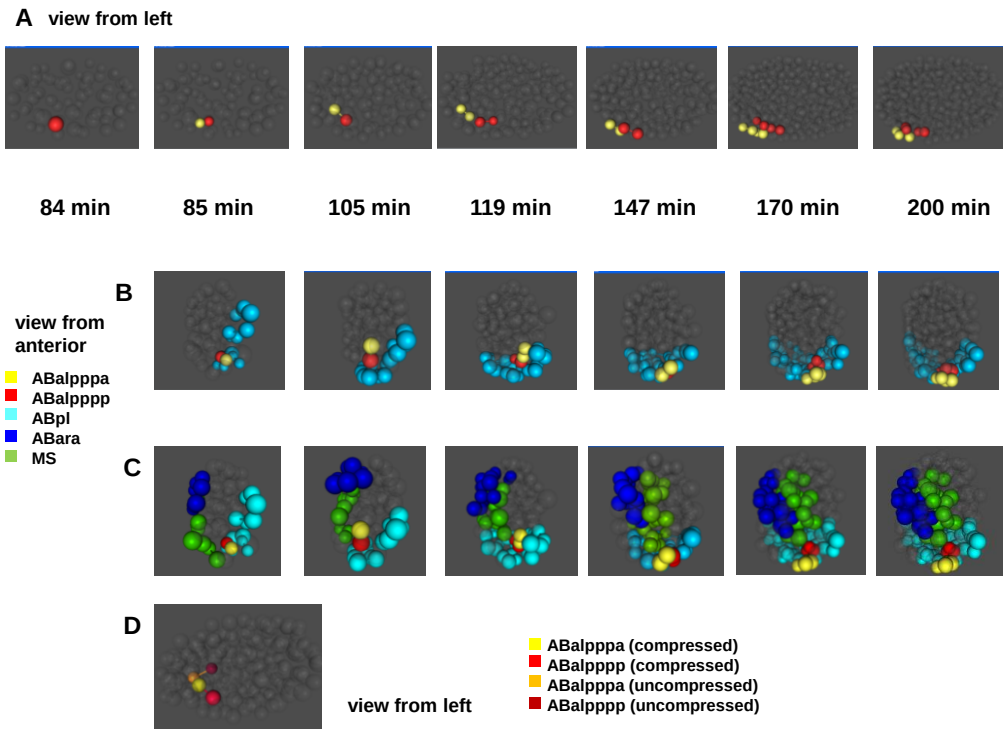

Figure 17: **ABalpppa and ABalpppp tunnel through the embryo.** Transgressing (tunneling) nuclei and surrounding cells are represented as balls in different colors as indicated. Other nuclei of the embryo are shown in gray in the background. Time is displayed in minutes after the ABa division. **(A)** ABalppp starts the ingression movement and divides interiorly (85 min). The daughters continue ingressing (105 min). After their division (119 min) the ABalpppa and ABalpppp immediately egress close to the site of ingression (147 min). Two of the ABalpppp daughters ingress again (170 min) so that at the granddaughter stage all four descendants are aligned inside of ABalpppa granddaughters (200 min). Later on, they will end up internal as well due to ventral enclosure by dorsal hypodermal cells. **(B)** ABalpppa and ABalpppp egress amongst ABpl descendants (147-200 min). The ingression of ABalpppa might drive the initial rotational movement of ABpl towards the anterior-ventral-left. **(C)** Ingression of MS descendants might push ABalppp descendants to the surface (147-200 min). **(D)** In uncompressed embryos, it is ABalpppp leading the ingression, not ABalpppa. Embryos are shown at 103 minutes after the four-cell division.

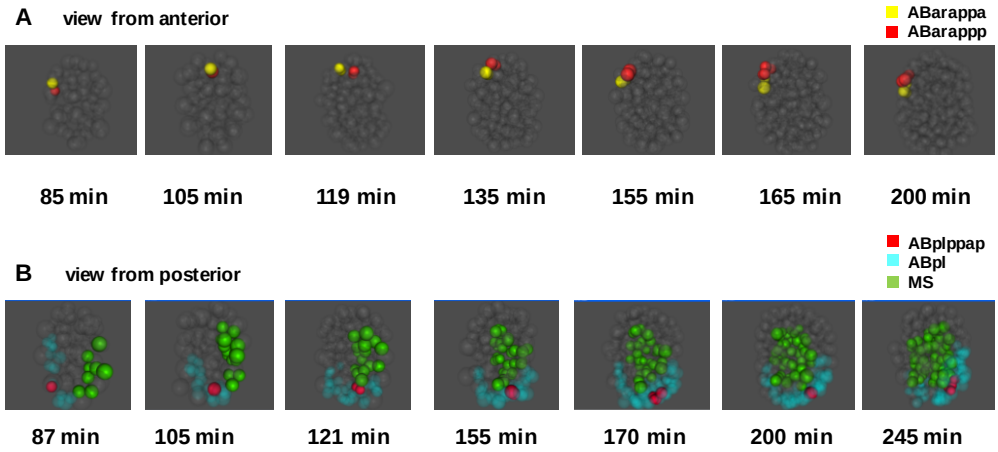

Figure 18: Cells of the anterior and posterior AB lineage exhibit egression behavior.
Transgressing (tunneling) nuclei and surrounding cells are represented as balls in different colors as indicated. Other nuclei of the embryo are shown in gray in the background. Time is displayed in minutes after the ABa division.
(A) ABarappa and ABarappp ingress as a pair and tunnel through the embryo. After division in the interior (119 min), cells immediately egress. The ingression and egression movement goes along with the overall embryonic rotation. Note that ABarappa internalization has not been reported before.
(B) ABplppap ingresses from the lateral left surface as ABpl cells move ventral during embryonic rotation (87-121 min). Granddaughters egress on the right surface (155-200 min), then internalize again (245 min).

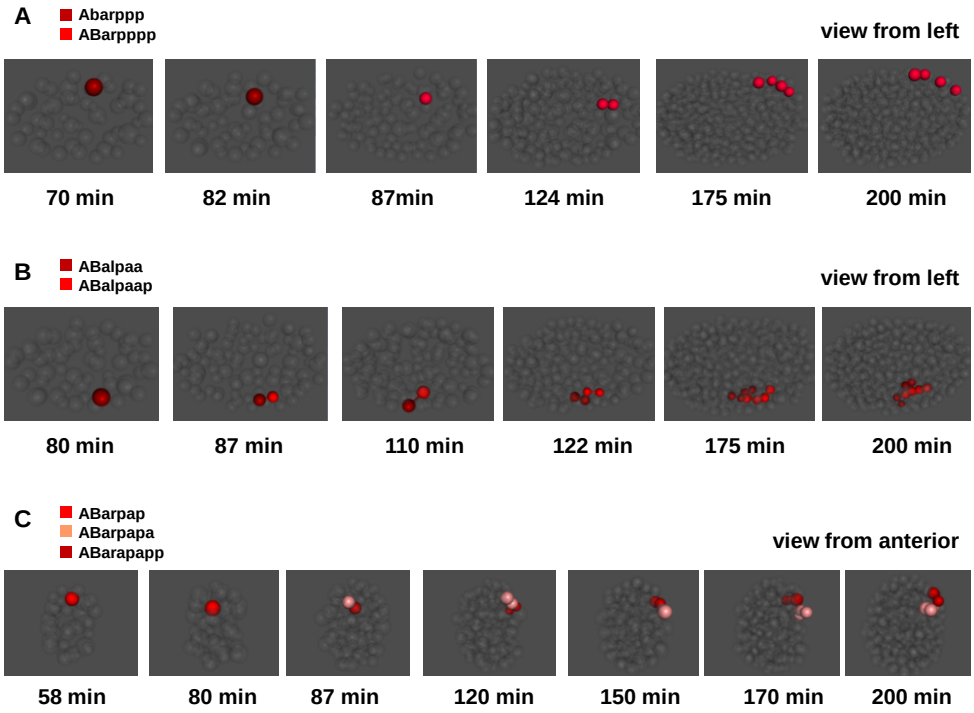

Figure 19: Newly identified ingressing and/or transgressing (tunneling) cells in the ABa lineage.

Nuclei of different cells are highlighted in different colors as indicated. Other nuclei of the embryo are represented in gray in the background. Time is displayed in minutes after the ABa division.

(A) ABarppp has not been reported to internalize before. After division in the interior (87 min), the daughters move further ventral (124 min). Granddaughters egress on the lateral left surface and move to further dorsal positions (200 min).

(B) The internal localization of ABalpaap has not been reported before. ABalpaap is internalized by displacement due to the division angle. Shortly afterwards, ABalpaap moves towards the anterior side and egresses again.

(C) The ingression of ABarpap has not been reported before. Right after division of ABarpap (87 min), its daughters egress again to the right dorsal surface.

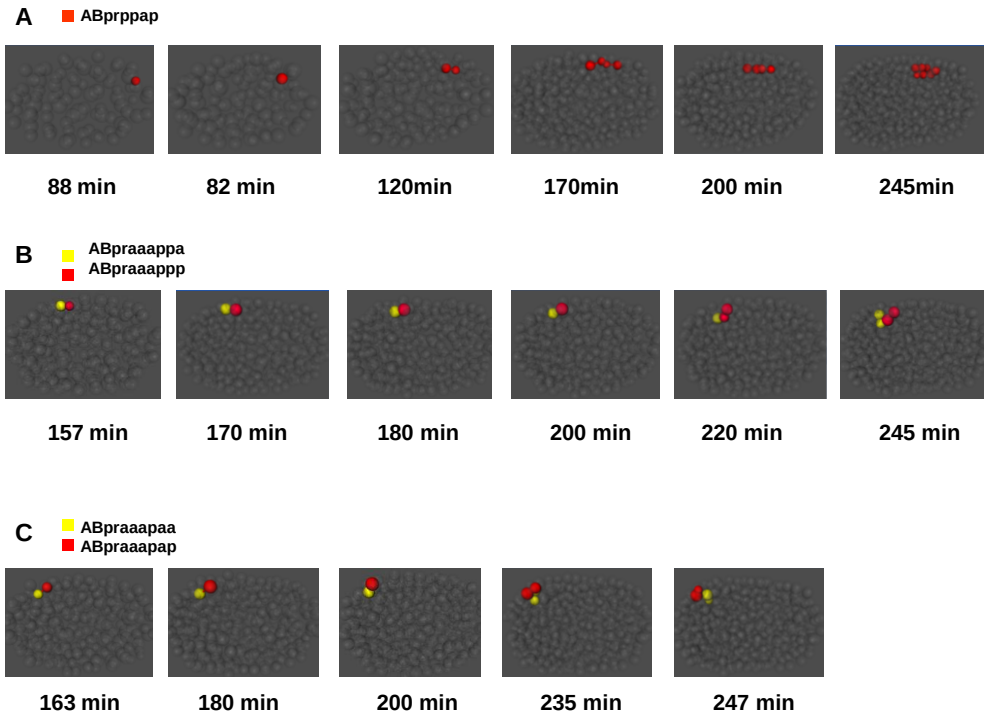

Figure 20: **Newly identified ingressing and/or transgressing (tunneling) cells in the ABpr lineage.**
Nuclei are represented as balls and colored as indicated. Other nuclei in the embryo are represented in gray in the background. Time is displayed in minutes after the ABa division. Embryos are aligned with anterior to the left, ventral to the bottom.
(A) ABprppap has not been reported to internalize before. It ingresses from the posterior and moves in anterior direction (87-170 min). Descendants do not egress but stay in the interior of the embryo (200+245 min).
(B) The internalization of ABpraaapp descendants has not been reported before. Cells ingress from the anterior-dorsal surface.
(C) The ingression of ABpraaapa descendants has not been reported before. Right after their birth, cells move from the dorsal-anterior inwards. ABpraaapap daughters later egress again.

2.3. Regulative cell movements in the *C. elegans* embryo confer robustness to physical compression

2.3.1. Morphological comparison of compressed and uncompressed embryos

As previously described, the pressure applied from a cover slip to an agarose pad or slurry bead mounted embryo causes alterations of the overall egg morphology. We observed that uncompressed embryos, in our case mounted with 45µm polystyrene beads (see Methods for details), are in average 34µm thick in the z-axis while compressed embryos mounted with 20µm beads are typically 26µm thick. Embryos mounted on agar pads were reported to be even more compressed, 18.4µm [109].

In compressed embryos, at the four-cell stage, the blastomeres are essentially lined up in a plane perpendicular to the z-axis. However, in uncompressed embryos there is no rotational preference. The four cells can be found in any orientation with respect to the y-axis. This random distribution reflects that the circular circumference of uncompressed embryos is essentially round.

2.3.2. Comparison of cell movements between compressed and uncompressed embryos

Early cell positioning is variable in uncompressed embryos and sets the blueprint for later positioning of cell groups

Additionally to the increased variability in the early AB division angles, initial cell positions and movements can differ substantially in uncompressed embryos. When comparing across uncompressed embryos (n=10), we found the positioning of early founder cells quite variable compared to compressed embryos (Figure 21). This continues until the beginning of gastrulation, at the 26-cell stage with relative positions of cell groups being rather variable, whereas cells in compressed embryos have stereotypical configurations (Figure 21, 30 minutes after four-cell stage).

In uncompressed embryos, at the eight-cell stage, both ABpl and ABpr are capable of moving towards the ventral side and there is variation in whether ABpl or ABpr move more (ABpr is located further ventral in two out of five embryos). In compressed embryos however, ABpl is always moving more ventrally (n=7) than ABpr (Figure 22). This is consistent with previously published data of compressed embryos [45] describing ABpl moving more ventrally than ABpr. Thus, compression of the embryo is constraining the variability of cell movements.

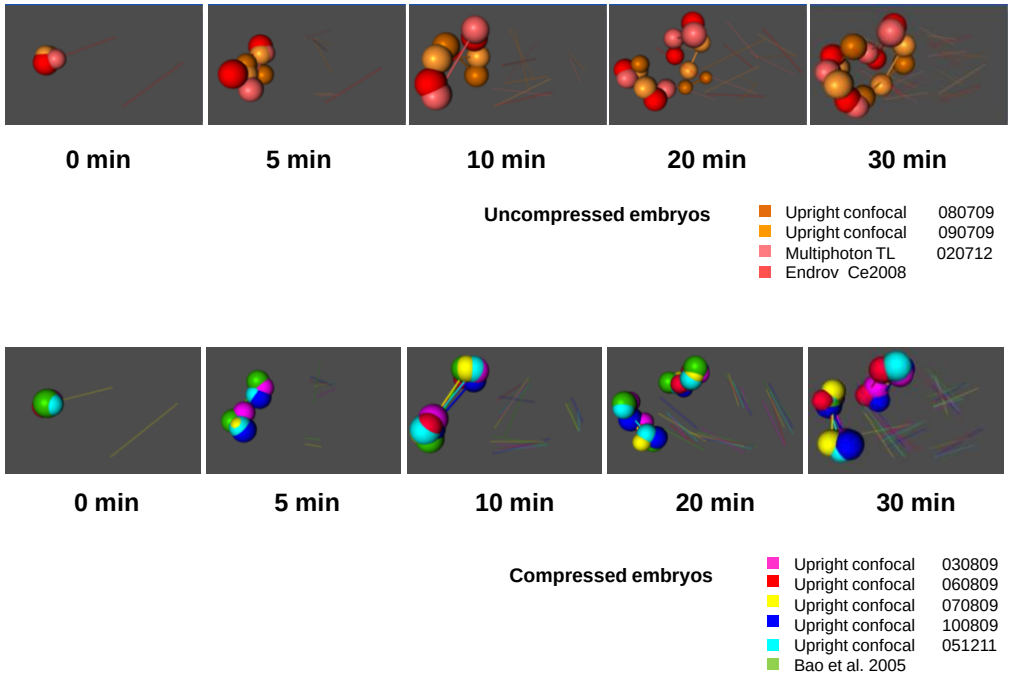

Figure 21: Early cell positioning is variable in uncompressed embryos, whereas in compressed embryos cells acquire stereotypical positions before the beginning of gastrulation.
In the upper panel, ABa (taken as example to highlight the variability) cell descendants of four different uncompressed embryos are represented as balls. Balls at the bottom panel represent ABa cells of six compressed embryos. Cells of each embryo dataset are depicted in a different color. Lines connect sister cells. Sticks in the background represent sister cell pairs of other lineages (ends of sticks correspond to one cell). Time is displayed in minutes after the ABa division.

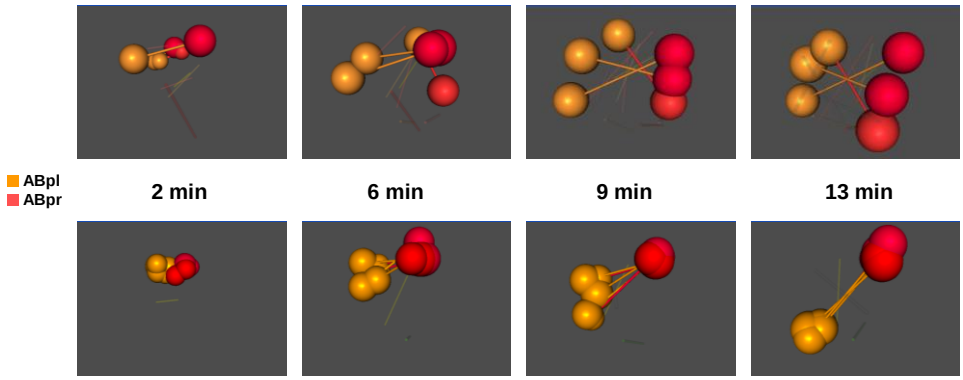

Figure 22: **In uncompressed embryos, ABpl and ABpr are both able to move towards the ventral side whereas this movement is limited to ABpl in compressed embryos.**
Embryos were aligned at the four-cell stage and are shown from a posterior view with dorsal to the top. In the upper panel, ABpl (red) and ABpr (orange) cell descendants of three different uncompressed embryos are shown as balls. Balls at the bottom panel represent ABpl/r cells of five compressed embryos (same color coding). Lines connect sister cells. Sticks in the background represent sister cell pairs of other lineages (ends of sticks correspond to one cell). Time is displayed in minutes after the ABa division.

At the eight-cell stage, this ABpl (or ABpr) movement is followed by a whole rotation of the embryo involving most of the other cells. In case of ABpl moving more to the ventral side than ABpr, the embryo rotates counterclockwise (looking from the posterior). When ABpr moves more towards the ventral side, the rotation is clockwise (n=5) (Figure 23). However, the outcome of this global rotation is an embryo with cells positioned stereotypically relative to each other (n=5). Afterwards, in uncompressed embryos, only minor adjustments occur in the body plan axes. These adjustments however, are not comparable to the substantial corrective cell movements in the compressed embryos.

Thus, in uncompressed embryos, early cell positioning sets the blueprint for later arrangements of cell groups. Due to the variability in division angles and positions of the early founder cells in uncompressed embryos, the final axes often differ substantially from those defined at the four-cell stage and between embryos (Figure 24).

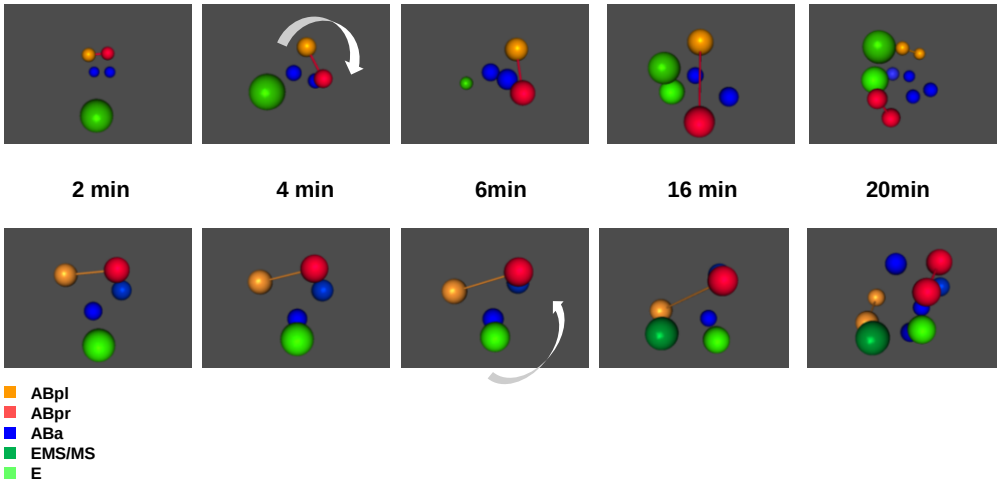

Figure 23: **At the eight-cell stage, in the case of ABpl moving more to the ventral side, the embryo rotates counterclockwise.** In contrast, if ABpr moves more towards ventral, the rotation is clockwise. Embryos were aligned at the four-cell stage and are shown from a posterior view with dorsal to the top. ABpl nuclei are shown in orange, ABpr in red, ABa cell descendants in blue and EMS descendants in green. Lines connect sister cells. Time is displayed in minutes after the ABa division. The upper panel shows an uncompressed embryo rotating clockwise. The bottom panel depicts an uncompressed embryo moving counterclockwise (rotation indicated by white arrows).

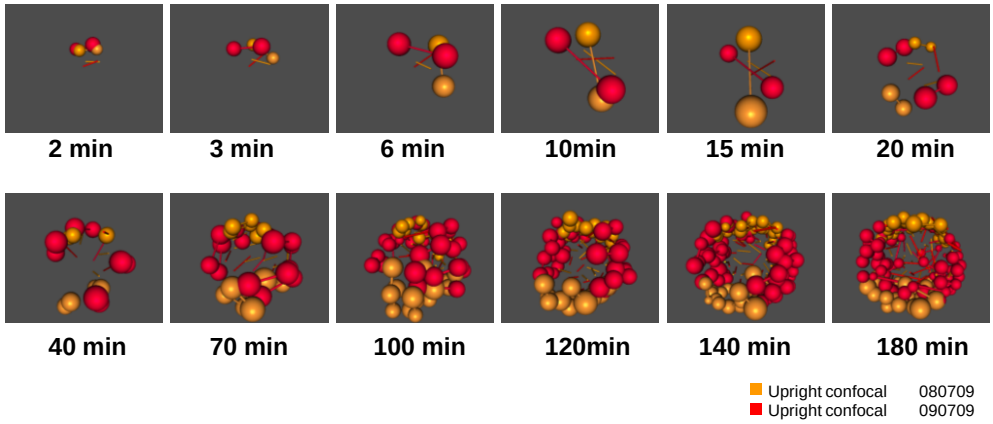

Figure 24: **Early cell positioning is variable in uncompressed embryos and sets the blueprint for later positioning of cell groups.** Two uncompressed embryos (nuclei of each embryo are represented in a different color, were aligned at the four-cell stage and are shown from a posterior view with dorsal to the top. ABpl and ABpr cell descendants are represented as balls. Lines connect sister cells. Sticks in the background represent sister cell pairs of ABa cell descendants (ends of sticks correspond to one cell). Cells of other lineages are not shown. Time is displayed in minutes after the ABa division. Two uncompressed embryos that are substantially different in cell positioning are shown to highlight variability. The ABp lineage was selected as example as it illustrates well the early establishment of the body axes at the eight-cell stage and little compensatory movements later, in contrast to compressed embryos (see Figure 25 and Figure 26).

2.3.3. Rotational movements during gastrulation compensate for distorted division angles and cell positioning in compressed embryos

As part of the pre-morphogenic movements, compressed embryos have been previously reported to rotate around their anterior-posterior axis, thus changing their position relative to the egg shell [3, 45, 107, 109]. However, in uncompressed embryos, we observed remarkably little rotational movements after the ingression of the E lineage, consistent with previous reports [109]. To understand this rotation behavior, we characterized the cell movements in more detail.

After the fourth division round, approximately 80 minutes after the four-cell stage, spatial constrains lead to substantial cellular crowding in compressed embryos. This is especially true in the anterior part of the embryo and may contribute to the large-scale embryonic rotation that occurs during the following 40 minutes (80-120 minutes after the four-cell stage). This rotational movement re-positions ABarp descendants stereotypically from the right to dorsal locations by ~90 degrees. Concomitantly, ABpl cells are moved by ~90 degrees from the dorsal to the left side of the embryo. Thus, at approximately the 200-cell stage, in compressed embryos new LR and DV axes are established, which are rotated ~ 90 degrees from the original axes defined at the four-cell stage (Figure 25 and Figure 26).

In addition to cellular crowding, spatial constraints lead to distorted division angles and cell positioning in compressed embryos, as

already apparent after the four-cell stage (Figure 25). At the eight-cell stage, in compressed embryos, ABal/r and ABpl/r cell groups are not positioned in parallel to each other as they are in uncompressed embryos. ABar and ABal instead align along the DV axis, ~ 90 degrees to the AP and LR axis (axes as defined at the four-cell stage). This is most likely due to the compression applied on the embryo which limits the ABa division angle in the LR plane (Figure 25).

Additionally, the division angle of the P2 cell is distorted in compressed embryos. Consequently, the C lineage (derived from the anterior daughters of P2) is shifted from dorsal towards the right (axes defined at the four-cell stage), compared to their positioning in uncompressed embryos (Figure 27). At the same stage, MS cells are found mis-localized, at positions further left and dorsal. In uncompressed embryos MS cells are positioned at the ventral right corner before their ingression (Figure 27).

In order to correct for these early displacements, a series of corrective cell movements takes place, starting with a change in the division angle of the ingressed intestinal precursor cells, Ea and Ep. In compressed embryos, these cells divide along the initial DV axis, aligning the E descendants in a plane parallel to this axis instead of orthogonal to it (Figure 27). Possibly, the primary reason for this change in division angle is the lack of space in the original LR axis: Ea and Ep are large cells, thus may be physically constrained from aligning in the original LR axis. In addition, at this time, the MS descendants are mis-localized by division (not by active movements), at positions further left and dorsal than in

uncompressed embryos (Figure 27). Therefore, they are already placed in the correct relative position to the four differentially aligned E cells, and so may potentially help define this new Eal-r and Epl-r plane.

During the subsequent movements and divisions, the other cell groups appear to align according to the newly orientated E- and MS-defined plane. For example, C descendants move to match the new orientation of the internal intestinal precursor cells prior to and during their ingression (Figure 27). The rotation of ABpl, ABarp and some ABal descendants then goes along with the ingression of the anterior ABal cells, MS cells, and C cells. Thus, ABpl/pr movements might be driven by the ingression of MS and C cells. This would imply that the embryonic ‘outside’ aligns to the ‘inside’, so establishing the new global LR and DV axes in the final pre-morphogenic stage.

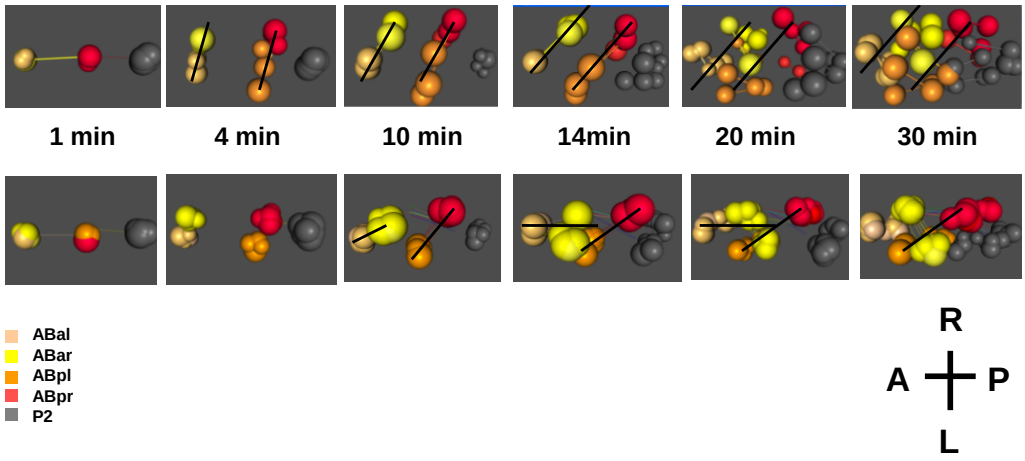

Figure 25: **In uncompressed embryos, ABpl-ABpr cells are parallel to ABal-ABar cells, thus defining a LR axis that is localized between the group of ABpl and ABpr cells as well as ABal-ABar cells. In compressed embryos, ABpl-ABpr cells are not positioned parallel to ABal-ABar cells, resulting in a conflict in LR axis definition.**
Two uncompressed (upper panel) and six compressed (bottom panel) embryos were aligned at the four-cell stage and are shown from a dorsal view with anterior to the left. ABpl (orange), ABpr (red), ABal (light pink), ABar (yellow) and P2 cells are shown as balls. Cells of other lineages are not shown. Time is displayed in minutes after the ABa division. Short black lines indicate the shifted planes set by ABal/r and ABpl/r group of cells.

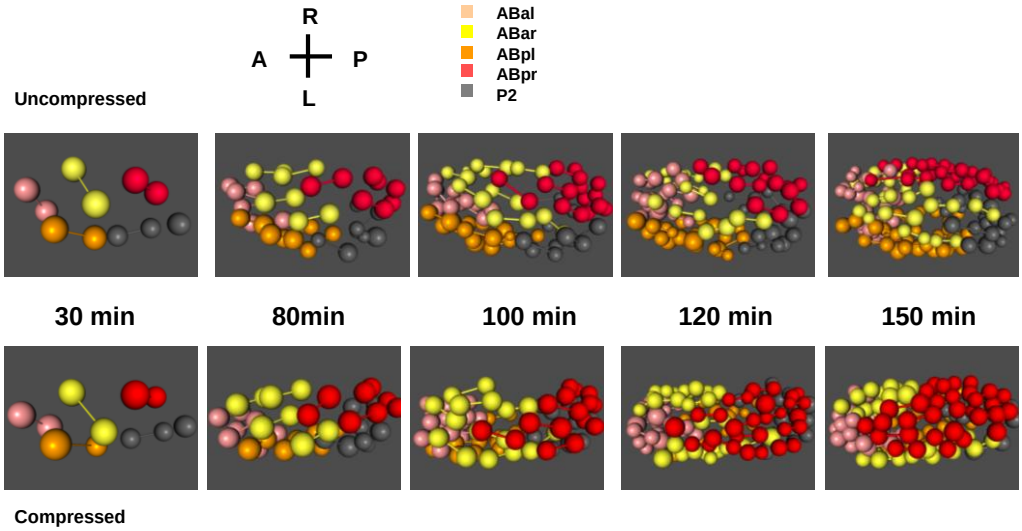

Figure 26: **In compressed embryos, ABarp descendants rotate from right to dorsal locations by ~90 degree. Concomitantly, ABpl cells move by ~90 degree from the dorsal to the left side of the embryo.**
Uncompressed (upper panel) and compressed (bottom panel) embryos were aligned after the early variable rotation (30 minutes after the four-cell stage). Embryos are shown from a dorsal view with anterior to the left and were aligned at the four-cell stage. ABpl (orange), ABpr (red), ABal (light pink), ABar (yellow) and P2 cells are shown as balls. Cells of other lineages are not shown. Time is displayed in minutes after the ABa division.

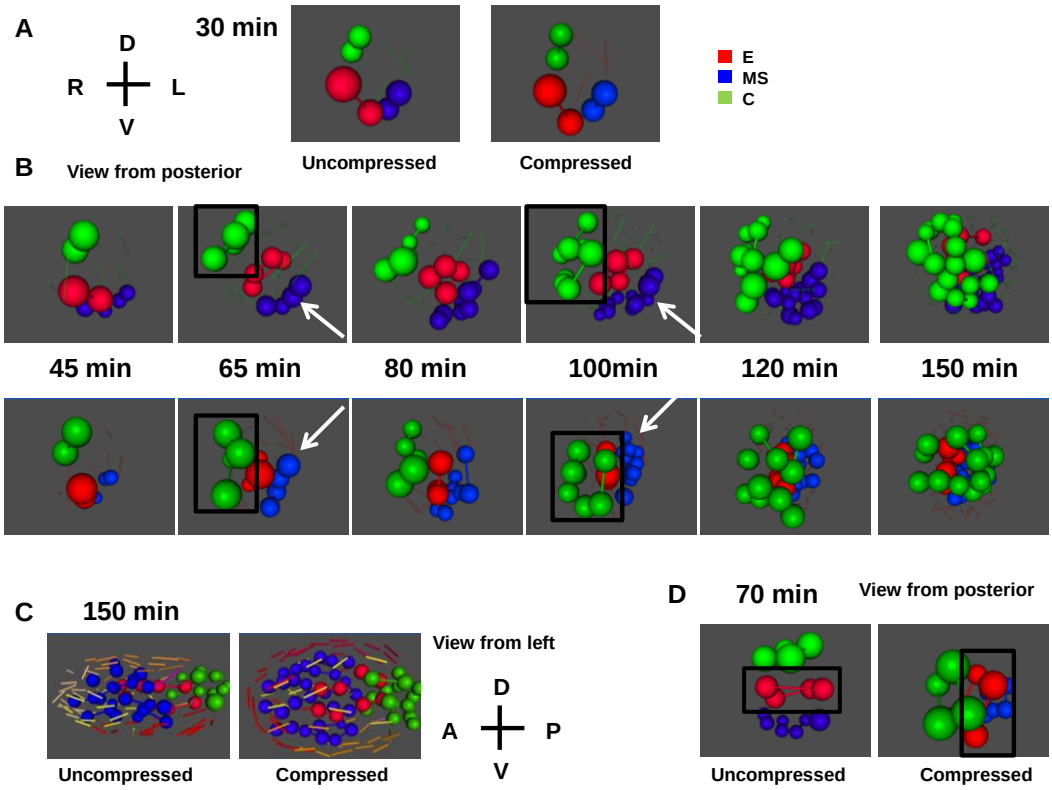

Figure 27: **In compressed embryos, C and MS cells are displaced and Ea and Ep divide along the original DV axis.**
Nuclei are represented by balls and colored as indicated. Time is displayed in minutes after the ABa division.
Compressed and uncompressed embryos were aligned after the early (variable) rotation, 30 minutes after the four-cell stage for further illustration in figure B. Embryos are shown from a posterior perspective with dorsal to the top

(A) In compressed embryos C cells (green) are positioned further right and ventral (black squares), and MS cells (red) are further left and dorsal (white arrows) compared to uncompressed embryos. Embryos are aligned as shown in A.

(B) In compressed embryos, the E cell plane (red balls) is aligned along the original DV axis and C and MS descendants re-align according to the “new” plane. View from the left side, with embryos being aligned at the four-cell stage with anterior to the left (axes defined at the four-cell stage). Nuclei of other lineages are shown as sticks in the background.

(C) In compressed embryos, Ea and Ep cells divide along the original DV axis, while in uncompressed embryos they divide

orthogonal to it. External cells then re-align to the axis of the internal E cells, as shown in Figure B and C. Posterior view, with embryos being aligned at the four-cell stage with dorsal to the top.

In summary, in a compressed embryo physical constraints cause cell groups to be mis-positioned with respect to each other. In particular, due to physical constraint and/or the altered positions of cell neighbors, in a compressed embryo the intestine precursors divide along the original DV axis rather than along the original LR axis, so establishing a new LR plane. Subsequently there is a global rotation of many external cells that realigns them to these new LR and DV axes.

The mechanisms underlying these global rotation movements remain to be identified. However, one possible cause is the increased cell crowding in the anterior of the embryo. Under conditions of cell crowding, the directed ingression, transgression and egression movements of cells in this region (see previous chapter) may trigger a global rotation of cells. Moreover, the location of the E and MS cells may also be instructive, specifying the ultimate axes of the embryo. Cell ablation and genetic experiments will be required to test these hypotheses.

The most important conclusion from this analysis is that the early embryo is a much more regulative developmental system than previously thought. We propose that the compensatory cell movements observed are part of a robustness mechanism to ensure that cell groups are correctly aligned even when division

angles and cell positions are distorted due to external compression.

2.4. Systematic and quantitative analysis of the function of chromatin remodeling complexes in *C. elegans*

Over 70 chromatin factors have been described either functionally or genetically in *C. elegans [300].* Many of them are embryonic lethal, however, their exact role in embryogenesis is not known. To gain further insights into their function during embryonic development, we chose this subset of genes for closer investigation.

In a genome wide screen performed by Kamath *et al*., approximately 65 embryonic lethal genes were classified as chromatin regulators (excluding histones) [168]. Among those we found 20 genes to have an embryonic lethal RNAi phenotype with high penetrance and decided to study those in more detail.

Table 4 and Table 5 list the chromatin regulators and associated factors as well as a few additional genes of unknown function analyzed in this study [300]. Their annotated or described function is shown. Apart from genes encoding chromatin regulators, genes of unknown function seemed to be an interesting target subset to analyze with our semi-automatic tracking method as quick detection of defects in nuclear positions, movements and division angles might provide first hints to biological function. In addition, we imaged genes involved in mitotic cell division to detect changes in fluorescence intensities that are caused by condensation and segregation defects as well as for phenotypic comparisons. Genes analyzed in this context are listed in Table 6.

Gene	Subunit of complex	Brief description	Cellular and developmental functions
lin-53	NuRD/CHD, ISWI/NURF, CAF1, HDAC, PRC2/EED-EZH2, DRM	Rb associated protein 48, NuRF55/CAF1/MSI1 ortholog	SynMuv B, embryonic development, RNAi
rba-1	NuRD/CHD, ISWI/NURF, CAF1, HDAC, PRC2/EED-EZH2	Rb associated protein 48, NuRF55/CAF1/MSI1 ortholog	SynMuv B, development, RNAi
hda-1	NuRD/CHD, HDAC	Histone deacetylase RPD3	SynMuvB, gonad and embyonic development
egl-27	NuRD/CHD	MTA1, transcr. corepressor Atrophin-1/DRPLA	**With lin-40:** posterior ventral hypodermal fate, emb. patterning, expression of hlh-8
lin-40 (*egr-1*)	NuRD/CHD, HDAC	MTA1	Vulval fate specification, morphogenesis
let-526	SWI/SNF	Iss-4	SynMuv, embryonic development
swsn-5	SWI/SNF	SNF5/Ini1	Asymmetric cell division, larval growth
swsn-7	SWI/SNF	Predicted transcript.regulator	Embryonic development
set-16	MLL (H3K4trimethylase)	Polycromb domain	Ras-mediated vulval development
cir-1		CBF1-interacting corepressor	Notch dep. transcriptional regulation
F55A3.3	FACT	Global transcript. regulator, division control protein	Global transcription, cell division
hmg-3	FACT, POB3	Nucleosome binding factor SPN	Embryonic development

Table 4: Genes encoding subunits of predicted *C. elegans* chromatin regulators and their known functions [300], (www.wormbase.org).

Gene	Subunit of complex	Brief description	Cellular and developmental functions
mdt-10	MeDiaTor	TF, SRB subcomplex of RNA pol II	Embryonic development, fertility, transcriptional regulation of developmental genes
mdt-15	MeDiaTor	two isoforms of human MED15 ortholog	Fat metabolism, lifespan
mdt-17	MeDiaTor		Embryonic development
let-49	MeDiaTor		Maternal: germline+embryonic development Zygotic: postemb. development
gei-4	GEX-2/GEX-3/GEI-4	Homolog to mammalian intermediate filament interacting protein	Embryonic viability, fertility, and vulval morphogenesis, regulation of intermediate filaments during rearrangement of the cytoskeleton
ubc-1	-	E2 ubiquitin-conjugating enzyme	Embryogenesis, larval + vulval development, posterior morphogenesis, DNA damage response
smo-1	-	SUMO ortholog	Vulva development
mel-28	-	ATHCTF, associates with NPC and kinetochores	Nuclear envelope assembly, mitotic spindle assembly, chromatin segregation
cdl-1	-	HBP/SLBP (3'UTR of histone mRNA)	Histone gene expression, cell division (late larval dev.), vulval morphogenesis, normally rapid apoptosis, fertility
let-858	-	Nucampholin, eIF4gamma	Tissue differentiation, protein synthesis/RNAbinding

Table 5: Chromatin associated factors and genes of unknown function studied in this project [300], (www.wormbase.org).

Gene	Subunit of complex / other description	Cellular and developmental functions
air-2	Chromosome passenger protein, Aurora-A family of serine/threonine kinases	Embryonic survival, germline proliferation and development, locomotion, and vulval development; recruitment of centrosomal gamma-tubulin during maturation, centrosome separation and spindle assembly
icp-1	Chromosomal passenger protein, INCENP homolog	Chromosome segregation during the first mitotic division
scc-3	Cohesin	Sister chromatid cohesion, mitotic chromosome segregation, embryonic development, vulval morphogenisis
him-1	Cohesin, SMC family	Embryonic viability, germline mitosis, chromosome pairing + segregation
smc-4	Mitotic condensin, SMC	Chromosome condensation and segregation
hcp-4	CeCENP-C, kinetochore	Mitotic spindle assembly, segregation

Table 6: Genes encoding essential cell division protein examined in this project [16].

2.4.1. Chromatin factors exhibit diverse and partly overlapping phenotypes

Analysis of time-lapse Nomarski and fluorescence microscopy of histone-GFP expressing embryos allowed us to subdivide the chromatin factors analyzed according to their phenotype: one group contains factors affecting chromosome behavior during mitotic cell divisions. Factors attributed to a second group had other cell cycle defects or affected particular cell groups. Figure 28 shows a summary of representative gross phenotypes observed for a selection of chromatin factors. The phenotype of *gei-4* is described further in Chapter 2.3.4.

let-49 was not analyzed in detail as GFP signal intensities of most time-lapse recordings were found too dim to be submitted to semi-automatic cell tracking. Also, *ubc-1* [301, 302] and *smo-1* [303] were not examined further in this study. However, their gross phenotypes (not listed in Figure 28) are very similar to *rba-1*.

Interestingly, factors predicted to encode subunits of the same complex do not necessarily show the same cellular defects when inhibited. For example, RNAi-depletion of only three (*lin*-53, *rba*-1, *hda*-1) of the four genes (*egl*-27 does not) encoding subunits of predicted NURD complex members exhibit cell division defects. Embryos with *lin-53* knock down show early onset of condensation and segregation defects with characteristic chromosome bridges. These bridges are similarly observed after depletion of cell division proteins such as condensins (SMC-4), kinetochore components (HCP-1) or the Aurora B kinase AIR-1 (Figure 31 and Figure 32, Chapter 2.4.2). The onset of segregation defects caused by *rba-1* and *hda-1* knock down, other members of the NURD complex, manifests much later, around the 60-cell stage. This delay might either be due to a less efficient RNAi knock down or might indicate that the function of those genes is compensated for early on in embryogenesis, either by maternally contributed factors or other pathways.

In contrast, double knockdowns - single knockdown embryos are viable and do not exhibit obvious phenotypes - of other components of the NURD complex, *egl-27* together with *lin-40*, do not show any affect on chromosome segregation. Yet, cells are mis-positioned in RNAi perturbted embryos, indicating a role in

global embryonic patterning as previously described and discussed in Chapter 2.3.4.2. [292, 304].

Similarly, knock-down of the MeDiaTor complex members *mdt-10* and *mdt-15*, does not give segregation phenotypes. Embryos depleted of *mdt-17,* however, exhibit late chromosome segregation defects. Yet, it is possible that these differences are due to a less efficient RNAi knockdown.

Similarly, the two members of the FACT complex, F55A3.3 and *hmg-3*, both seem to play a role in cell division, however with a distinct onset of phenotype. F55A3.3 depleted embryos show early segregation defects from the first divisions on, while *hmg-3* (RNAi) embryos exhibit defects after the 150-cell stage. As the observed embryonic lethality of *hmg-3* RNAi is only about 30%, the later onset might be due to less efficient RNAi knockdown (Figure 28).

As expected, the mRNA binding protein CDL-1 which regulates histone expression, and the nuclear assembly factor MEL-28, both show early chromatin compaction and segregation defects (Figure 28) [170, 305-309].

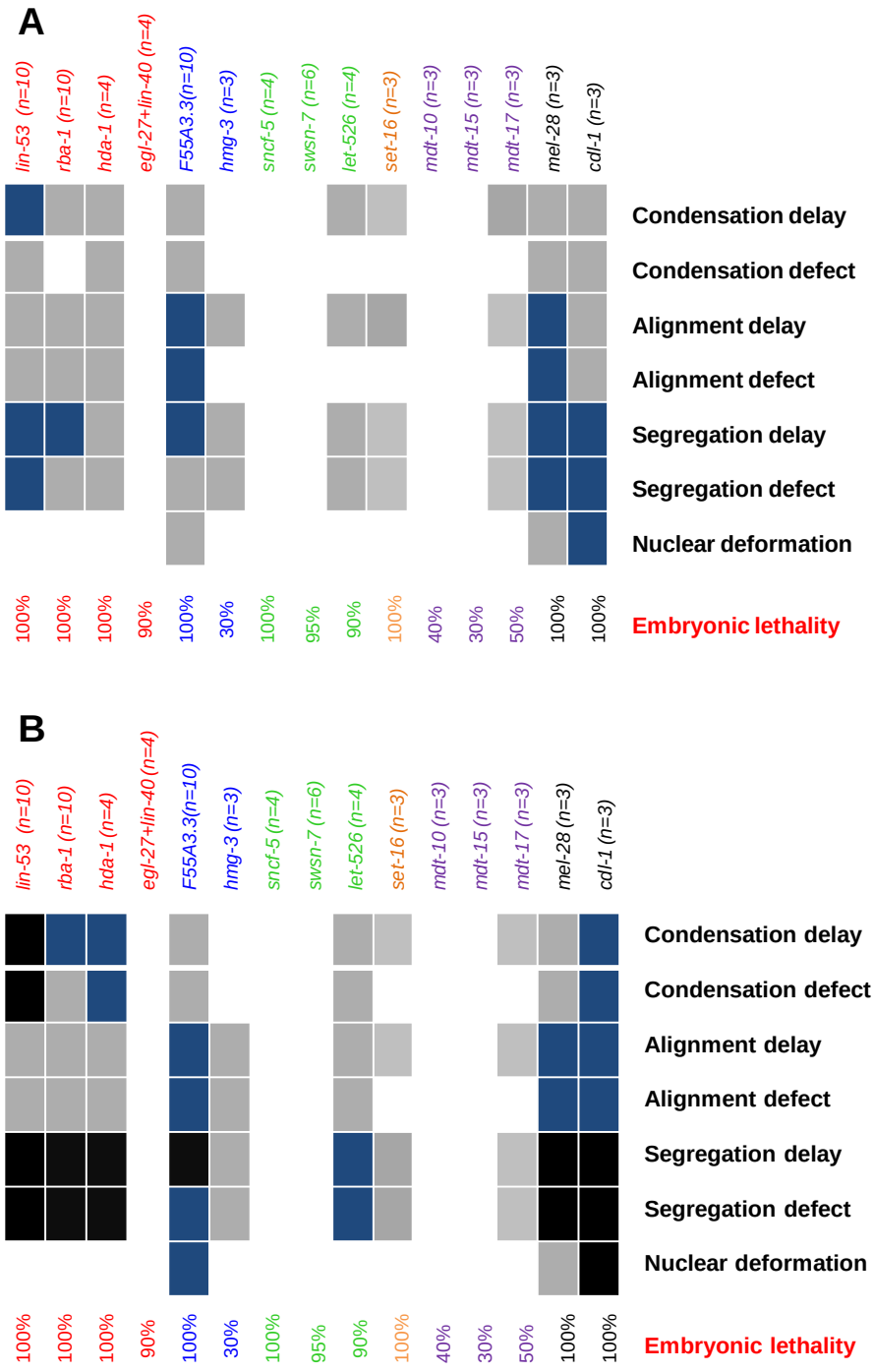
A
lin-53 (n=10)
rba-1 (n=10)
hda-1 (n=4)
egl-27+lin-40 (n=4)
F55A3.3(n=10)
hmg-3 (n=3)
sncf-5 (n=4)
swsn-7 (n=6)
let-526 (n=4)
set-16 (n=3)
mdt-10 (n=3)
mdt-15 (n=3)
mdt-17 (n=3)
mel-28 (n=3)
cdl-1 (n=3)
Condensation delay
Condensation defect
Alignment delay
Alignment defect
Segregation delay
Segregation defect
Nuclear deformation
100%
100%
100%
90%
100%
30%
100%
95%
90%
100%
40%
30%
50%
100%
100%
Embryonic lethality
B
lin-53 (n=10)
rba-1 (n=10)
hda-1 (n=4)
egl-27+lin-40 (n=4)
F55A3.3(n=10)
hmg-3 (n=3)
sncf-5 (n=4)
swsn-7 (n=6)
let-526 (n=4)
set-16 (n=3)
mdt-10 (n=3)
mdt-15 (n=3)
mdt-17 (n=3)
mel-28 (n=3)
cdl-1 (n=3)
Condensation delay
Condensation defect
Alignment delay
Alignment defect
Segregation delay
Segregation defect
Nuclear deformation
100%
100%
100%
90%
100%
30%
100%
95%
90%
100%
40%
30%
50%
100%
100%
Embryonic lethality

Figure 28: Comparison of phenotypes of chromatin factors analyzed.
Red color marks members of the NURD complex, blue predicted members of the FACT complex, green members of the SWI/SNF complex, orange the MLL family member set-16, purple MeDiaTor complex members, and black other genes giving rise to cellular defects. Below, the percentage of embryonic lethality under RNAi knockdown conditions is shown. N corresponds to the number of embryos analyzed. Colors code for the severity of the defect, according to visual inspection, with black being the most severe one.
(A) First defects observed
(B) Later (most likely secondary) defects observed

Embryos depleted of all genes that lead to an early onset of defects (*lin-53, F55A3.3, cdl-1* and *mel-28*), also arrest earlier, before the 100-cell stage. Embryos depleted of all other genes tested develop further at least to 100 minutes after the four-cell stage, arresting development at 100 to 200 cells. The onset of division round delay usually corresponds to the onset of the first defects (Figure 29).

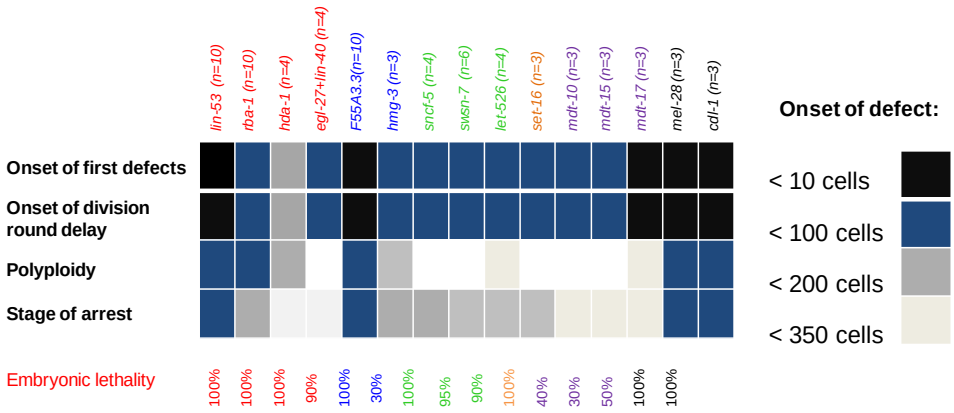

Figure 29: Onset of first defects, division-round-delay, polyploidy and stage of arrest for the chromatin factors studied.
Red color marks members of the NURD complex, blue predicted members of the FACT complex, green members of the SWI/SNF complex, purple MeDiaTor complex members, and black other genes giving rise to cellular defects. Below, percentage of embryonic lethality under knockdown conditions is shown. N corresponds to the number of embryos analyzed. Colors code for the defective cell stage.

Except for the genes not exhibiting any chromosome segregation phenotypes (*egl-27+lin-40*, and *mdt-10, mdt-15*), knockdown of all genes examined eventually leads to duplication of chromosome sets and polyploidy with enlarged nuclei (Figure 30). In some cases (e.g. for SWI/SNF factors, see Chapter 2.3.4.), prior to the segregation defects, other defects such as cell mis-positioning are observed. Thus, the late impairment of segregation might be a secondary defect. Alternatively, it might indicate the existence of multiple SWI/SNF complexes with different functions.

In contrast, in *rba-1* mutants, condensation and segregation delay and failure are the first defects observed (Figure 30). Partially condensed chromosomes fail to segregate to opposite poles approximately at the 30- to 80-cell stage, depending on the efficiency of the RNAi knockdown. The chromosomes then frequently de-condense, and cells appear to leave mitosis without cytokinesis. (Figure 30) This cytokinesis defect results in enlarged nuclei with polyploid genomes. As chromosome segregation defects alone are not sufficient to disrupt cytokinesis [196, 200] secondary defects are likely to have accumulated in *rba-1* depleted embryos at that time as well. As no DNA condensation, segregation or cytokinesis defect was observed in the early cleavages, *rba-1* may not play a role in early cleavages or may act redundantly with other genes in early divisions.

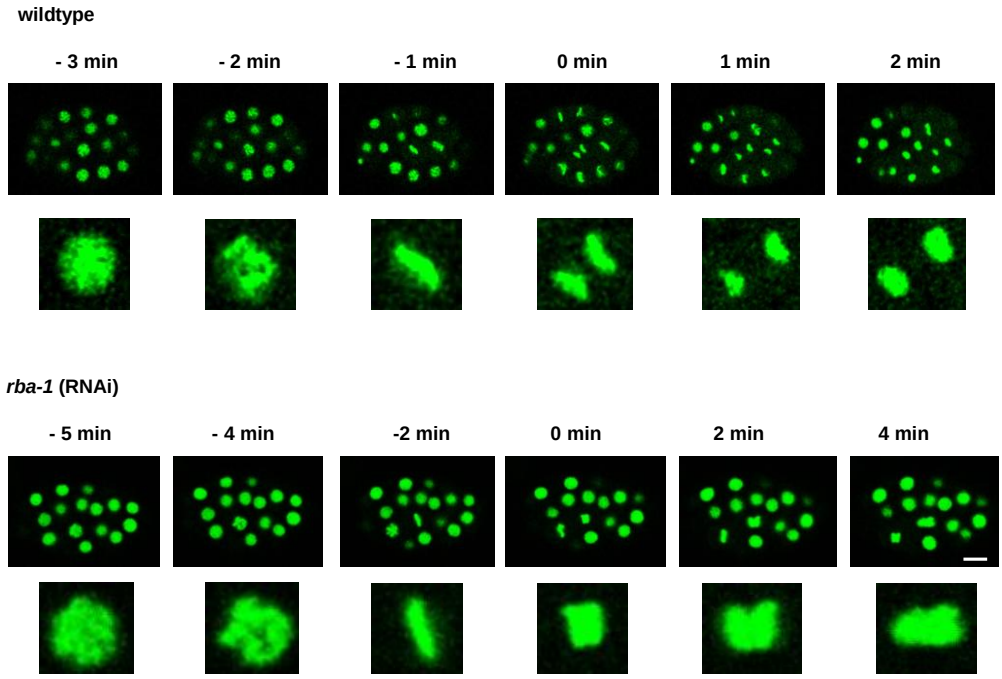

Figure 30: Onset of segregation defects in an *rba-1* (RNAi) depleted embryo 85 minutes after the four-cell division with 38 cells. Condensation and segregation is delayed compared to wild-type mitosis (see time scale, 0 min refers to the time point when the two chromatin masses first segregate at the onset of anaphase). Daughter nuclei fail to segregate, leading to a cell containing a duplicated set of chromosomes. Images are representative for other RNAi embryos exhibiting segregation defects accompanied by duplication of chromosomes, like *hda-1* and *let-526*. In white, scale bar 10µm.

2.4.2. Chromatin regulators involved in mitosis

We divided the chromatin factors listed above into those involved in cell division processes and those regulating rather broad developmental functions. The first group can be subdivided again according to early and late onset of defects. Hereby, multiple

different molecular defects most likely give rise to similar cellular defects that are difficult to distinguish. Particularly, cellular defects arising at late stages are difficult to characterize as cells are already very small and at the limit of image resolution. Also, at that stage defects might be caused indirectly (secondary defects). Therefore, we primarily analyzed genes with an early onset of defects. As *mel-28* and *cdl-1* are not chromatin regulators, we chose F55A3.3, a member of the FACT complex, and *lin-53*/NURD for detailed characterization.

2.4.2.1. F55A3.3 and *lin-53* are required for chromosome segregation

To semi-quantitatively assay the segregation defects observed, we monitored chromosome dynamics of RNAi embryos expressing either the GFP::H2B fusion protein, alone or in combination with a GFP::TBB-2 fusion protein, marking the mitotic spindle. Analysis was performed by time-lapse Nomarski and fluorescence microscopy. In contrast to *hda-1* and *rba-1* (RNAi) embryos, which show normal chromosome segregation until the ~ 30- to 60-cell stage, *F55A3.3* and *lin-53* (RNAi) embryos exhibit continuous defects beginning already at the first cell division. Anaphase chromosome bridges were first detected between the one- to four-cell stage and were observed throughout the following cell divisions until arrest occurred at approximately the 30-cell stage (Figure 31 and Figure 32). Onset of defects as well as stage of arrest varied from embryo to embryo, likely due to variable

efficiency of the RNAi knockdown. However, defects always manifested early on and became increasingly severe over time with secondary defects accumulating (n=66 for *lin-53*, n=61 for *F55A3.3* (RNAi)). In general, AB descendants were affected stronger and at earlier stages. This could also be observed in *rba-1* and *hda-1* depleted embryos (see Chapter 2.4.4).

Formation of chromosome bridges at anaphase, a hallmark of division defects, is observed similarly in both *F55A3.3* and *lin-53* (RNAi) embryos (Figure 31 and Figure 32). However, closer inspection of chromosome dynamics reveals differences between the phenotypes of the two genes. In wild-type embryos, chromosomes condensed mainly in late prophase (Figure 31, Figure 32 and Figure 33, white arrows), aligned at a narrow metaphase plate and segregated to the opposite poles in anaphase (Figure 31 and Figure 32, red arrow). In contrast, in the affected *lin-53* (RNAi) embryonic cells, chromosomes fail to condense properly (Figure 31 - Figure 34, white arrows), and anaphase bridges can be observed (Figure 31 and Figure 32, red arrow). Condensation as well as segregation is delayed in *lin-53* (RNAi) depleted embryos (Figure 31 and Figure 33) leading to progressive developmental delay. At the onset of defect at the first divisions, condensation takes at least two minutes longer than in wild-type embryos. Complete chromosome segregation, if achieved at all, takes at least five minutes more. This delay worsens over time, leading eventually to a complete stop of divisions and arrest around the 25- to 35-cell stage (depending on the RNAi efficiency).

In contrast, in *F55A.3.3* (RNAi) embryos, chromosome condensation appears to be normal (Figure 31 - Figure 33), although it takes longer (Figure 33). At anaphase, chromosomes are not segregated properly and bridges are formed (Figure 31 and Figure 32, red arrow). Consequently the onset of the new cell division cycle is delayed similar to *lin-53* (RNAi) embryos (Figure 31).

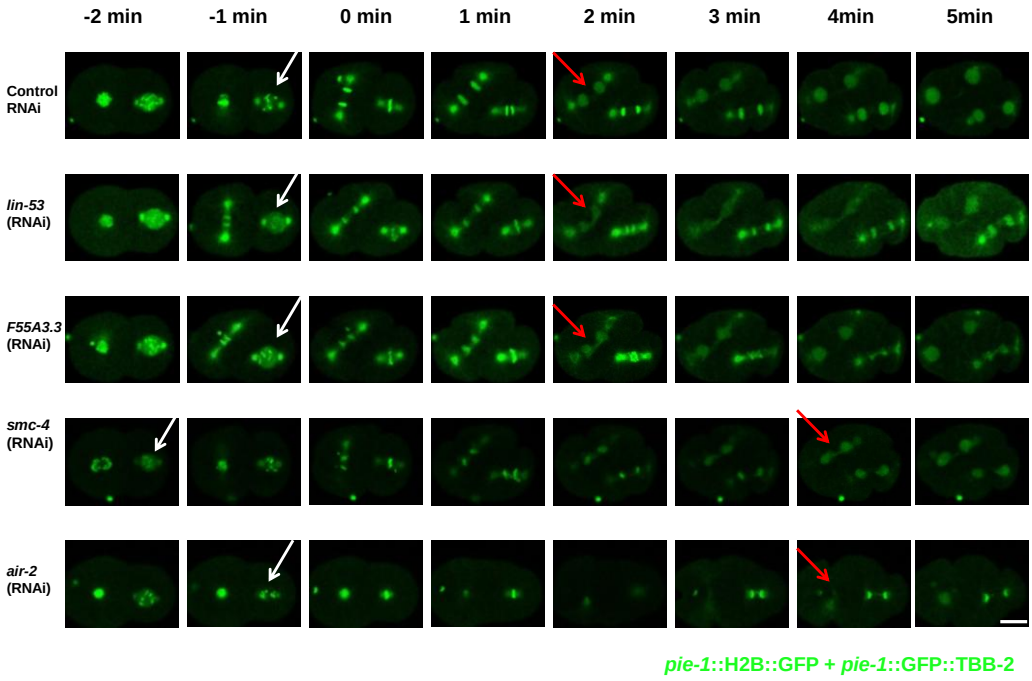

Figure 31: Condensation and segregation defects in embryos that are RNAi depleted of genes involved in cell division.
Time 0 is set to the time point when the two chromatin masses first segregate at the onset of anaphase of the AB cell. Imaged worm strains are expressing GFP::H2B and TBB-2::GFP (β-tubulin) fusion proteins, marking histones and the mitotic spindle, respectively. Depletion of all genes shown leads to lagging chromosomes during anaphase (red arrows) and delay in segregation, which is most severe in *smc-4* and *air-2* depleted

embryos. Chromosome condensation reaches wild-type levels before segregation in *F55A3.3* and *air-2* (RNAi) embryos (white arrows). Late chromosome compaction is visible in *smc-4* (RNAi) embryos, while it is not observed in *lin-53* (RNAi) embryos. White scale bar: 10µm. White arrows show differences in condensation before chromosome alignment at metaphase. Red arrows point to lagging chromosomes at anaphase.

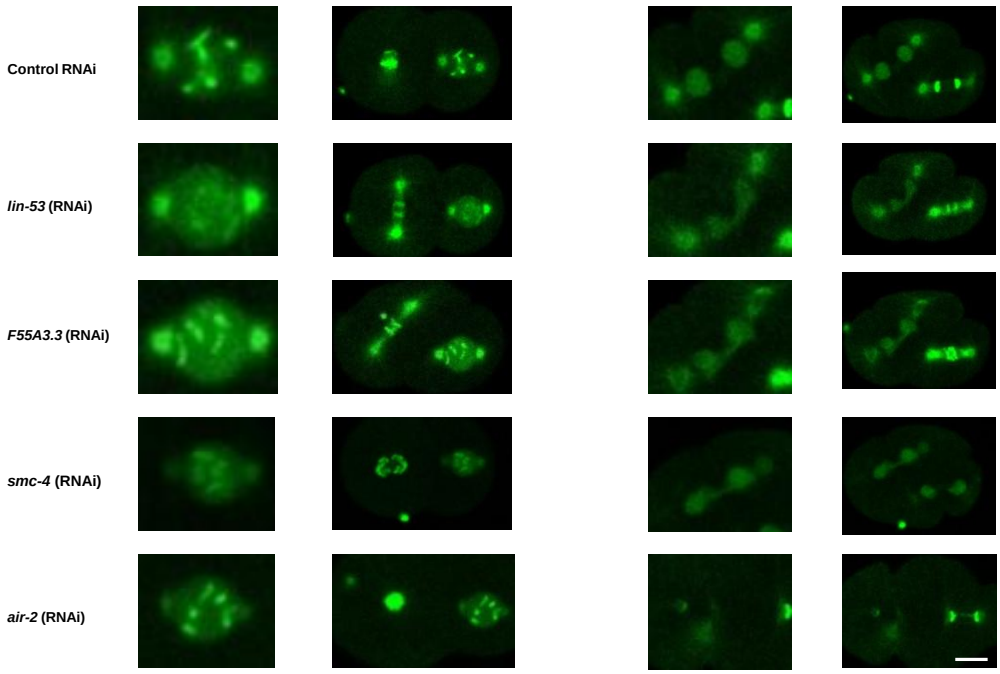

Figure 32: Condensation and segregation defects in embryos that are RNAi depleted of genes involved in cell division.
Imaged worm strains are expressing GFP::H2B and TBB-2::GFP (β-tubulin) fusion protein, marking histones and the mitotic spindle, respectively. Shown are enlarged images of the arrow marked nuclei in Figure 9a. Chromosome condensation reaches wild-type levels before segregation in *F55A3.3* and *air-2* (RNAi) embryos. Residual condensation (although strongly delayed) is achieved in *smc-4* (RNAi) embryos, while it is not observed in *lin-53* (RNAi) embryos. In white, scale bar 10µm.

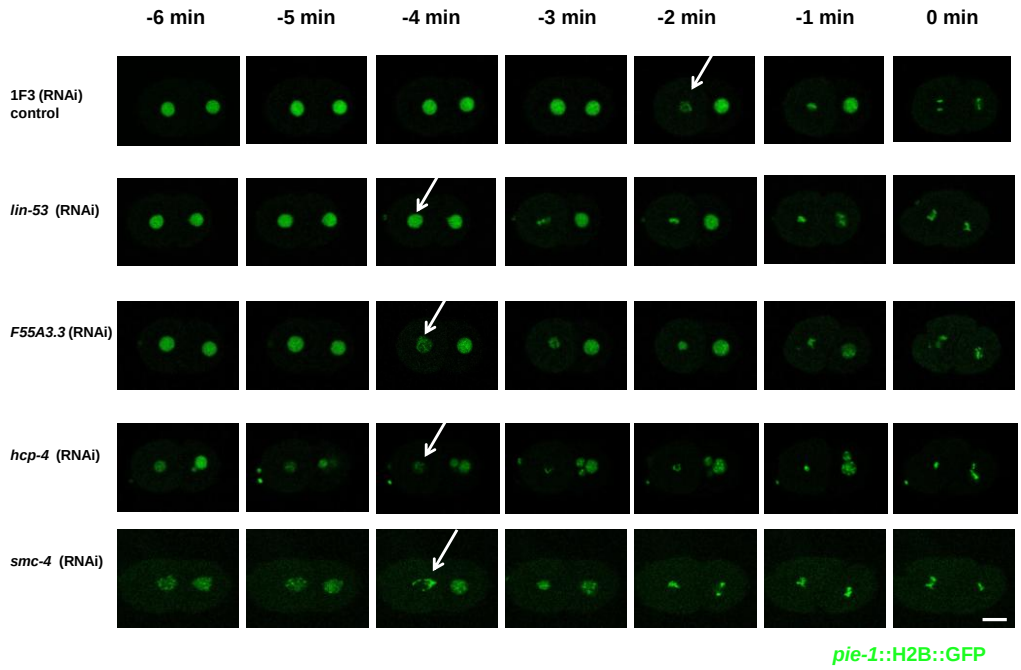

Figure 33: Condensation defects in embryos that are RNAi depleted of cell division genes.
Time 0 is set to the time point when the two chromatin masses first segregate at the onset of anaphase. Imaged worm strains are expressing GFP::H2B fusion protein. Depletion of all genes studied leads to timely delay in chromosome compaction during prophase. However, condensation reaches wild-type levels before segregation in F55A3.3 and hcp-4 (RNAi) embryos, while some residual of compaction is also achieved in embryos depleted of the Condensin I and II subunit SMC-4. Chromosome condensation is not observable in *lin-53* (RNAi) embryos. In white, scale bar 10µm. White arrows indicate different compaction states immediately prior to metaphase alignment.

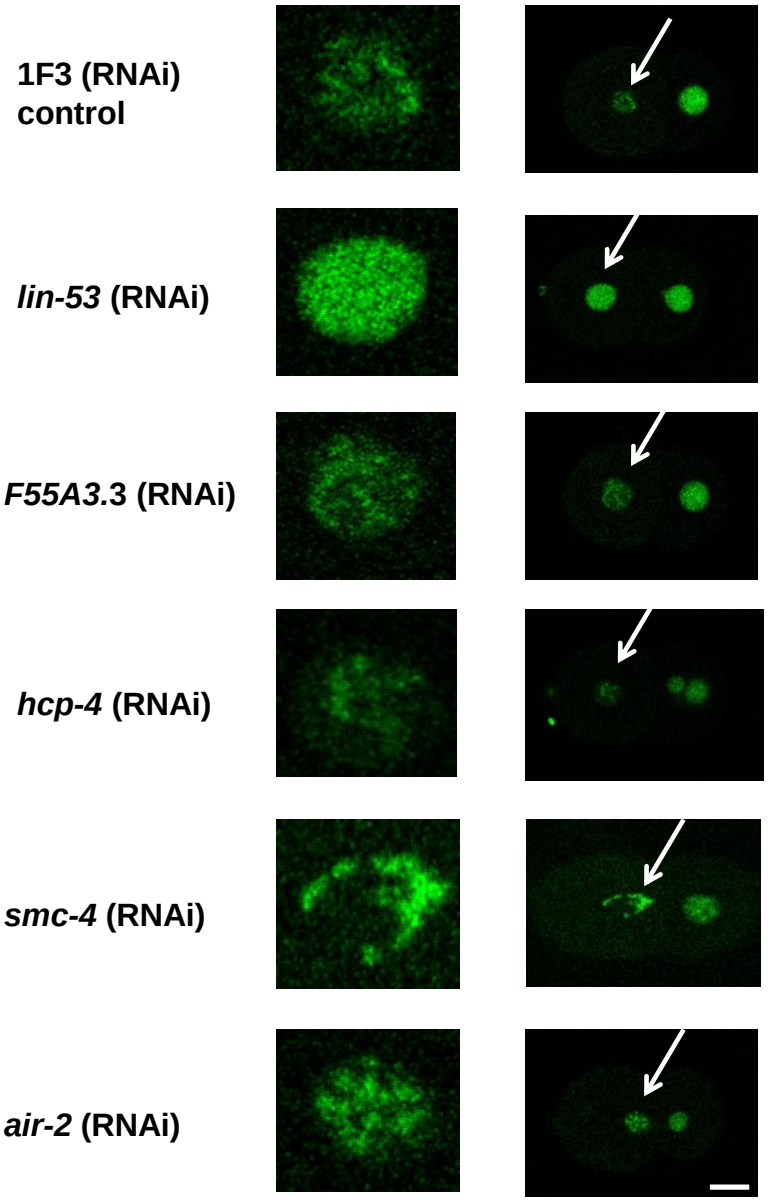

Figure 34: Condensation defects in embryos depleted of genes affecting mitotic division.
Imaged worm strains are expressing GFP::H2B fusion protein. Arrows point to the nuclei that are enlarged in the image on the left and mark the same nuclei as in Figure 10a. In white, scale bar 10µm.

2.4.2.2. The chromosome condensation defect is most severe in *lin-53 (*RNAi) embryos

To gain insight into the molecular mechanisms of observed phenotypic differences between *lin-53* and *F55A3.3* (RNAi) embryos, we compared chromosome dynamics and segregation defects to the ones observed after depletion of well-characterized cell division proteins such as the condensin I and II subunit SMC-4, the centromeric protein CeCENP-C/HCP-4, and the Aurora B kinase AIR-2.

In 27 out of 34 *lin-53* (RNAi) depleted embryos (79%, Table 7) we did not observe condensation of chromosomes at prophase (Figure 31, Figure 33 and Figure 34). In contrast, in *smc-4* (RNAi) depleted embryos, condensation is delayed (15/16 embryos). However residual, although abnormal, compaction is achieved and distinct compacted chromosomes are visible before alignment at the metaphase plate (Table 7, Figure 31 - Figure 34).

Hcp-4/CeCENP-C (RNAi) depleted embryos exhibit a slight condensation delay at early prophase. However compaction is achieved and reaches wild-type levels before sister chromatids are separated (16/17 embryos, Table 7, Figure 33, Figure 34). This phenotype is very similar to that of *F55A3.3* depleted embryos where we observe a delay in condensation but final compaction of chromosomes (Table 7, Figure 31 - Figure 34). In *air-2* (RNAi) mutants, chromosome condensation takes place (Figure 31, Figure 32, Figure 34, Table 7), however position of the spindle is random (Figure 35). Subsequently, severe segregation defects

with anaphase bridges are observed. Membranes are pulled in at wrong positions, preventing the stereotypical positioning of the four-cell stage embryo (Figure 35, bright-field image) and leading to unequal segregation of chromatin. This observation is in consensus with published results [196, 202] and clearly different from the situation in *lin-53, F55A3.3*, *smc-4* or *CeCENP-C* (RNAi) embryos. Here, only condensation and/ or segregation of chromosomes is impaired but not the general sequence of division or spindle positions. Thus, membranes are pulled in at the right time and at correct positions. However, in *lin-53, F55A3.3*, and *smc-4* (RNAi) embryos spindle morphology is abnormal due to lagging chromosomes and segregation delay (Figure 35).

RNAi clone	lethality	delay	abnormal condensation	defect in final compaction	abnormal alignment	lagging chromosomes	cytokinesis defect	abnormal nuclear shape
1F3	0%	0/30 (0%)	0/30 (0%)	0/30 (0%)	0/30 (0%)	0/30 (0%)	0/30 (0%)	0/30 (0%)
lin-53	95-100%	29/34 (85%)	27/34 (79%)	27/34 (79%)	17/34 (50%)	27/34 (79%)	4/34 (12%)	17/34 (50%)
F55A3.3	95-100%	9/30 (30%)	7/30 (23%)	2/30 (7%)	20/30 (67%)	24/30 (80%)	1/30 (3%)	24/30 (80%)
smc-4	95-100%	15/16 (94%)	13/16 (81%)	2/16 (13%)	12/16 (75%)	15/16 (94%)	2/16 (13%)	11/16 (69%)
hcp-4	10-100%	2/17 (12%)	2/17 (12%)	1/17 (6%)	7/17 (41%)	7/17 (41%)	0/17 (0%)	7/17 (41%)
air-2	95-100%	12/13 (92%)	5/13 (38%)	0/13 (0%)	12/13 (92%)	12/13 (92%)	9/13 (69%)	6/13 (46%)

Table 7: **Chromosomal defects observed in embryos depleted of proteins affecting mitotic cell division.**
Numbers correspond to the number embryos in which the specified defect was observed.

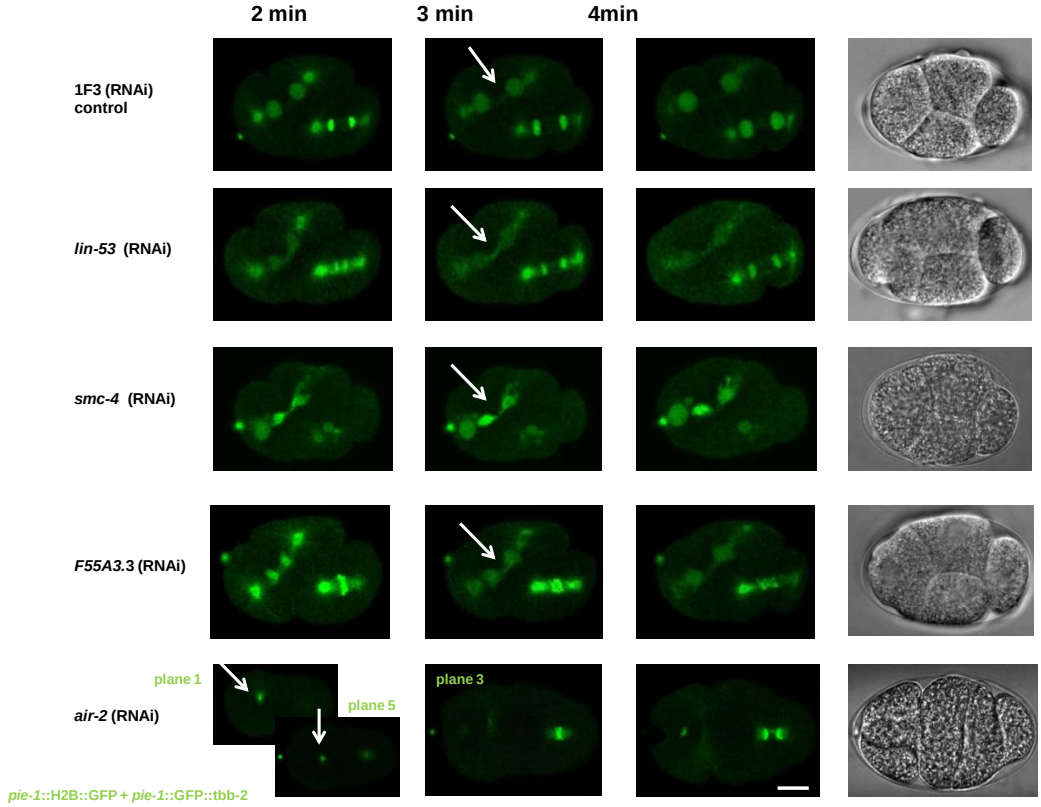

Figure 35: Spindle morphology in *lin-53*, *smc-4* and *F55A.3.3* (RNAi) embryos is different from wild-type embryos.
Spindle positioning is affected in *air-2* (RNAi) depleted embryos, leading to improper arrangement of cell. White scale bar, 10µm. Imaged worm strains are expressing GFP::H2B and TBB-2::GFP (β-tubulin) fusion proteins, marking histones and the mitotic spindle, respectively. Time 0 is set to the time point when the two chromatin masses first segregate at the onset of anaphase as in previous figures.

fluorescently tagged protein	RNAi clone	embryonic lethality	chromosome defect	abnormal spindle positioning	spindle morphology defect
TBB-2 (β-tubulin)	1F3	0%	0/5 (0%)	0/5 (0%)	0/5 (0%)
	lin-53	95-100%	7/7 (100%)	0/7 (0%)	5/7 (71%)
	F55A3.3	95-100%	3/4 (75%)	0/4 (0%)	3/4 (75%)
	smc-4	95-100%	4/4 (100%)	0/4 (0%)	4/4 (100%)
	air-2	95-100%	4/6 (66%)	4/6 (66%)	4/6 (66%)

Table 8: **Defects in spindle morphology and spindle positioning in RNAi depleted embryos.**
Time-lapse recordings embryos expressing beta-tubulin::GFP as well as histone H2B::GFP fusion proteins where studied. N corresponds to the number of embryos in which the specified defect was observed.

2.4.2.3. Condensin I loading is abnormal in *lin-53*, *F55A3.3* and *smc-4* (RNAi) depleted embryos

As the condensation defect observed in *lin-53* depleted embryos is more pronounced than in embryos depleted of the Condensin I and II subunit SMC-4, we asked whether LIN-53 might act in condensin independent compaction of chromatin. Condensin complexes have well studied roles in organizing DNA structures. They are important for DNA condensation in mitosis and meiosis [310]. *C. elegans* possesses two mitotic condensin complexes, I

and II. The mitotic Condensin I complex plays a role in chromosome segregation while Condensin II in chromosome condensation and segregation[191, 194]. Consistent with the observations described above, it has been reported that condensation is delayed in condensin depleted embryos. However some late DNA compaction is ultimately achieved, indicating the action of factors independent of condensin that can compact mitotic chromatin [196]. To test whether condensin is loaded properly in *lin-53* (RNAi) depleted embryos or if the impaired condensation is due to defects in an alternative condensation pathway, we analyzed early cell divisions of embryos carrying a GFP fusion of the Condensin I complex subunit CAPG-1.

Comparable to wild-type embryos, in *lin-53* (RNAi) depleted embryos, CAPG-1::GFP was associated with DNA in metaphase and anaphase, despite DNA condensation and segregation defects (Figure 36, Table 8). CAPG-1::GFP appeared to be at least partly localized to the condensed region of incompletely compacted chromosomes (8/8 embryos). However, it is difficult to unambiguously determine if CAPG-1::GFP also binds to DNA that failed to condense with the compact chromosome mass as this DNA was found spread out in the nucleus. The signal of CAPG-1::GFP, if associated with this type of DNA, may have been too weak to be detected. Similar observations were made in embryos depleted in *F55A3.3*. Condensin I signal was found at abnormal positions due to segregation defective chromosomes (7/7 embryos). CAPG-1::GFP was visible on metaphase chromosomes with a congression defect and bridged anaphase chromosomes.

This goes along with an abnormally disorganized localization pattern compared to wild-type. Delocalized CAPG-1::GFP signal could also be detected in *smc-4* (RNAi) depleted embryos (8/8 embryos), although it appeared dimmer in five out of eight embryos (Figure 36, Table 8). This hints at an impaired loading of Condensin I to chromatin, compared to wild-type, *lin-53* and *F55A3.3* (RNAi) depleted embryos.

Taken together, these results indicate that CAPG-1::GFP localization is abnormal in RNAi embryos due to lagging chromosomes and a delay in segregation. That is, the changes in CAPG-1 localization are likely a secondary defect. It cannot be ruled out entirely that the lower GFP signal in *smc-4* (RNAi) embryos is not caused by variability in expression of the transgene. Thus, it cannot be faithfully distinguished whether the condensation defect in *lin-53* (RNAi) embryos is independent of condensin.

fluorescently tagged protein	RNAi clone	embryonic lethality	segregation defect	abnormal Condensin I localization	dimmer signal than wt
CAPG-2	1F3	control-0%	0/8 (0%)	0/8 (0%)	0/0 (0%)
	lin-53	95-100%	7/8 (87.5%)	7/8 (87.5%)	3/8 (37.5%)
	F55A3.3	95-100%	7/7 (100%)	7/7 (100%)	0/7 (0%)
	smc-4	95-100%	8/8 (100%)	8/8 (100%)	5/8 (62.25%)

Table 9: **Defects in loading of CAPG-1::GFP in RNAi embryos with condensation and/or segregation defects.**
N corresponds to the number of embryos in which the specified defect was observed.

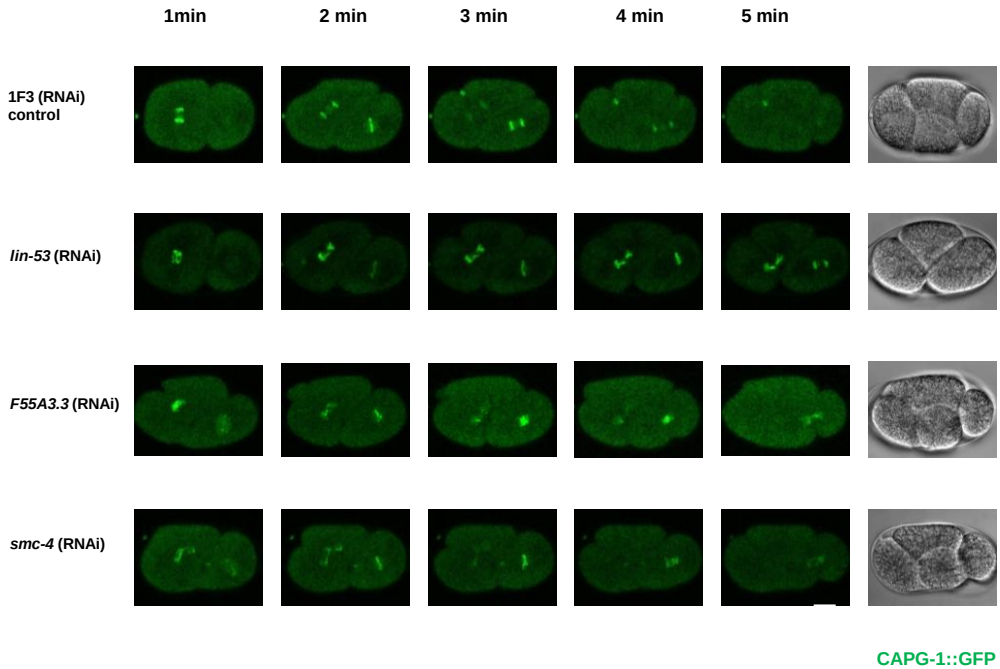

Figure 36: CAPG-1::GFP loading is abnormal in RNAi embryos with condensation and segregation defects.
In white, scale bar 10µm. Time is set 0 at the time point when the two chromatin masses first segregate at the onset of anaphase as in previous figures.

2.4.2.4. Kinetochore assembly is impaired in embryos depleted of *lin-53* and *F55A3.3*

To examine whether other proteins essential for the sequence of mitotic cell division are improperly assembled properly in *lin-53* and *F55A3.3* (RNAi) embryos, we next analyzed time-lapse recordings of early divisions in embryos expressing kinetochore proteins fused to GFP.

Figure 37 shows that depletion of all examined chromatin factors and cell division proteins leads to improper localization of KNL-3::GFP, marking a kinetochore protein downstream of CeCENP-A and CeCENP-C. Two discrete kinetochore bands, as observed in wild-type embryos, were not visible at metaphase in any of the RNAi depleted embryos (Table 10). However, no explicit difference in localization or signal intensity between different RNAi depleted embryos could be established. Thus, it is unfortunately not possible to conclude if the abnormal KNL-3::GFP localization is caused by impaired compaction of chromosomes, thus being a secondary defect, or directly by defective kinetochore assembly itself.

fluorescently tagged protein	RNAi clone	embryonic lethality	segregation defect	abnormal kinetochore localization
KNL-3	1F3	control-0%	0/7 (0%)	0/7 (0%)
	lin-53	95-100%	15/17 (88%)	15/17 (88%)
	F55A3.3	95-100%	10/14 (71%)	10/14 (71%)
	smc-4	95-100%	4/5 (80%)	4/5 (80%)
	hcp-4	10-20%	3/8 (38%)	3/8 (38%)
	air-2	95-100%	4/4 (100%)	4/4 (100%)

Table 10: Defects in KNL-3::GFP loading in RNAi mutants with segregation defects.
N corresponds to the number of embryos in which the specified defect was observed.

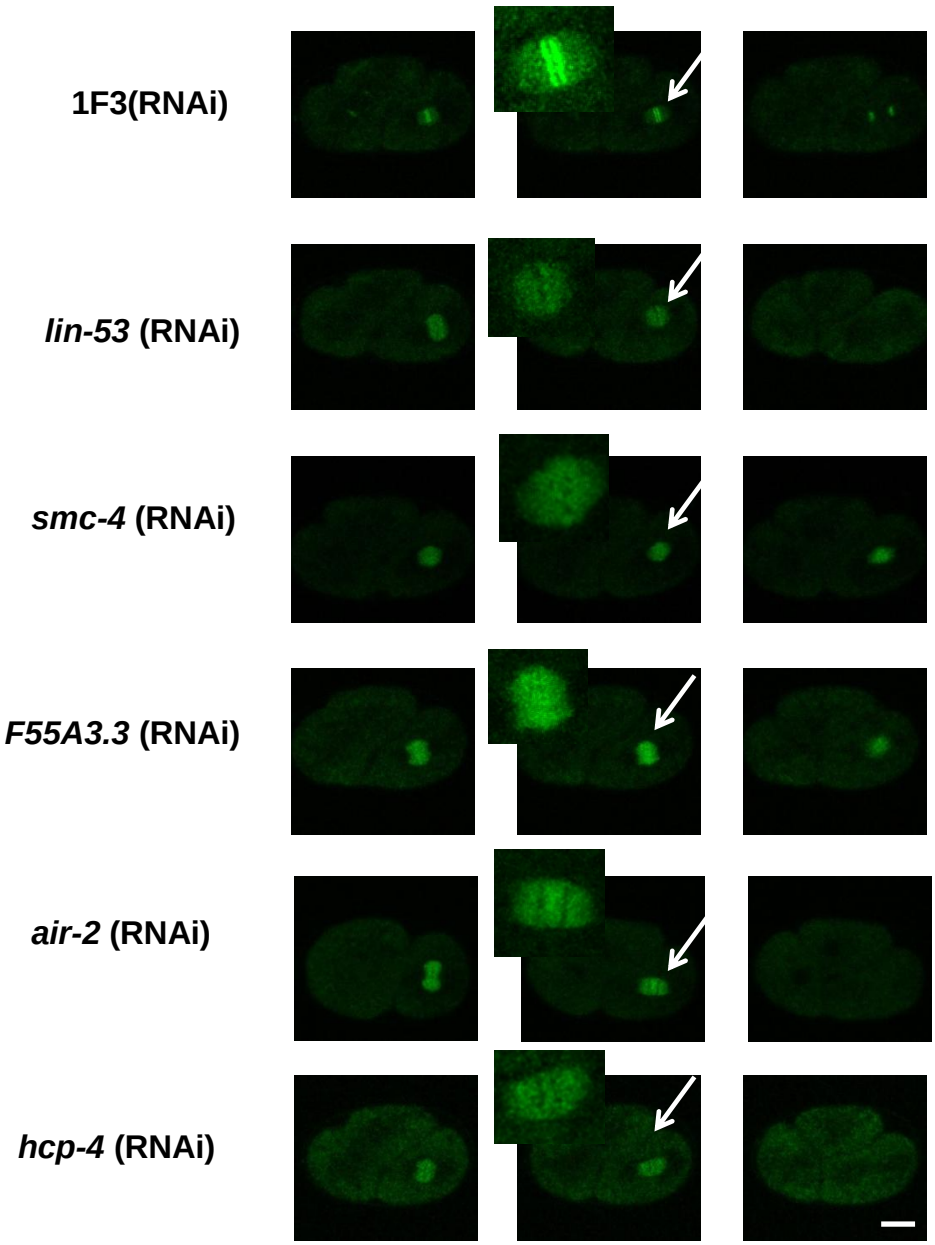

Figure 37: Kinetochore assembly is impaired in embryos RNAi depleted for the factors indicated.
In white, scale bar 10µm. Arrows point to the mislocalized kinetochore signal of the P1 cell at metaphase. Imaged worm strains are expressing KNL-3::GFP fusion protein.

2.4.2.5. AIR-2 localization is normal in *lin-53* and *F55A3.3* (RNAi) embryos

To examine whether localization of the Aurora B kinase AIR-2 is impaired in *lin-53* and *F55A3.3* (RNAi) embryos, we imaged embryos expressing AIR-2::GFP and H2B::GFP fusion proteins.
In wild-type embryos, GFP::AIR-2 was localized to prophase and metaphase chromosomes as described previously (Figure 38). Following chromosome separation, GFP::AIR-2 was present on both chromosomes and midzone microtubules. In telophase, GFP::AIR-2 was predominately localized at the midzone. In *lin-53* (RNAi) mutants, GFP::AIR-2 signal appeared to be normal, despite chromosome condensation and segregation defects. The same normal localization pattern was observed in *F55A3.3* and *smc-4* (RNAi) depleted embryos (Figure 38). This suggests that the condensation and segregation defects observed are independent of AIR-2. Consistent with this hypothesis, *air-2* (RNAi) depletion leads to an apparent mislocalization of AIR-2::GFP together with characteristic cytokinesis defects (Figure 38, Table 11).

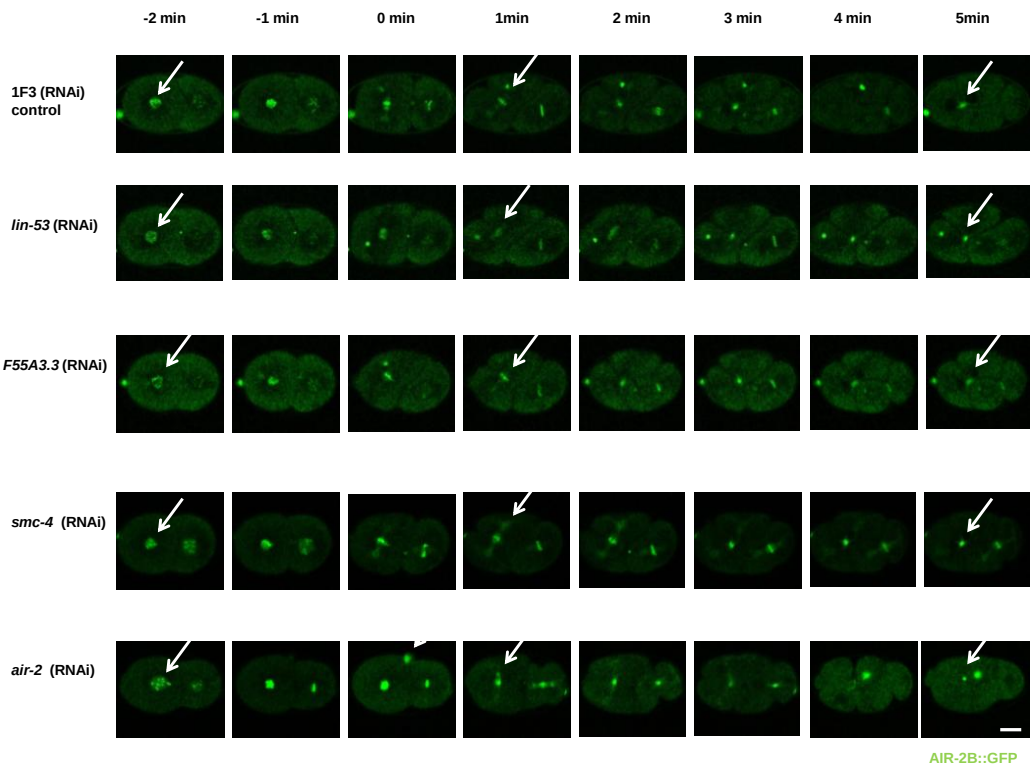

Figure 38: Localization of the Aurora B kinase appears normal in all RNAi depleted embryos analyzed, with exception of *air-2* (RNAi).
Time is set to 0 at anaphase onset, when chromatin masses first segregate, as in previous figures. Imaged embryos are expressing AIR-2B::GFP fusion protein. Scale bar, white, 10µm. Arrows point to AIR-2::GFP signal at prophase (-2 min), onset of anaphase (1 min) and after cytokinesis (5 min).

fluorescently tagged protein	RNAi clone	embryonic lethality	chromosome defect	abnormal localization
AIR-2	1F3	control-0%	0/5 (0%)	0/5 (0%)
	lin-53	50-100%	2/4 (50%)	0/4 (0%)
	F55A3.3	90-100%	4/6 (66%)	0/6 (0%)
	smc-4	95-100%	3/3 (100%)	0/3 (0%)
	air-2	95-100%	3/3 (100%)	3/3 (100%)

Table 11: **Localization of the Aurora B kinase appears normal in all RNAi depleted embryos analyzed, with exception of *air-2* (RNAi).**
N corresponds to the number of embryos in which the specified defect was observed.

2.4.2.6. Nuclear envelope dynamics are abnormal in *lin-53* and *F55A3.3* (RNAi) embryos due to lagging of chromosomes and delay in segregation

To examine the effect of *lin-53* and *F55A3.3* depletion on nuclear envelope dynamics we imaged embryos expressing CeMAN-1/LEM-2::GFP fusion protein together with histone H2B::GFP.

In wild-type embryos, inner nuclear membranes containing Ce-MAN-1 remained largely intact and surrounded the mitotic spindle except a region surrounding spindle poles during metaphase and early anaphase (Figure and Figure 39). During mid to late anaphase, disassembly was completed. As remnants of the old

nuclear envelopes dispersed, the formation of new envelopes around the segregated chromatin was detected beginning about one minute after anaphase onset. These observations are consistent with previous reports [176, 177].

In contrast, in *lin-53* and *F55A3.3* (RNAi) embryos, nuclear membrane dynamics were abnormal. Due to the lagging of chromosomes, assembly of the nuclear membrane appeared to be more disorganized. The signal for LEM-2::GFP appeared more dispersed around segregated chromatin masses because of their delayed decondensation. In *lin-53* (RNAi) embryos, daughter nuclei did not completely separate after division and remained associated with the membrane. LEM-2::GFP could be detected at the membrane connection point (Figure). Due to the general delay in segregation, nuclear membrane assembly was delayed in both RNAi embryos. In addition, as in *lin-53* depleted embryos condensation is also delayed, nuclear membrane disassembly was delayed here as well (Figure). The more subtle segregation defects in *F55A3.3* (RNAi) embryos compared to lin-53 (RNAi) coincide with a less severe assembly defect (Figure and Figure 39). In summary, the observed abnormalities in nuclear envelope dynamics are most likely secondary defects arising from primary condensation and segregation defects.

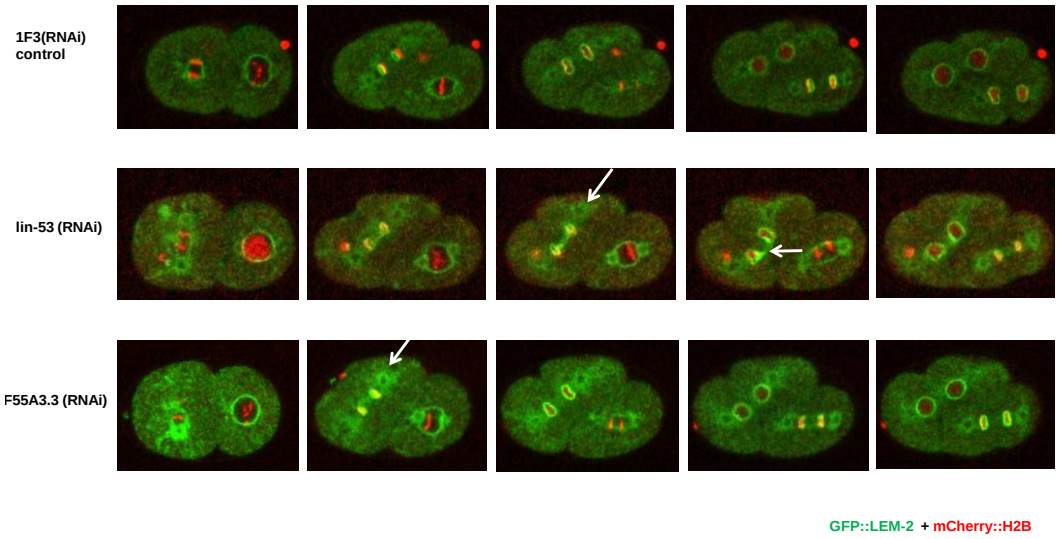

Figure 39: Nuclear envelope dynamics is abnormal in *lin-53* and *F55A3.3* (RNAi) embryos.
Time is set to 0 at anaphase onset, when chromatin masses first segregate, like in previous figures. Imaged embryos are expressing LEM-2::GFP and H2B::mCherry fusion proteins. Scale bar, white, 10µm. Arrows point to dispersed LEM-2::GFP signal at time points when nuclear envelope assembly is normally accomplished.

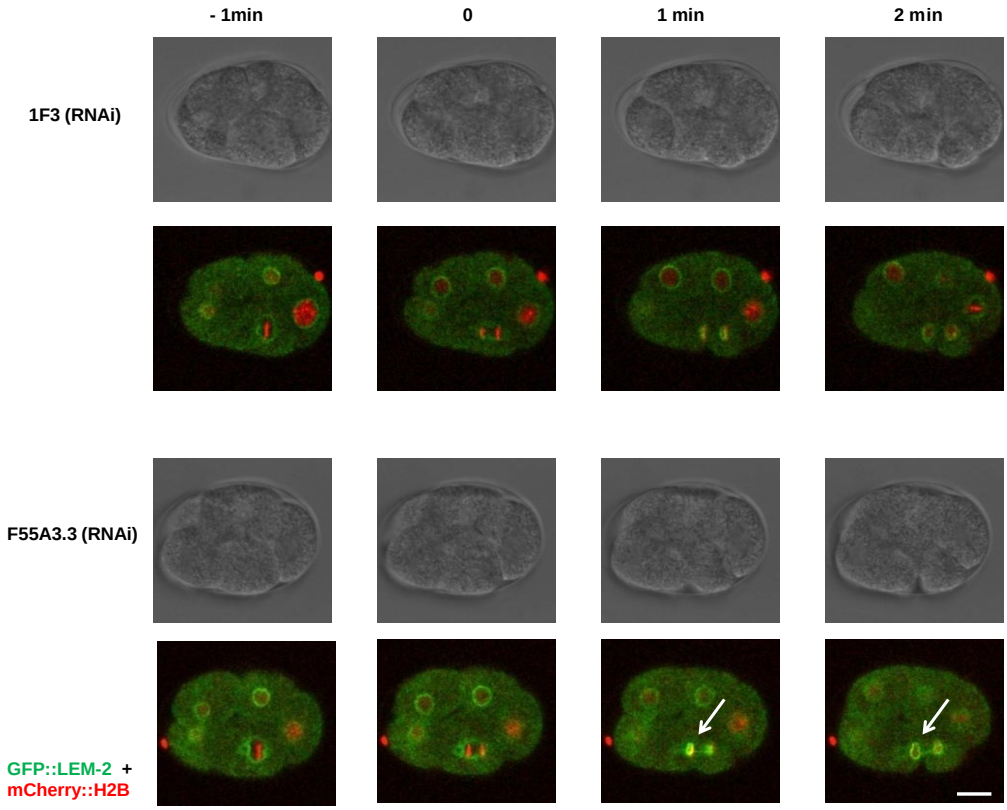

Figure 39: **Nuclear envelope assembly defects are more subtle in *F55A3.3* (RNAi) embryos in connection with more subtle segregation defects.**
Time is set to 0 at anaphase onset, when chromatin masses first segregate, like in previous figures. Imaged embryos are expressing LEM-2::GFP and H2B::mCherry fusion proteins. Scale bar, white, 10µm. Arrows point to dispersed LEM-2::GFP signals at time points indicated, when nuclear envelope assembly is accomplished. Upper images Nomarski, lower images fluorescence detection by confocal microscopy.

2.4.3. Chromatin factors with cellular phenotypes other than chromosome segregation

2.4.3.1. Depletion of *let-858, cir-1,* and *F55A3.3* leads to a re-arrangement of chromosomes to the nuclear periphery

In depth analysis of time-lapse recordings of Histone-GFP labeled embryos depleted of chromatin factors revealed another interesting phenotype. In *let-858* (RNAi) embryos we first observed that the GFP/chromosome signal is missing at the nuclear centers (Figure 40 A, Figure A). To elucidate this 'ring' phenotype, we lineaged three *let-858* (RNAi) embryos semi-automatically up to 180 minutes after the four-cell stage.

Hereby, we noticed that the cell cycle length of the two cells initiating gastrulation, the daughters of the E cell, Ea and Ep, was shorter compared to wild-type embryos (Figure 40 B). In normal embryos, those two cells exhibit a characteristically prolonged cell cycle at that stage, which allows them to ingress before their division. Indeed, further analysis revealed a defect in the initiation of gastrulation. Ea and Ep did not ingress in all embryos examined (n=5) (Figure A).

Two possible reasons could explain this phenotype: either the fate of the E cells changed which has been described to concomitantly lead to a change in cell cycle length and ingression behavior. Alternatively, embryos depleted of *let-858* could lack zygotic gene expression which has also been shown to stop E cell ingression

due to the loss of expression of E cell fate markers [311]. LET-858 is homologous to nucampholin and displays sequence similarities to the eukaryotic translation initiation factor eIF-5 gamma. In yeast, eIF-5 is associated with the spliceosome [312]. Thus, it is likely to be involved also in general protein expression. Moreover, in our time-lapse recordings we observed that in *let-858* (RNAi) embryos nuclei become smaller and dimmer over time and eventually exhibit a sudden stop of cell division and movement. This phenotype seemed a plausible result of death caused by impaired zygotic gene expression (Figure 40 A).

In addition, in *F55A3.3* and *cir-1* (RNAi) embryos, we observed a similar nuclear re-arrangement of chromosomes (Figure A). F55A3.3 is thought to be a general transcriptional regulator while CIR-1 acts as Co-repressor in mammals [313] and its homologue is involved in ribosomal biogenesis in *S. cerevisiae* [314]. Taken together, we suggested that impairment of zygotic gene expression in *let-858* (RNAi), *F55A3.3* (RNAi) and *cir-1* (RNAi) embryos leads to re-arrangement of chromosomes to the nuclear periphery.

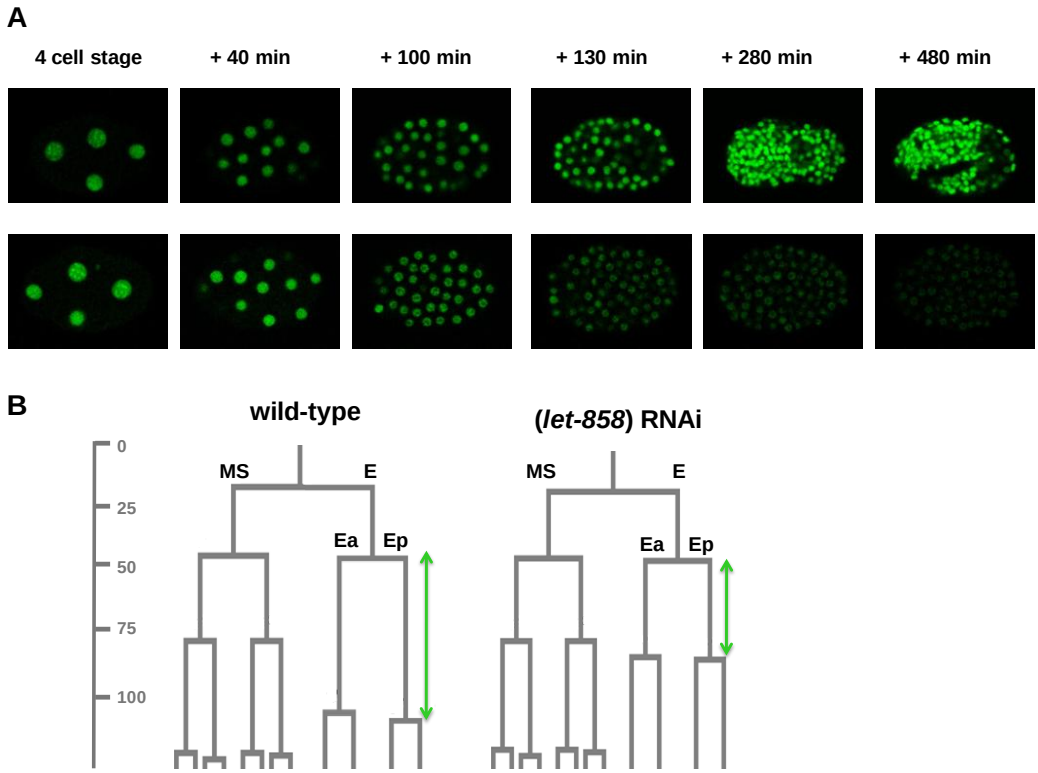

Figure 40: **Decrease in H2B::GFP signal intensity during embryogenesis in *lin-858* (RNAi) embryos.**
(A) The first row shows pictures of a wild-type, the second row of a *let-858* (RNAi) embryo.
(B) Schematic diagram (lineage tree) of cell divisions. In *let-858* (RNAi) embryos (right) the cell cycle length of the E cell daughters is shortened compared to wild-type embryos. On the left, time scale in minutes after the four-cell division.

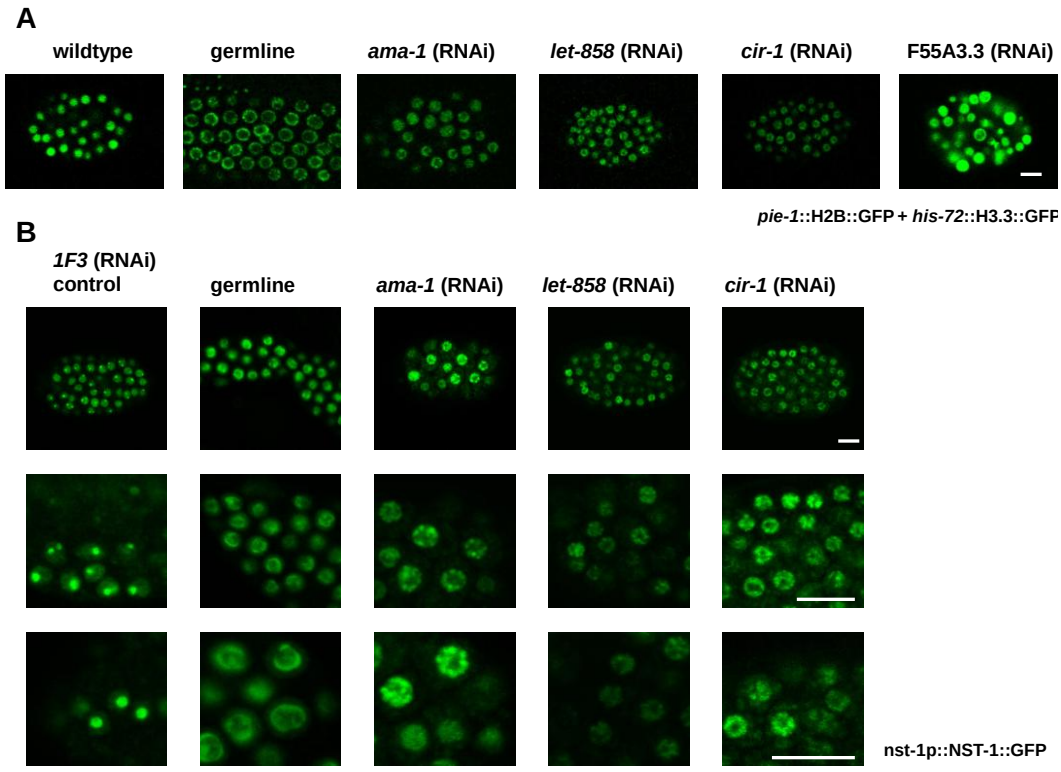

Figure 42: Nuclear re-arrangement in cells with impaired gene expression. White scale bar corresponds to 10µm.
(A) Imaged embryos/germline expressing the *pie- 1*::H2B::GFP + *his-72*::H3.3::GFP construct.
(B) Embryos expressing NST-1::GFP fusion protein. After depletion of *let-858, cir-1* and *ama-1,* nucleostemin is localized at the nuclear periphery. This localization is similar to that described in transcriptionally silent germ-line cells [315], and different from wild-type embryos where it is confined to the nucleolus.

2.4.3.2. Impairment of gene expression leads to the re-arrangement of nuclear architecture

To test this hypothesis, we compared the observed phenotypes to those of genes with a known lack of zygotic transcription. RNAi

depletion of *ama-1*, encoding for the large subunit of the RNA polymerase II, leads to the same defect in E cell cycle length and ingression. Interestingly, knockdown of *ama-1* induced embryonic lethality with depletion of H2B::GFP signal in the nuclear center at arrest of development (Figure A). As the phenotype is very similar to *let-858* (RNAi), we assumed that it results from a general failure of gene expression.

Interestingly, when imaging nuclei of the germ line of embryos expressing H2B::GFP fusion protein, we observed the same nuclear organization. H2B::GFP signal was absent in the nuclear center and confined to the nuclear periphery (Figure).

2.4.3.3. Nuclear re-arrangement is not a consequence of enlargement of the nucleolus

As it is known that in germ line cells the chromosomal re-arrangement is due to an enlargement of the nucleolus [316], we asked whether this is the case in *let-858* and *ama-1* (RNAi) depleted embryos as well. To address this question, we stained *ama-1* (RNAi), *let-858* (RNAi) and control embryos as well as dissected wild-type gonads with a α-NOP-1/Fibrillarin antibody, a specific nucleolar marker. Unexpectedly, RNAi depleted embryos showed similar staining patterns as control embryos despite re-arrangement of chromosomes to the periphery (Figure 41). Dissected wild-type gonads instead exhibited the typical staining pattern of germ line nuclei, with α-NOP-1/Fibrillarin signal

concentrated in the enlarged nucleolus (Figure 41, top line). Thus, we propose that the re-arrangement of DNA in *let-858* and *ama-1* (RNAi) depleted embryos is not a result of enlargement of the nucleolus, but consequence of impaired gene expression.

To further examine the observed phenotype, we imaged embryos expressing NST-1::GFP, a nucleolar marker. *Nst-1* encodes for a homologue of human GNL3, a nucleolar GTPase called nucleostemin. It is concentrated in the nucleolus and diffusely present in the nucleoplasm, corresponding to reports of mammalian nucleostemin localization [317]. NST-1 is generally absent from regions of the nucleolus where rRNA transcription and processing occurs. This differs from localization of NOP-1/fibrillarin which is directly involved in rRNA processing. In contrast to mammalian nucleostemin, NST-1 is found in both terminally differentiated, non-cycling cells as well as in proliferating cells. Indeed, NST-1::GFP localization in nuclei of arrested *let-858*, *ama-1*, and *cir-1* (RNAi) embryos was different from wild-type localization, however similar to the described localization in germ line nuclei (Figure B). In wild-type embryos, NST-1::GFP is concentrated and distributed uniformly in the nucleolus, whereas it localizes to the periphery of the enlarged nucleolus in germ line nuclei and nuclei of arrested *let-858*, *ama-1*, and *cir-1* (RNAi) embryos. This similar nucleostemin localization indicates impaired gene expression in those embryos and further confirms our hypothesis.

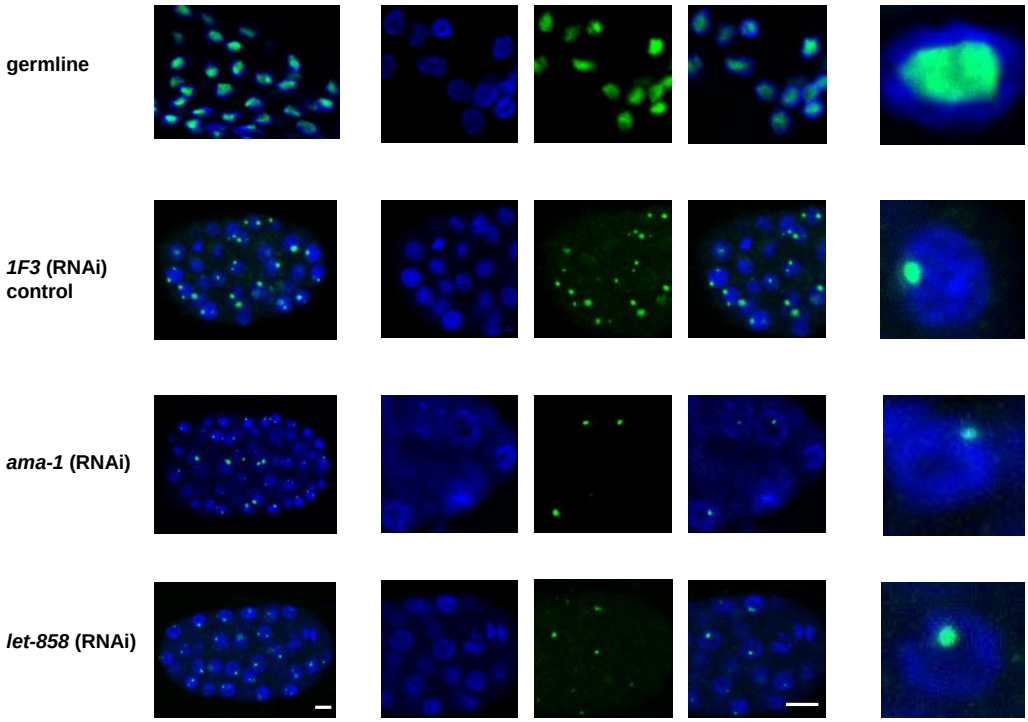

Figure 41: **α-NOP-1/Fibrillarin antibody and DAPI staining, marking the nucleolus (green) and DNA (blue) respectively.**
Shown are embryos depleted of *let-858* and *ama-1*, control embryos (1F3, empty vector) and dissected germ lines. White scale bar: 5 µm.

2.4.4. Quantitative analysis of developmental phenotypes

To study the group of chromatin factors presumably mediating global developmental functions, we subjected semi-automatically tracked time-lapse recordings to detailed systematic and quantitative analysis of cell cycle length, positions, movements and division angles.

By doing so, we could group factors into distinct phenotypic classes. One class, comprising many of the chromatin factors analyzed, shows a delay in development after depletion by RNAi. Knockdowns leading to rather lineage specific defects were assigned to a second group. RNAi depleted embryos showing defects most likely attributed to a failure of zygotic gene expression define a third class of chromatin factors.

2.4.4.1. RNAi depletion of many chromatin factors delays cell cycle progression

Knockdown of many genes analyzed slowed down embryogenesis with an observed increase of cell cycle length during development. Onset of the developmental delay was usually during the 4th round of division (Figure 42, first green line). The most pronounced decrease in developmental speed was observed in embryos depleted of *rba-1*. Here, the increase in cell cycle length during the 4th round of division affected all cells uniformly. Knockdown of *hda-1* also led to a uniform (yet less pronounced than in *rba-1* (RNAi) embryos) increase of cell cycle times during the 4th round of

division (Figure 42). In embryos depleted of *set-16*, and the SWI/SNF family members *swsn-5*, *swsn-7*, and *let-526,* onset of cell cycle length prolongation could be observed during the fourth round of division only in the cells of the AB lineage. Beginning after the fifth round of division, other cells were affected as well, however to a lesser extent than observed in *rba-1* (RNAi) embryos (Figure 42 and Figure 43). Except for *swsn-5* and *swsn-7*, RNAi depletion of this first group of chromatin factors also led to segregation defects at late time points in addition to the observed division delay (see Figure 30). Interestingly, RNAi knockdown of *egl-27* in combination with *lin-40* did not result in a general deceleration of development, with some specific lineages being the exception (Figure 44).

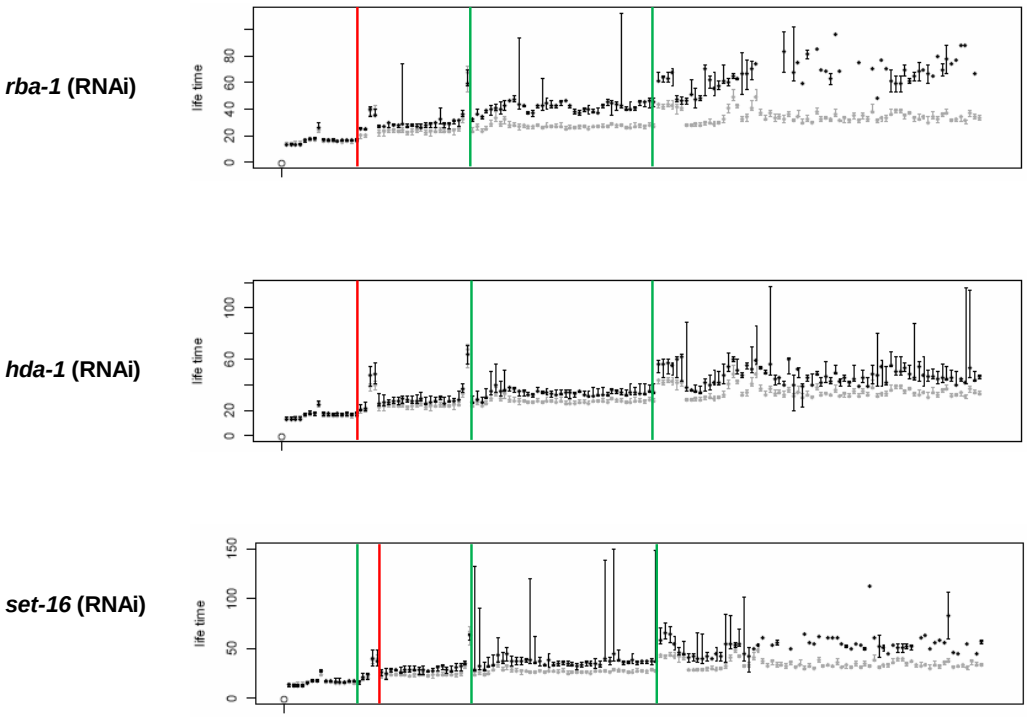

Figure 42: Development is slowed down after RNAi knockdown of *rba-1, hda-1* and *set-16.*

Life times of cells (cell cycle length in minutes) are shown on the y-axis. On the x-axis each point represents a particular cell, arranged according to their time of birth. Indices of all cells can be found in the appendix. Red lines mark the onset of developmental delay (first cell that shows a longer cell cycle). Green lines mark the beginning of a new division round (first cell that divides at the particular division round). The first green line corresponds to the fourth division round. If onset of delay goes along with the start of a new division round, only the red line is shown. Cells of an RNAi depleted embryo are represented in black. Wild-type cells are shown in gray. Box plots indicate the median (point at center) and extreme values (outer bounds) of n=3 embryos. Plots adapted from Rob Jelier.

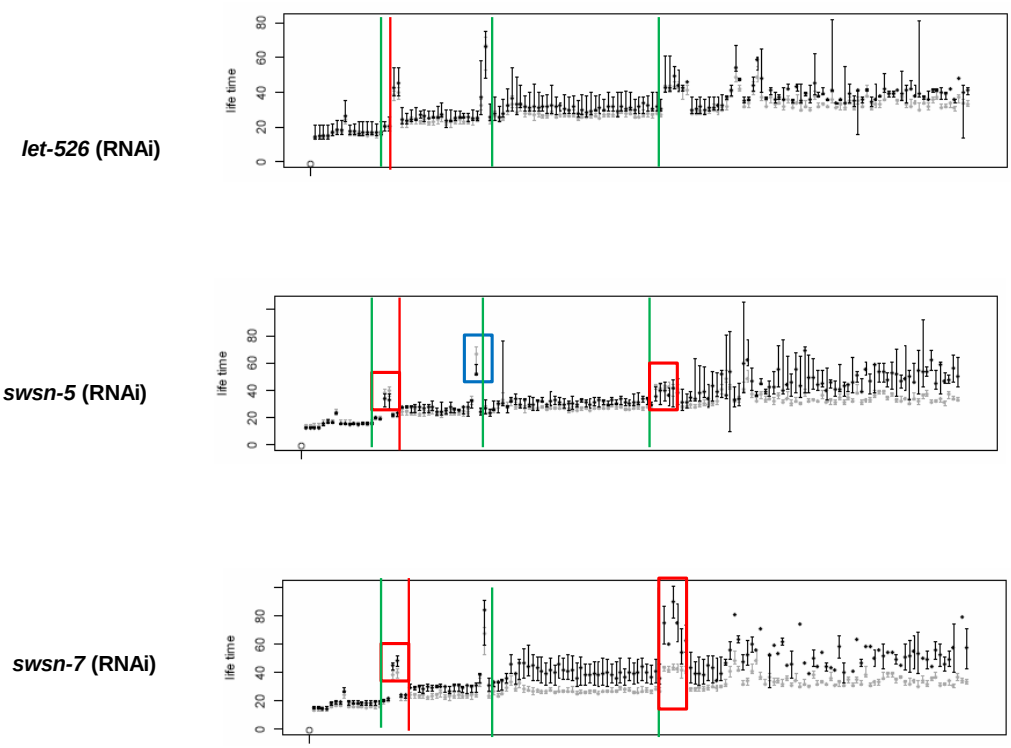

Figure 43: Development is slowed down after RNAi knockdown of *let-526, swsn-5* and *swsn-7.*
Cell life times (cell cycle length in minutes) are shown on the y-axis. On the x-axis each point represents a particular cell, arranged according to their time of birth. Indices of all cells can be found in the appendix. Red lines mark the onset of developmental delay (first cell that shows a longer cell cycle). Green lines mark the beginning of a new division round (first cell that divides at the particular division round). The first green line corresponds to the fourth division round. If onset of delay goes along with the start of a new division round, only the red line is shown. Cells of an RNAi depleted embryo are represented in black. Wild-type cells are shown in gray. Red squares mark descendants of the E lineage, exhibiting particularly altered life times. The blue square highlights the shorter life time of the P4 cell. Box plots indicate the median (point at center) and extreme values (outer bounds) of n=3 embryos.Plots adapted from Rob Jelier.

2.4.4.2. *egl-27/lin-40* is required for MSp cell fate

In contrast to chromatin factors whose depletion appears to affect all cells, double RNAi knockdown of *egl-27* together with *lin-40* leads to defects specifically in cells of the MS lineage (Figure 44, Figure 45, Figure 46 B). There is no general delay of division times. Only MS cell divisions are delayed. In particular, after the 5th cell division only posterior MSp descendants are affected (Figure 44). Curiously, after the 4th division round, the cell cycle of Ea and Ep is shortened (as well as of the P4 cell), while at the fifth division round it is prolonged (Figure 44). This indicates an additional involvement in the development of the E lineage as well. Consistent with the particularly strong delay in division times of MSp descendants, cell group analysis revealed that positions and division angles of MSp cells are also more variable than those of MSa descendants (Figure 45). Despite this variability, however, cells re-organize in such a way that after their ingression, 140 minutes after the ABa division, overall alignment of cells of the MS lineage is largely correct (Figure 45, Figure 46 B).

2.4.4.2.1. *swsn-5* but not *swsn-7* or *let-526* are required for E cell fate

In *swsn-5* (RNAi) embryos, E cell descendants seem to be, to some extent, more affected than cells of other lineages. In contrast to the general delay in division timings, cell cycle lengths of E cell descendants as well as of the P4 cell are shorter (Figure 44, red

squares). This is consistent with the partial failure in ingression of Ea and Ep (Figure 46 A, Figure). It is known that proper E cell ingression requires a delay in the division of the E cell [78]. In *swsn-5* (RNAi) embryos, Ea and Ep divide before having moved completely into the interior of the embryo (Figure 47, top). In addition, division angles of E cell descendants seem to be more variable (Figure B and C, Figure 47). As embryos depleted of other members of the SWI/SNF family, namely *swsn-7* and *let-526*, do not show a similar defect in E cell lineage behavior, the observed effect seems to be specific to *swsn-5* (RNAi) embryos. In *swsn-7* and *let-526* depleted embryos, E cells ingress to their normal positions despite their slowed development and thus later division (Figure 44 and Figure 48) and movement (Figure 48 top). The positioning of C and D cell descendants is, in contrast to E cells, impaired in all three SWI/SNF factor depleted embryos (Figure 48 middle and bottom line). C cells are positioned more anterior than wild-type (Figure 48 middle), while D cells are located more posterior (Figure 50 bottom). This is probably due to a lack of active movements and ingression at this time of development (mis-positioning is observed 100 minutes after the four-cell stage). After abnormal displacement due to different cell division angles, Ca and Cp/Da and Dp fail to acquire their proper positions and solely stay at the locations where they were born. C descendants do not move to the posterior, and D descendants do not move in an anterior-left direction to ingress from there. Also, ingression of ABa lineage descendants is affected in these three SWI/SNF factor depleted embryos, mainly after approximately 100 minutes after

the four-cell stage (Figure 46 A). Yet, positioning of C and D lineage descendants is not impaired in general after depletion of chromatin and other factors. E.g. *egl-27+lin-40* and *gei-4* (RNAi) embryos show correct cell arrangements (Figure 46 B). Depletion of the NuRD complex members, *hda-1* and *rba-1,* does not affect cell positioning at all. Cells of all lineages move to their correct positions until development slows down to such an extent that no more movements take place in general (Figure 49). Thus, *swsn-5* might have a more specific role in the proper expression of E cell fate markers, while defects in other lineages are most likely due to a general loss of proper gene expression at that stage of embryogenesis after SWI/SNF factor depletion.

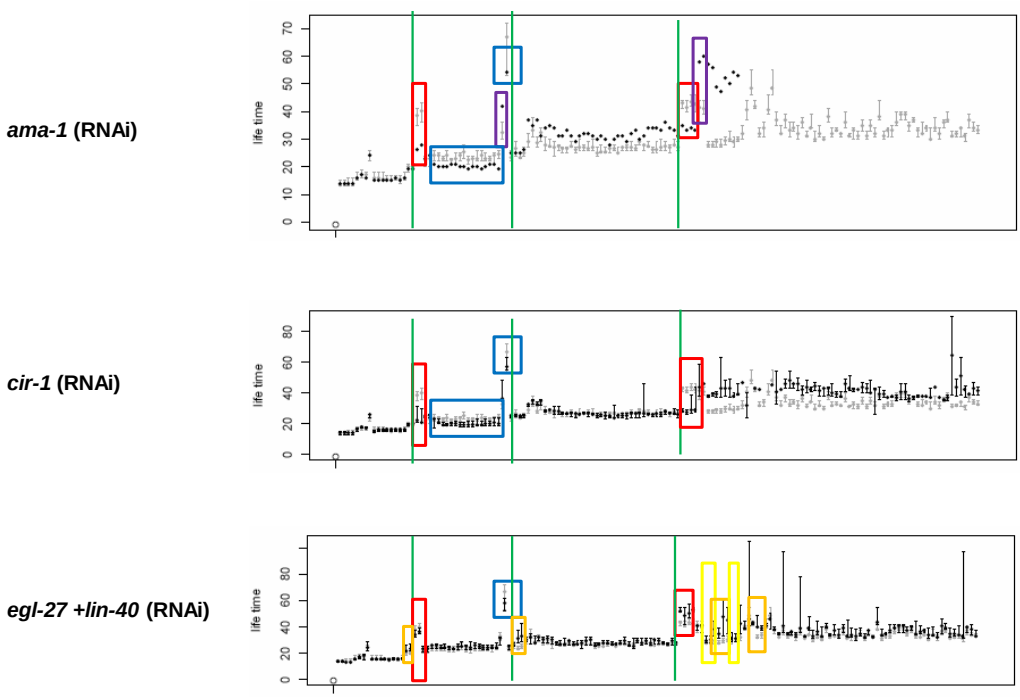

Figure 44: Cell cycle lengths of E cell descendants and the P4 cell are shortened in *ama-1* and *cir-1* depleted embryos, whereas *egl-27+lin-40* (RNAi) embryos show a cell cycle delay in the MS lineage.

Cell life times (cell cycle length in minutes) are shown on the y-axis. On the x-axis, each point represents a particular cell, arranged according to their time of birth. Indices of all cells can be found in the appendix. Red lines mark the onset of developmental delay (first cell that shows a longer cell cycle). Green lines mark the beginning of a new division round (first cell that divides at the particular division round). The first green line corresponds to the fourth division round. If onset of delay goes along with the start of a new division round, only the red line is shown. Cells of an RNAi depleted embryo are represented in black. Wild-type cells are shown in gray. Red squares mark the particularly altered life times of descendants of the E lineage. Blue squares highlight the shorter life time of the P4 cell in *egl-27+lin-40* (RNAi) depleted embryos. In *cir-1* (RNAi) depleted embryos blue squares highlight P4 and early AB lineage descendants. Descendants of the MS cell are marked in yellow, while later shortening in life time of MSp descendants is highlighted in orange. D cell descendants are surrounded by a purple square. Box plots indicate the median (point at center) and extreme values (outer bounds) of n=3 embryos. Plots adapted from Rob Jelier.

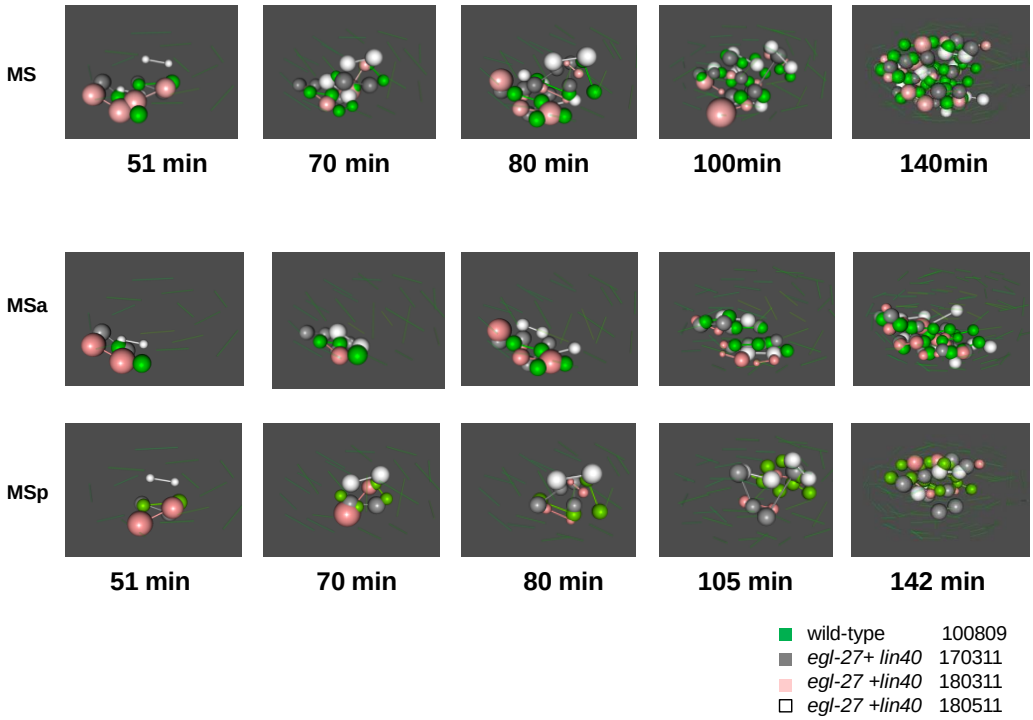

Figure 45: In *egl-27+lin-40* depleted embryos, division angles and positions of MSp descendants are more affected than MSa descendants.

Nuclei of three different *egl-27+lin-40* (RNAi) depleted embryos and one representative wild-type embryo were aligned at the four-cell stage. Embryos are shown with anterior is to the left and ventral to the bottom. Below each picture, time is displayed in minutes after the ABa cell division. Nuclei of MS cell descendants of *egl-27+lin-40* (RNAi) depleted embryos are represented as white, grey and light pink balls. Nuclei of MS cell descendant of one representative wild-type embryo are displayed as green balls. Sister nuclei are connected by a line. Nuclei of other lineages are displayed as sticks in the background, connecting sister cell pairs (each end of a stick represents one nucleus).

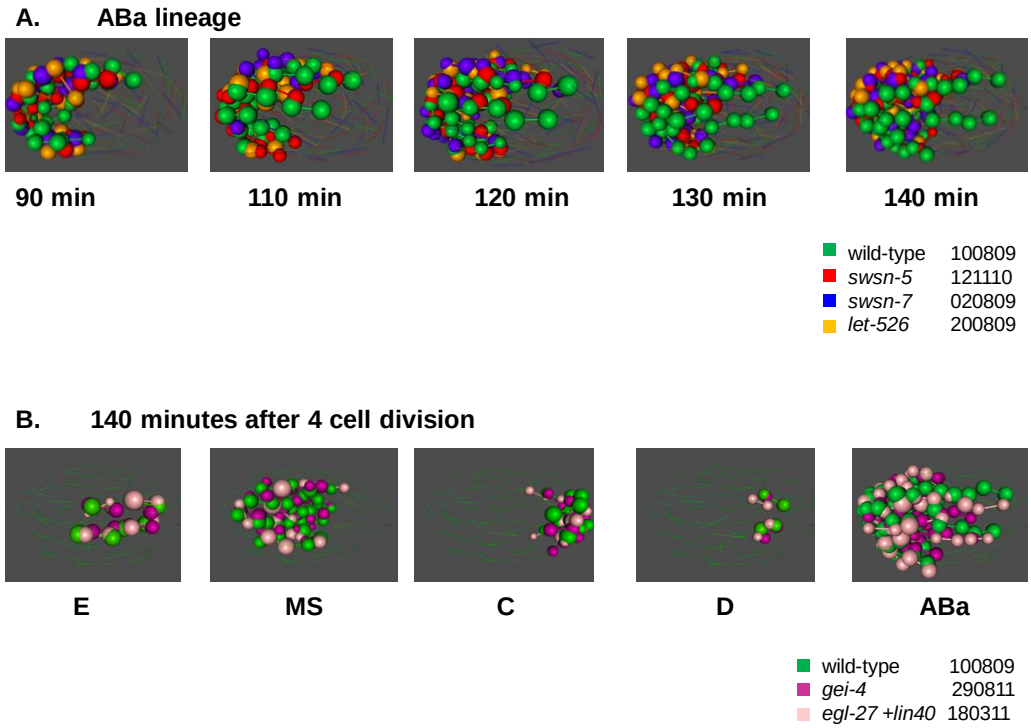

Figure 46: Ingression movements and positioning of cell lineages in different RNAi embryos.
Displayed embryos were aligned to at the four-cell stage.
In the images, anterior is to the left and ventral to the bottom.
(A) Ingression of ABa descendants is impaired in *swsn-5, swsn-7, and let-526 (RNAi)* embryos. Nuclei of ABa cell descendants of one representative *swsn-5* (red), *swsn-7* (blue), *let-526* (yellow) (RNAi), and wild-type (green) embryo are represented as balls. Sister nuclei are connected by a line. Nuclei of other lineages are displayed as sticks in the background, connecting sister cell pairs. Below the images, time is displayed in minutes after the ABa cell division.
(B) 140 minutes after the four-cell stage, relative cell positions of all lineages are correct in *egl-27+lin-40 (RNAi)* embryos. Wild-type, *gei-4* (RNAi) and *egl-27+lin-40* (RNAi) nuclei are represented in green, dark, and light pink, respectively. Below the images, the specific lineage depicted by the balls, is shown at 140 minutes after the four-cell division. Nuclei of other lineages are displayed as sticks in the background, connecting sister cell pairs.

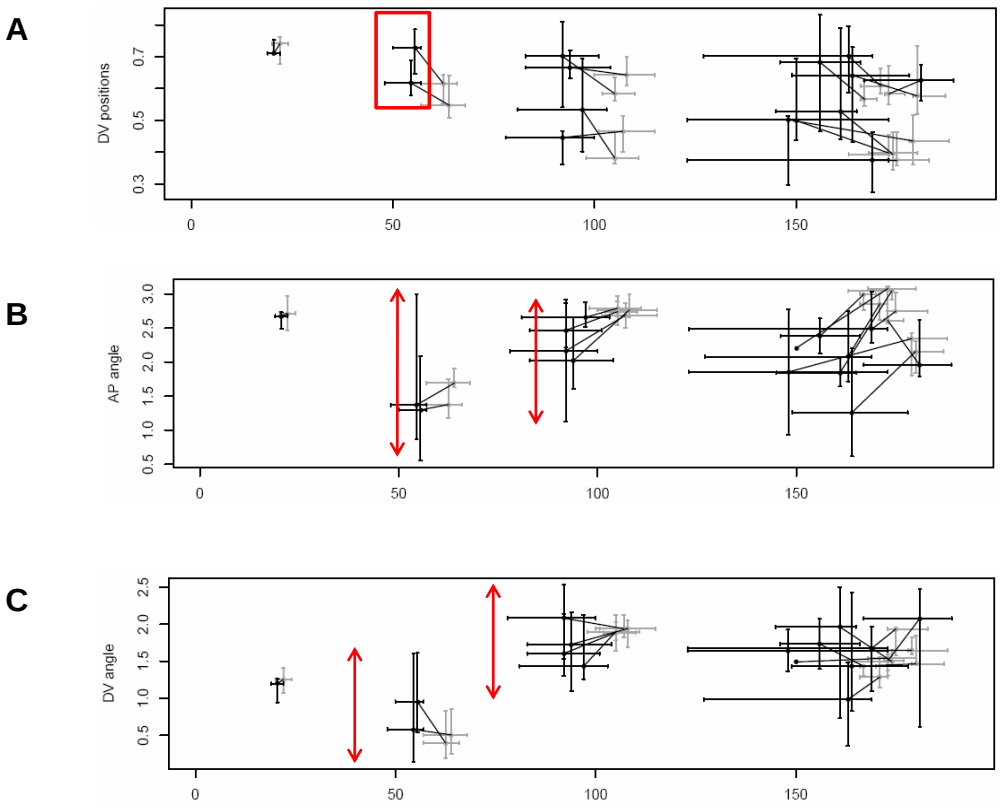

Figure 49: **In *swsn-5 (RNAi)* depleted embryos, E cell descendants show different positioning and division angles.**
On the x-axis, time is displayed in minutes after the ABa cell division. Cell division angles of RNAi depleted embryos are shown in black, of wild-type embryos in gray. Box plots indicate the median (point at center) and extreme values (outer bounds) of n=3 embryos. Plots adapted from Rob Jelier.
(A) Positions of E descendants along the dorsal-ventral axis are shown as fraction of the embryo. Red squares highlight the shift to further ventral positions of E descendants, indicating a defect in ingression.
(B) Division angles [rad] of E cell descendants along the anterior-posterior axis. Arrows highlight an increase in variability.
(C) Division angles [rad] of E cell descendants along the dorsal-ventral axis. Arrows highlight an increase in variability.

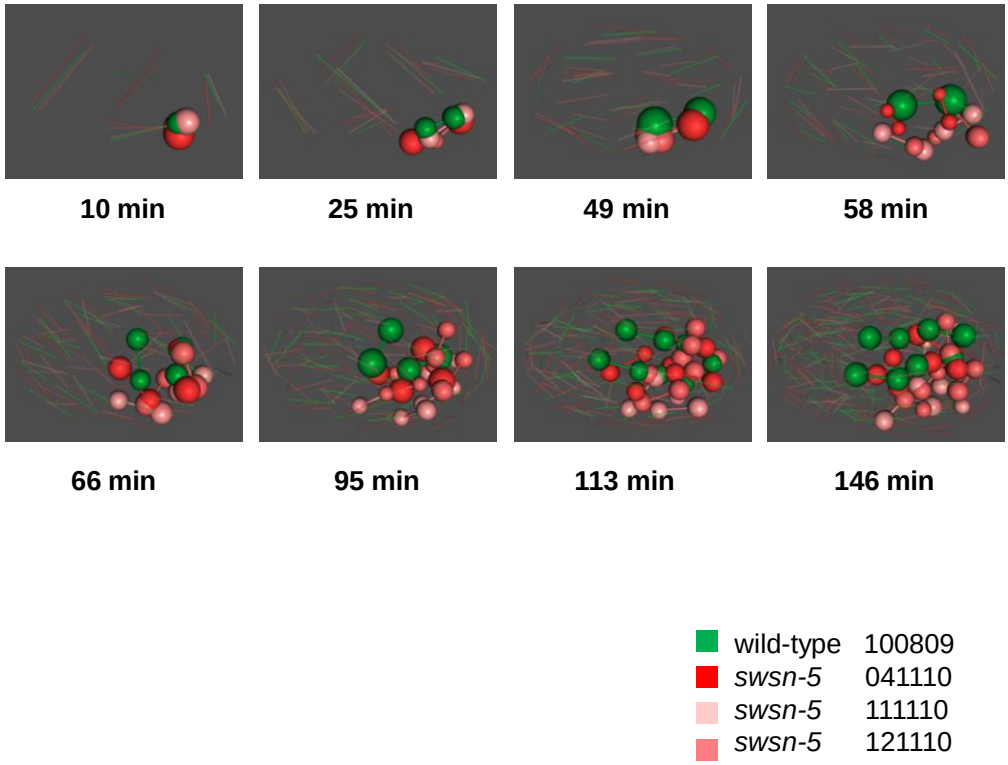

Figure 47: Division angles and positions of E cell descendants are altered in *swsn-5* (RNAi) embryos.
Nuclei of E cell descendants of three different *swsn-5* (RNAi) embryos are displayed as red, light pink and dark pink balls. Wild-type nuclei of the E lineage of one representative embryo are shown as green balls. Other nuclei in the embryo are represented as sticks, connecting sister cell pairs (each end of a stick represent one nucleus). Embryos are aligned with anterior to the left and ventral to the bottom. Time is shown after the four-cell stage.

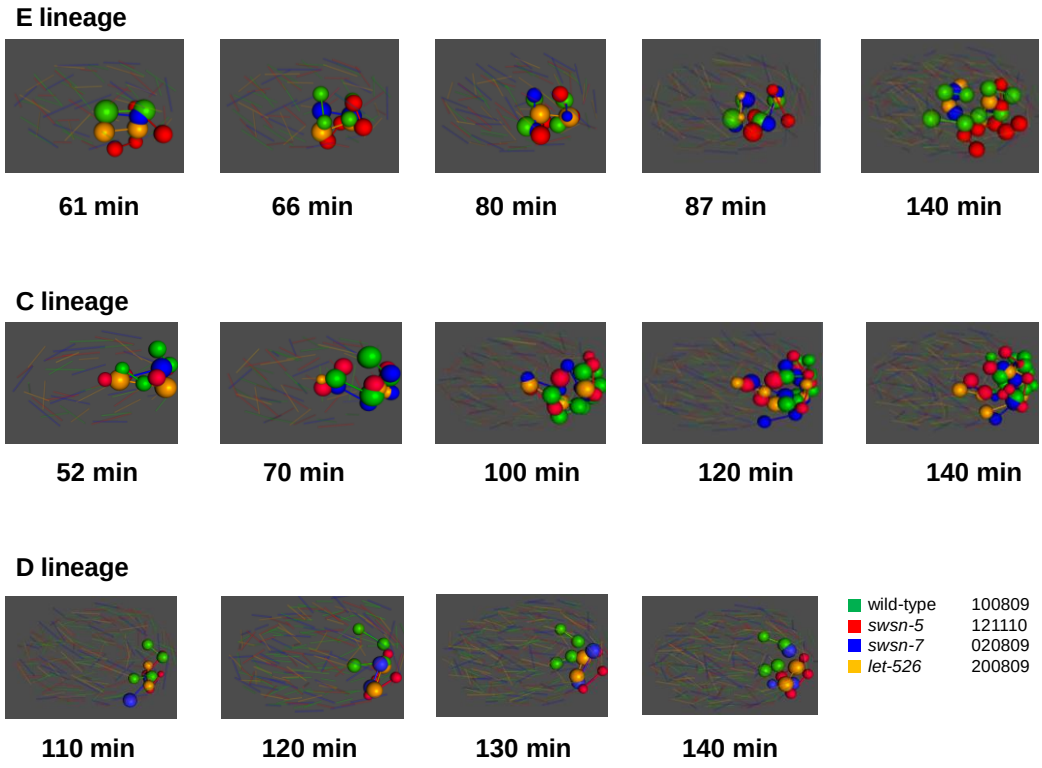

Figure 48: **Division angles and positions of E, C and D cell descendants in *swsn-5, swsn-7, and let-526* (RNAi) embryos.**
Shown are nuclei of one representative embryo for each gene knockdown/wild-type, each depicted in a different color. Each row of images shows descendants of a different lineage displayed as balls. Nuclei of other lineages are represented as sticks in the embryo, connecting sister cell pairs (each end of a stick represents one nucleus). Embryos are aligned with anterior to the left and ventral to the bottom. Time is shown after the ABa cell division.

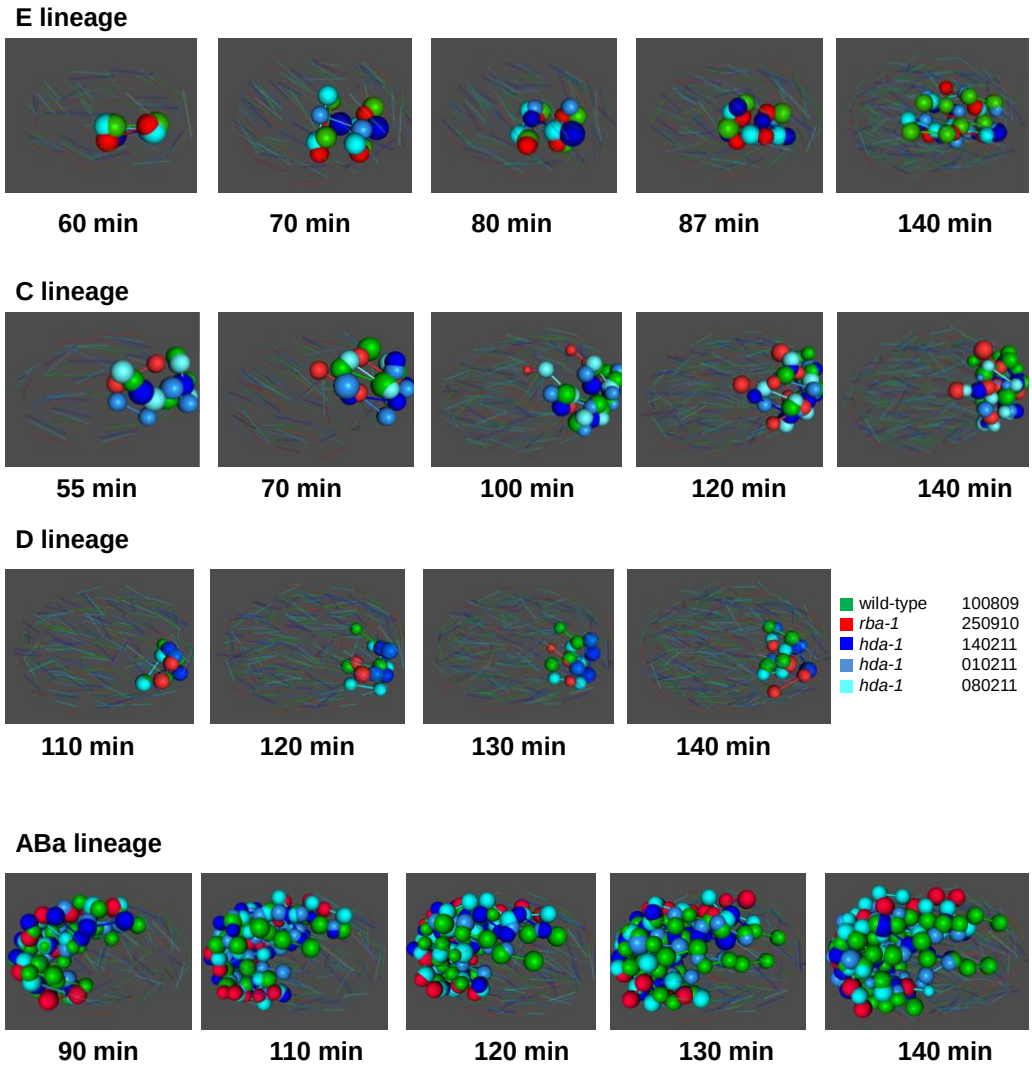

Figure 49: **E, C, D and ABa cell descendants are positioned properly in *hda-1 and rba-1* (RNAi) embryos.**
Nuclei of three different *hda-1* (RNAi) embryos are colored in dark blue, light blue and turquoise. Wild-type nuclei of one representative embryo are shown in green. *Rba-1* (RNAi) nuclei are shown in red. Each image row depicts nuclei of a different lineage as balls. Nuclei of other lineages are represented as sticks in the background, connecting sister cell pairs. Embryos are aligned with anterior to the left and ventral to the bottom. Time is shown after the ABa cell division.

2.4.4.3. Chromatin factors exhibiting phenotypes consistent with a lack of zygotic gene expression

Analysis of *cir-1* RNAi depleted embryos first revealed defects in cells of the E lineage. Cell cycle times of E descendants are strikingly shorter than wild-type (Figure 44). Interestingly, after the forth division, not only E cell cycle lengths are affected. Also a set of AB cell descendants and the P4 cell display shorter life times (Figure 44, blue squares). The same phenotype was observed in embryos depleted of a subunit of Polymerase II, *ama-1* (Figure 44), where transcription is impaired. In addition to altered life times, in *cir-1* and *ama-1* (RNAi) embryos E cells are shifted to more ventral locations, also at later time points (Figure 50 A). Further examination showed that this is due to a failure in E cell ingression (Figure 51). Also the division angles of Ea and Ep are different from wild-type (Figure 50 B and C, Figure 51). The planes of divisions of Ea and Ep seem to lie more orthogonal to the anterior-posterior axis and to the dorsal-ventral axis (Figure 50 B and C). In general, division angles are more variable in cells of the E lineage compared to other lineages in *cir-1* and *ama-1* (RNAi) embryos (Figure 49 B and C, Figure 50).

Also, depletion of both genes affects the division angles of C and D cell descendants. D cells seem to divide further orthogonal to the a-p axis and d-v axis (Figure 52 A and B, Figure 53). The division angles of Ca and Cp seemed to be skewed towards the a-p axis, while division axes of all C descendants appear to be more orthogonal to the dorsal-ventral axis (Figure 54 A and B, Figure

55). Thus, the location of D cells further left in the embryo (Figure 52 C, Figure 53) and of C cells further anterior (Figure 54 C, Figure 55) might be a consequence of the change in division angles. Most likely, there is no more active cell movement at that time in development and cell displacement only takes place by division. As the observed defects are very similar in *ama-1* (RNAi) embryos, we hypothesize a role for *cir-1* in zygotic gene expression.

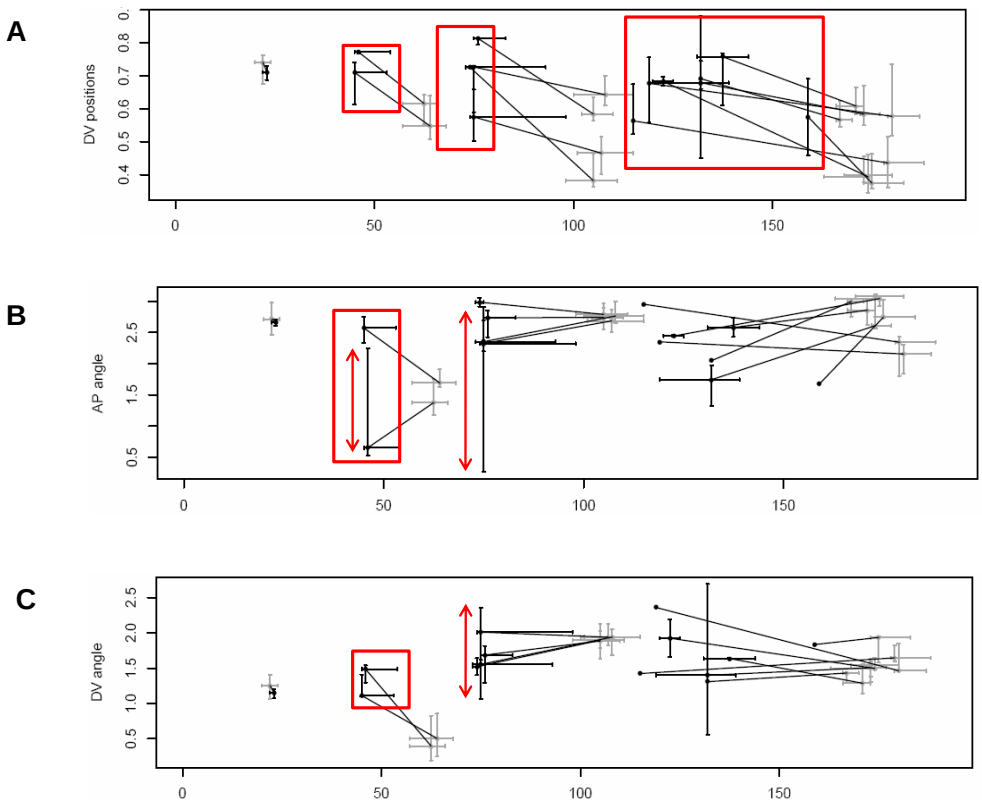

Figure 50: **In *cir-1 (RNAi)* embryos, E cell descendants show different positioning and division angles.**
On the x-axis, time is displayed in minutes after the ABa cell division. Cell division angles of RNAi depleted embryos are shown in black, of wild-type embryos in gray. Box plots indicate the median (point at center) and extreme values (outer bounds) of n=3 embryos.
(A) Positions of E descendants along the dorsal-ventral axis are shown [fraction of embryo]. Red squares highlight the more ventral positions of E descendants, indicating a defect in ingression.
(B) Division angles [rad] of E cell descendants along the anterior-posterior axis are shown. Arrows highlight an increase in variability.
(C) Division angles [rad] of E cell descendants along the dorsal-ventral axis are displayed. Arrows highlight an increase in variability. The red square marks the further ventral position of Ea and Ep.

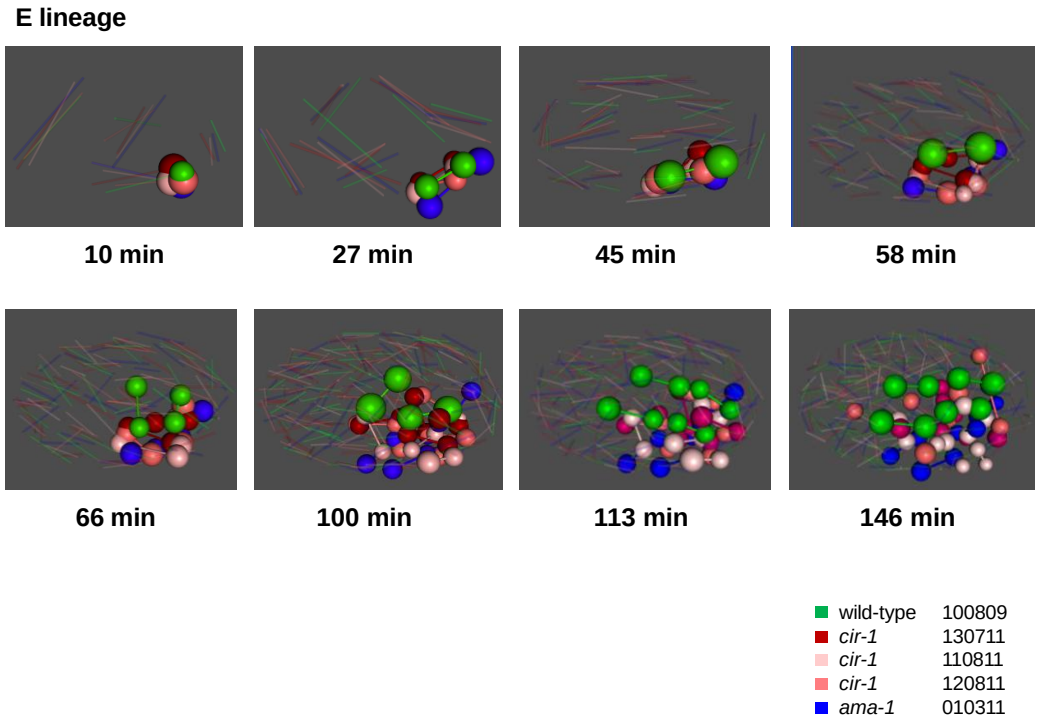

Figure 51: **In *cir-1 and ama-1 (RNAi)* embryos, E cell descendants do not ingress and exhibit variable division angles.**
Nuclei of three different *cir-1* (RNAi) embryos are colored in dark red, light and dark pink. Wild-type nuclei of one representative embryo are shown in green. Nuclei of one representative embryo *ama-1* (RNAi) embryo are shown in blue. Balls depict nuclei of the E lineage. Lines between balls connect sister nuclei. Nuclei of other lineages are represented as sticks in the background, connecting sister cell pairs (each end of a stick represents one nucleus). Embryos are aligned with anterior to the left and ventral to the bottom. Time is shown after the four-cell stage.

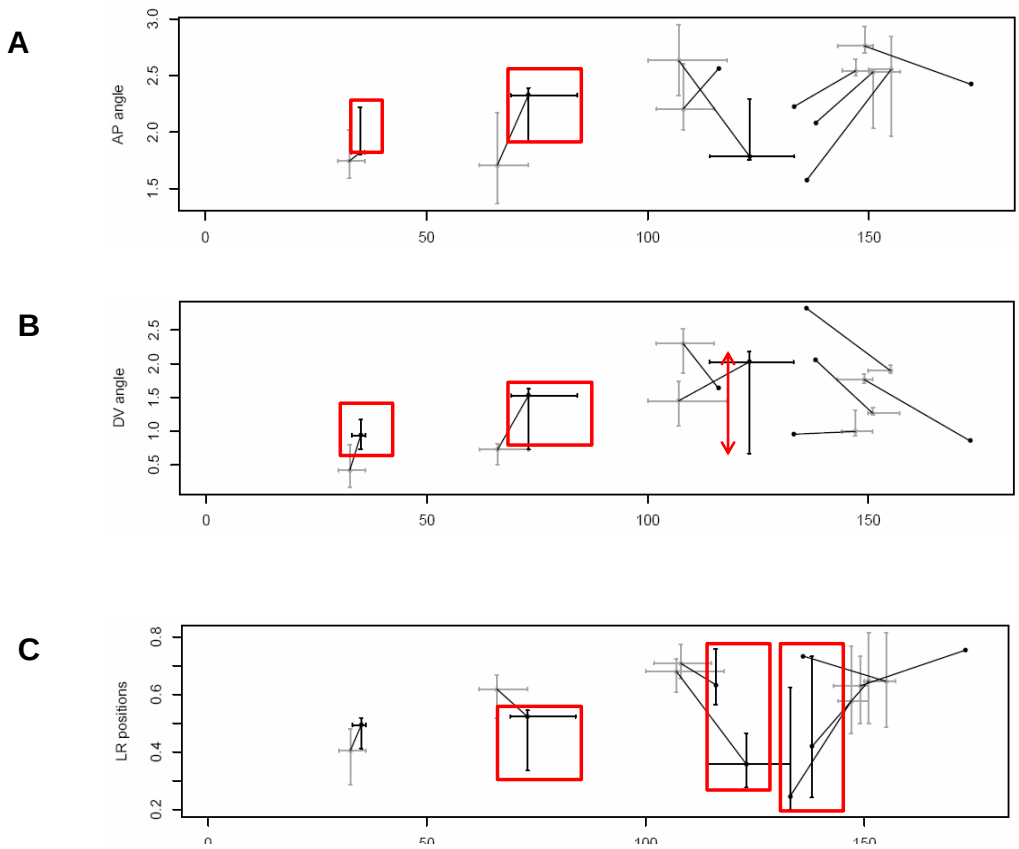

Figure 52: **In *cir-1 (RNAi)* embryos, D cell descendants show different positioning and division angles.**
On the x-axis, time is displayed in minutes after the ABa cell division. Cell division angles of RNAi depleted embryos are shown in black, of wild-type embryos in gray. Box plots indicate the median (point at center) and extreme values (outer bounds) of n=3 embryos. (A) Division angles [rad] of D cell descendants along the anterior-posterior axis. Red squares highlight the shift directed further orthogonal to a-p. (B) Division angles [rad] of D cell descendants along the dorsal-ventral axis. Red squares highlight the shifted division angles to further orthogonal to d-v. The red arrow depicts an increase in variability. (C) Positions of D descendants along the left-right axis [µm]. Red squares highlight the shift in positioning of D descendants towards the left side of the embryo.

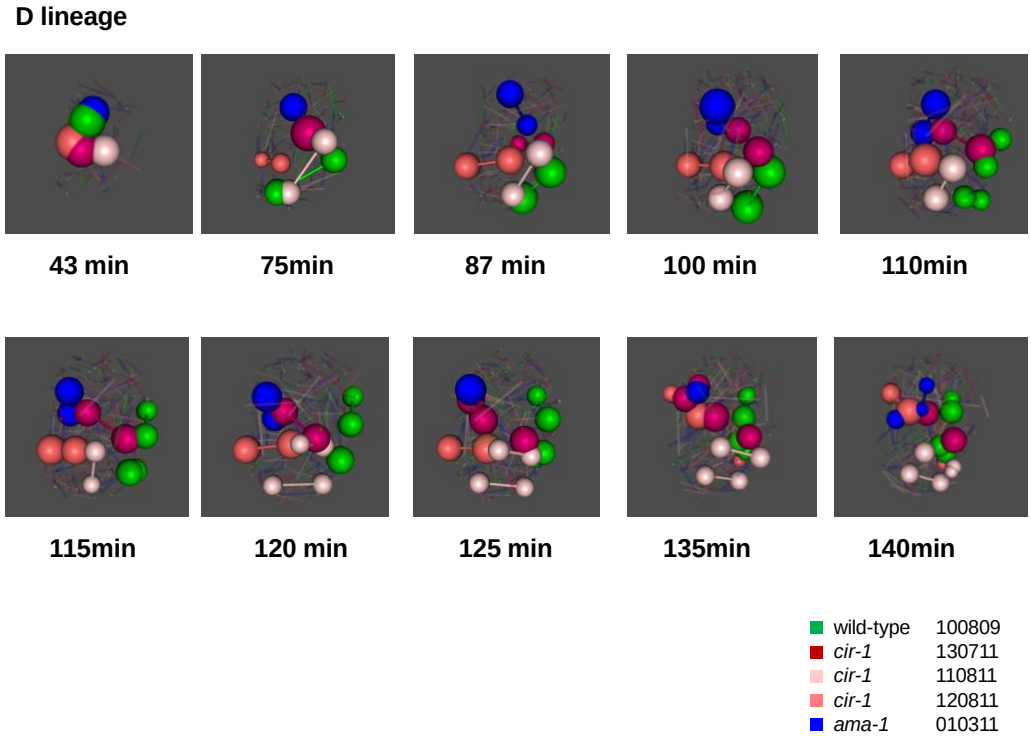

Figure 53: **In *cir-1 and ama-1 (RNAi)* embryos, D cell descendants do not ingress and exhibit variable division angles.**
Embryos are shown as looking from the posterior end, with ventral to the bottom and dorsal to the top. Time of development is indicated below each picture, counting from the ABa cell division on. Nuclei of three different *cir-1* (RNAi) embryos are colored in dark red, light and dark pink. Wild-type nuclei of one representative embryo are shown in green. Nuclei of one representative embryo *ama-1* (RNAi) embryo are shown in blue. D lineage nuclei are highlighted as balls, with lines connecting sister nuclei. Nuclei of other lineages are represented as sticks in the background, connecting sister cell pairs.

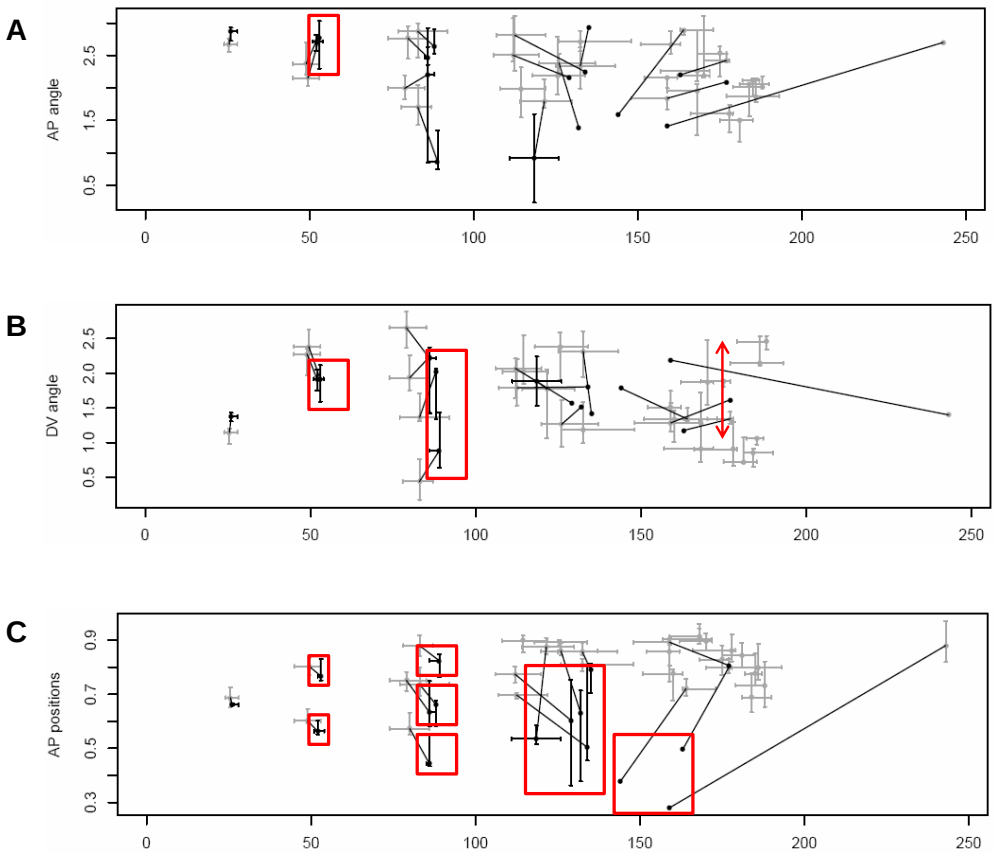

Figure 54: **In *cir-1 (RNAi)* embryos, C cell descendants show different positioning and division angles.**
On the x-axis, time is displayed in minutes after the ABa cell division. Cell division angles of RNAi depleted embryos are shown in black, of wild-type embryos in gray. Box plots indicate the median (point at center) and extreme values (outer bounds) of n=3 embryos.
(A) Division angles [rad] of C cell descendants along the anterior-posterior axis. The red square highlights a skew towards the a-p axis.
(B) Division angles [rad] of C lineage cells along the dorsal-ventral axis. Red squares highlight the further orthogonal (to d-v) division angle. The red arrow shows an increase in variability.
(C) Positions of C descendants along the anterior-posterior axis [fraction of embryo]. Red squares highlight a shift of C descendants towards the anterior side of the embryo.

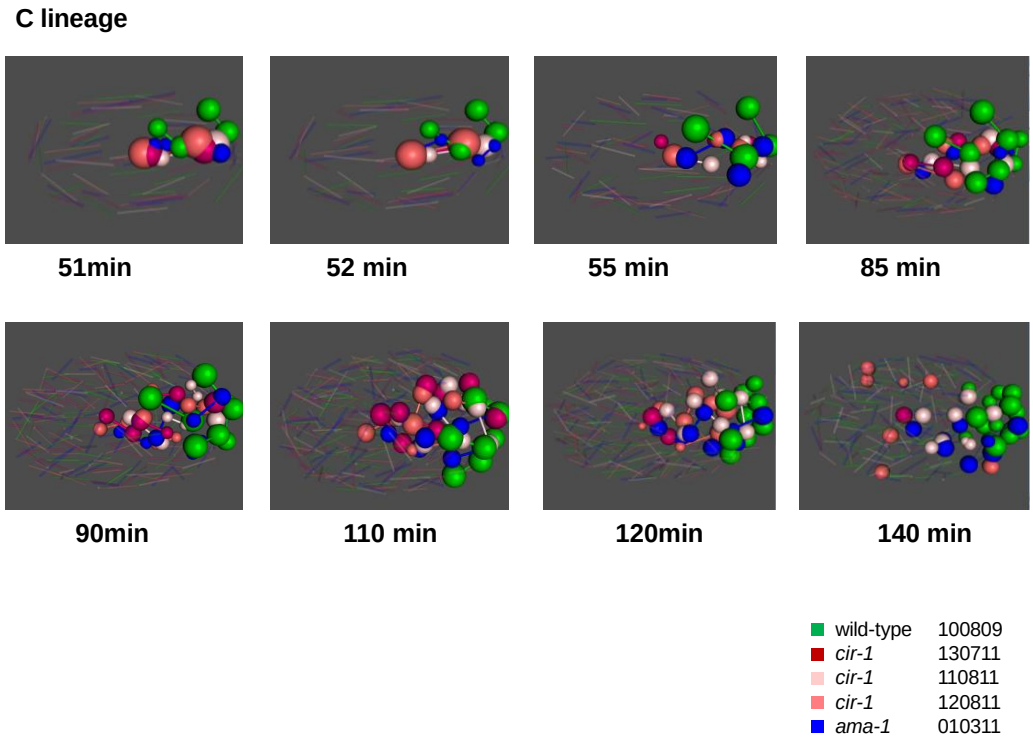

Figure 55: **In *cir-1 and ama-1 (RNAi)* embryos, C cell descendants do not ingress and exhibit variable division angles.**
Nuclei of three different *cir-1* (RNAi) embryos are colored in dark red, light and dark pink. Wild-type nuclei of one representative embryo are shown in green. Nuclei of one representative embryo *ama-1* (RNAi) embryo are shown in blue. C lineage nuclei are highlighted as balls, with lines connecting sister nuclei. Nuclei of other lineages are represented as sticks in the background, connecting sister cell pairs. Embryos are aligned with anterior to the left and ventral to the bottom. Time is shown after the four-cell stage.

3. Discussion

3.1. New insights into *C. elegans* gastrulation

The results presented in this thesis provide new insights into the behavior of gastrulating cells in *C. elegans.* We identified cells that have previously not been known to internalize as well as previously undescribed cell behaviors.

By following cells systematically during embryogenesis we confirmed the previously reported internalization of many cells of the AB derived nervous system [92] (Table 2, Figure 16, Figure 17 and Figure 18 B). Seven of the eight reported precursor cells (that give rise to 60 neurons) were observed to ingress. ABprpaap descendants however, were not found to internalize. In addition to the previously reported 66 cells that gastrulate, we could identify additional early internalizations of AB derived precursors of the nervous system, hypodermis, arcade cells and pharynx. Also, we found several cells that end up in the interior of the embryo because of an oriented cell division, not because of an ingression movement (Table 3, Figure 18 A, Figure 19 and Figure 20).

Unexpectedly, we observed that movements during gastrulation are not restricted in direction into the interior of the embryo (ingressions), but can also take place in the opposite direction, from the inside to the outside (egressions). Cell lineages that undergo both directional movements, i.e. first internalize and then continue to move until finally reemerging on the surface, we considered to “transgress” or “tunnel” through the embryo. Many of

the previously described ingressing cell lineages were found to egress again at later time points (Table 2, Figure 16, Figure 17 and Figure 18 B). Other cells, were internalized by division, and egressed immediately afterwards, thus only carrying out the externalization movement (Table 3, Figure 17 and Figure 19 B). The observation of these unexpected cellular displacements together with a detailed and precise characterization of movements will provide the basis for a deeper understanding of the interplay between single cell and global movements during gastrulation in the pre-morphogenetic embryo.

3.1.1. Egressions are directed cell movements

By closer inspection of surrounding cell groups we found that some cells ingress and egress exclusively in between specific neighboring cells. In particular, comparing between compressed and uncompressed embryos reveals that cellular egressions always occur between specific cell groups, even when the positions of these groups differ relative to the site of ingression. For example, ABalaap and ABalapp descendants always egress between the anterior ABara and ABarp lineages (Figure 16B) and ABalpppa and ABalpppp always egress amongst ABpl descendants (Figure 17 B and C). The differing paths of transgressing cells in compressed and uncompressed embryos demonstrate that cellular transgressions are directed movements.

3.1.2. Ingressions and egressions might drive global cell movements

By further studying the global movements associated with these specific cell displacements, we observed that some egressions are likely a consequence of ingressions of other cells that clear them out of the way. For example, the egression of ABalaap/ABalapp occurs as MS descendants move to the interior of the embryo and further dorsal (Figure 16 C). MS descendants seem to push ABalaap descendants to the dorsal surface. As a further consequence, ABara and ABarp make space for egressing ABalaap descendants and move towards the ventral and dorsal midlines, respectively. Thus, this egression might serve the purpose to move other cells, switching their relative positions. ABalpppa and ABalpppp descendants showed a similar behavior and appear to reemerge on the anterior-ventral surface due to MS cell movements (Figure 17 C). Thus, although it is not clear what exactly powers egression movements, at least in some cases it could be the ingression of other cells.

Coinciding with the egression of ABarpapa/p and ABalppa, in a compressed embryo a sheet of cells primarily consisting of ABpl descendants becomes displaced towards the anterior-ventral-left side of the embryo (Figure 17 C). Thus, the egressions of ABarpapa/p and ABalppa might initiate the rotation movements of the ABpl group of cells. Similar movements can be observed for ABplppap, which ingresses from the lateral left surface as ABpl cells move more ventral during their rotation (Figure 18 B). Moreover, the ingression movements of ABalpppa/p on the left of

the embryo precede the initial movements of the most ventral ABalp cells towards the future ventral surface. The strikingly coinciding movements suggest a precisely orchestrated interplay between left/ventral ingressions, right/dorsal egressions, and the global rotations of cell groups.

3.1.3. Cellular ingressions differ between compressed and uncompressed embryos

Interestingly, we observed differences in ingressions between compressed and uncompressed embryos. ABalpppa and ABalpppp consistently ingress as a pair but in uncompressed embryos, ingression is led by ABalpppp, whereas in compressed embryos the movement is led by the anterior cell ABalpppa (Figure 17 D). Similarly, descendants of ABarpppp emerge onto the surface only in compressed embryos. The differential positioning of cells in compressed and uncompressed embryos is likely to be the cause of these differences, maintaining correct relative cellular positions. In addition, at least some of the observed egressions in compressed embryos are likely to be caused by other internalizing cells pushing them out of their way as a consequence of increased cell crowding.

3.2. Regulative cell movements during gastrulation confer robustness to physical compression

After the 4th division round, approximately 80 minutes after the four-cell stage, the spatial constraints result in substantial cellular crowding in compressed embryos. This is especially true in the anterior part of the embryo and may contribute to the large-scale embryonic rotation that occurs during the following 40 minutes (80-120 minutes after the four-cell stage). This rotational movement re-positions ABarp descendants stereotypically from the right to dorsal locations by ~90 degrees. Concomitantly, ABpl cells are moved by ~90 degrees from the dorsal to the left side of the embryo. Thus, at approximately the 200-cell stage, in compressed embryos new LR and DV axes are established which are rotated ~ 90 degrees from the original axes defined at the four-cell stage (Figure 26 and Figure 27).

In addition to the cellular crowding, spatial constrains lead to distorted division angles and cell positioning in compressed embryos, as already apparent at the four-cell division (Figure 25). The result is that the relative positions of cell groups differ between compressed and uncompressed embryos. In order to correct for these displacements, a series of later rearrangements occur repositioning cells and resulting in a ~90 degree rotation in the overall LR and DV axes. These corrective movements start with a change in the division angle of the ingressed intestinal precursor cells, Ea and Ep. In compressed embryos, these cells divide along the initial DV axis, aligning the E descendants in a plane parallel to this axis instead of orthogonal, as observed in uncompressed

embryos. At this time, MS cells are mis-localized by division (not by active movements), at positions further left and dorsal than in uncompressed embryos (Figure 27). Thus, they are already placed in the correct relative position to the four differentially aligned E cells, indicating that they may be instructive in specifying the Ea and Ep division angles. During the following movements and divisions, all cells appear to align according to the newly orientated E cell plane that is with the axes defined by the E and MS lineages. This might imply that the embryonic 'outside' aligns to the 'inside' to resolve contradictions in relative cell positioning between different cell groups.

Taken together, these observations suggest a regulatory mechanism that aligns cells properly even when division angles and relative cell positions are perturbed due to external compression. Without such compensatory movements, compression of the embryo would likely cause lethality as the relative positions of cell groups are altered and this would interfere with subsequent morphogenesis and tissue differentiation. We therefore propose that these regulative movements are an intrinsic 'design principle' of *C. elegans* embryogenesis, conferring robustness to mechanical deformation.

Most likely it is the combination of physical forces (pushing due to spatial constraints) together with the need to preserve the correct relative cell positions within the embryo (signaling between cell groups for correct movements and development), leading to the substantial embryonic rotation that re-defines the DV and LR axis. This connects gastrulation movements with an important

compensation mechanism for the correct positioning of cells in response to external compression.

Further systematic analysis of the differences in ingression and egressions between compressed and uncompressed embryos will help to explain differential global movements and rotation behaviors. In addition, analysis of cortical tensions and forces underlying ingressions and egressions of single cells as well as of global cellular rearrangements might give further hints into the mechanisms of observed movements. Moreover, by performing cell ablation experiments it should be possible to determine which cells are instructive or powering the rotation movements. For example ablation of the Ea and Ep cells to prevent their division and ablation of the MS cell would test the hypothesis that these cell groups specify the final LR and DV axes of the pre-morphogenetic embryo.

It has previously been shown that otherwise equivalent cells (by fate), display differential movement behavior due to different cortical morphologies and actomyosin dynamics [45]. Thus it is possible that the pronounced rotational behavior of cells in compressed embryos is caused by mechanical differences between cells. The spreading of cells is usually accompanied by the formation of apical NMY-2-cap–like structures and cortical flow. Cortical flow originates from dynamic contractions of actomyosin, thus reflecting the contractility of cells [8]. By analyzing the distribution of non-muscle myosin NMY-2 in moving cells one could reveal mechanical asymmetries. Alternatively, perturbation of cortical actin dynamics by depleting WAVE-Arp2/3 complex

components, required for polymerization of branched actin filaments and for strengthening of the cortex, might give insights into the mechanism of global cell movements.

In future work, the systematic study of ingression and egression patterns and the balance of forces might enable one to predict the scale of rotations and movements. Open questions are how differences in ingression between compressed and uncompressed embryos explain the LR-DV axis rotation and how ingressions drive global cellular movements. These might be addressed by systematical analysis of variable movement defects in pleiotropic mutants, such as the chromatin factors described in the following section, and by perturbation of cytoskeletal components and signaling pathways.

The results obtained in this study set the foundation for dissecting the molecular mechanisms underlying adaptive cell movements. As the molecular basis for this fascinating robustness mechanism is completely unknown, it is a highly interesting area for future studies.

3.3. Systematic and quantitative analysis of the functions of chromatin factors in *C. elegans*

Genome-wide reverse genetic screens have identified chromatin regulators required for the early development of *C. elegans*. However the exact role of these proteins in cell division and embryogenesis is often not known. For these reasons, chromatin

regulators were interesting targets for a directed candidate approach in the course of this study. Using the semi-automatic tracking method described in the previous chapter allowed us to quickly detect defects in nuclear positions, movements and division angles, and so to describe the *in vivo* functions of these chromatin regulators.

In *C. elegans, o*ver 70 chromatin factors have been characterized either functionally or genetically [300]. Among these, 22 genes targeted by the Kamath library [168, 318], had high penetrance embryonic lethal RNAi phenotypes.

Analysis of time-lapse Nomarski and fluorescence microscopy of histone-GFP expressing embryos allowed us to subdivide the chromatin factors analyzed according to their phenotype: one group contains factors affecting chromosome behavior during mitotic cell divisions. Factors attributed to the second group had other cell cycle defects or affected particular cell groups and are discussed in the following section.

3.3.1. Many essential chromatin factors are required for cell division

By visualizing cell divisions we could observe that knockdown of many of the genes examined eventually leads to duplication of chromosome sets and polyploidy with enlarged nuclei (Figure 30, Table 12). In fact, depletion of all factors that lead to a delay in cell cycle timings (see next chapter), also show a mitotic phenotype. However, after depletion of some factors (SWI/SNF factors, *set*-

16), prior to division failures, other defects such as cell mis-positioning are observed.

Gene	Subunit of complex	Brief description	Cell division defect
lin-53	NuRD/CHD, ISWI/NURF, CAF1, HDAC, PRC2/EED-EZH2, DRM	Rb associated protein 48, NuRF55/CAF1/MSI1 ortholog	Early condensation and segregation defects
rba-1	NuRD/CHD, ISWI/NURF, CAF1, HDAC, PRC2/EED-EZH2	Rb associated protein 48, NuRF55/CAF1/MSI1 ortholog	Late segregation defects, unequal distribution of chromosomes
hda-1	NuRD/CHD, HDAC	Histone deacetylase RPD3	Later segregation defects, unequal distribution of chromosomes
egl-27/ lin-40	NuRD/CHD	MTA1	No mitotic phenotype
let-526	SWI/SNF	Iss-4	Late segregation defects
swsn-5	SWI/SNF	SNF5/Ini1	Late segregation defects
swsn-7	SWI/SNF	Predicted transcript.regulator	Late segregation defects
set-16	MLL (H3K4trimethylase)	Polycromb domain	Late segregation defects
cir-1		CBF1-interacting corepressor	Division arrest
F55A3.3	FACT	Global transcript. regulator, division control protein	Early segregation defects
hmg-3	FACT, POB3	Nucleosome binding factor SPN	Late segregation defects

Table 12: Summary of analyzed chromatin factors and their segregation phenotypes (www.wormbase.org).

In *rba-1* depleted embryos, condensation and segregation delay and failure are the first defects observed and occur concomitantly (Figure 30). Depending on the efficiency of the RNAi knockdown, partially condensed chromosomes fail to segregate to opposite poles between the 30- to 80-cell stage. The chromosomes then frequently de-condense, and cells appear to leave mitosis without cytokinesis. (Figure 30) This cytokinesis defect results in enlarged nuclei with polyploid genomes. A similar defect late in the cell cycle was observed for *hda-1*. As no DNA condensation, segregation or cytokinesis defect was observed in the early

cleavages, *rba-1* and *hda-1* do not seem to play a role in early cleavages or may act redundantly with other genes in early divisions. Alternatively, the late onset of observed defects might be due to a less efficient RNAi knock down.

These defects observed are consistent with previously described phenotypes of the protein homologues in other species.

RBA-1 is a homologue of the human retinoblastoma (Rb) – associated protein RbAp46/48, a subunit of many different chromatin remodeling complexes [319]. RbAp46/48 proteins belong to the class of WD40 proteins (40 times Trp and Asp amino acid repeats), a sequence motif that forms the basis for beta-propeller structures and enables the formation of protein interaction surfaces [320]. In fission yeast, two centromeric proteins, Mis15 and Mis16, show a strong similarity with human RbAp48 and RbAp46. Mis15 and 16 are part of the CENP-A recruitment pathway, forming the most upstream factors in kinetochore assembly [321]. Their described mutant phenotype is unequal segregation of chromosomes, generating aneuploid cells that undergo a few rounds of divisions but lose viability. Mis16 and Mis18 form a complex that is required for maintaining histones in the central domains of centromeres in a deacetylated state [321]. The human homologues of Mis16, RbAp 46 and RbAp48, are thought to influence chromatin assembly and remodeling and are also required for proper localization of CENP-A. In HeLa cells, CENP-A recruitment is abolished after depletion of both RbAp46 and RbAp 48 together, but not after single depletion [321]. These

phenotypes are consistent with the segregation defects observed for *rba-1* in this study and imply a similar function in *C. elegans*.

HDA-1 is a histone deacetylase with similarities to the RPD3 histone deacetylases from yeast and fly. In *C. elegans,* its function in cell migration and axon guidance has been reported [322]. Together with RBA-1 it is a predicted subunit of the NURD complex. The NURD complex contains the histone deacetylases HDAC-1 and HDAC-2, RbAp46/48 (Rb-associated proteins), CHD-3 and/or CHD-4 (highly similar chromodomain helicase proteins), MDB-3 (similar to methyl-CpG-binding proteins) and several uncharacterized polypeptides [285, 323-325]. All NURD subunits are highly conserved, and several orthologues may exist for each subunit. In *C. elegans*, at least two different NURD complexes exist, that contain LIN-53/RbAP and HDA-1/HDAC but not RBA-1/RbAP. One of these complexes also contains LET-418 as the CHD component. LET-418 was found to be required for the down-regulation of a subset of 44 early expressed genes that are specifically enriched in mitotic and meiotic functions [326]. Together with our observations of segregation defects after depletion of predicted subunits of the NURD complex, this implicates a role for at least some specific NURD complexes, in cell division. The existence of multiple genes encoding similar yet distinct subunits may allow to alter the protein composition of different NURD complexes and play an important role in regulating and fine tuning their various cellular functions. This might also explain the different segregation phenotypes observed for different NURD subunits in this study.

Embryos depleted of another predicted NURD complex subunit, *lin-53* (in contrast to *rba-1* and *hda-1* (RNAi) embryos) show early onset of condensation and segregation defects with characteristic chromosome bridges as discussed in the following section. *F55A.3.3*, a member of the FACT complex, also exhibits early segregation defects. In contrast*, hmg-3*, the other predicted FACT subunit studied here, exhibits segregation defects after the 200-cell stage. The later onset is most likely due to a less efficient RNAi knockdown as embryonic lethality of *hmg-3* (RNAi) is observed in only about 30% of embryos (Figure 6). As cellular defects arising at late stages are difficult to characterize because cells are already very small and at the limit of image resolution, we chose *F55A3.3.* and *lin-53* for a more detailed characterization.

F55A3.3. is known to be a global transcriptional regulator and cell division control protein. It is a predicted component of the abundant nuclear FACT complex, which was originally identified in mammalian systems as a factor required for transcription elongation on chromatin templates. FACT is composed of two proteins that are evolutionarily conserved in all eukaryotes and homologous to mammalian SPT16 and SSRP1 [327, 328]. In metazoans, the SSRP1 homologue contains an HMG domain; however in fungi and protists, it does not. For example, in *S. cerevisiae* the Pob3 protein is homologous to SSRP1 (and F55A3.3), but lacks the HMG chromatin binding domain. Instead, the yeast FACT complex of Spt16p and Pob3p, binds to nucleosomes occupied with multiple copies of the HMG-domain containing protein Nhp6p, but isolated Nhp6p fails to form a stable

complex with the Spt16p/Pob3p heterodimer [329]. Pob3 has been shown to facilitate RNA Polymerase II transcription initiation and elongation by destabilizing the interaction between the H2A/H2B dimers and the H3/H4 tetramers of the nucleosome and reassembling nucleosomes after passage [327, 330-332]. By this activity, it also plays a role in DNA replication and other processes that require efficient passage through chromatin [331]. Additionally, a function in DNA damage response has been suggested [333].

lin-53 encodes a class B SynMuv protein containing a 7 WD40-repeat similar to the mammalian homologue RbAp48/48 and is a paralog of *rba-1*. Interaction between LIN-53 and LIN-9 is important for the incorporation of LIN-53 into the DRM complex. A complete loss of LIN-53 disrupts DRM complex formation and results in the degradation of other complex members. Null mutations in lin-53 lead to a decrease in protein levels of other DRM complex components, including LIN-9, LIN-37, LIN-52, and LIN-54 for transcriptional repression. LIN-53 is present in both the DRM complex and a NuRD-like complex, and like its mammalian orthologues may be a component of many different chromatin remodeling complexes [282].

3.3.2. F55A3.3 and LIN-53 are required for chromosome segregation

To semi-quantitatively assay the segregation defects observed, we monitored chromosome dynamics of RNAi embryos expressing

either the GFP::H2B fusion protein, alone or in combination with a GFP::TBB-2 fusion protein, marking the mitotic spindle.

At first glance, *F55A3.3* and *lin-53* both exhibited similar RNAi phenotypes. Formation of anaphase chromosome bridges could be detected between the one- to four-cell stage and was observed throughout following cell divisions until arrest occurred at approximately the 30-cell stage. Depletion of both genes delayed the onset of a new cell division cycle to a similar extent, causing a progressive developmental delay (Figure 31 and Figure 32).

Despite these similarities, closer inspection of chromosome dynamics revealed differences between the RNAi phenotypes of the two genes. In *lin-53* (RNAi) embryos condensation of chromosomes could not be observed (Figure 32 and Figure 33). In *F55A.3.3* (RNAi) embryos however, condensation is delayed but takes place, reaching wild-type levels of compaction (Figure 32 and Figure 33). To understand the molecular basis for these differences in phenotype, we compared chromosome dynamics and segregation defects to the ones observed after depletion of well-characterized cell division proteins.

The *F55A.3.3* (RNAi) condensation and segregation phenotype resembled that of *hcp*-4/CeCENP-C depleted embryos (RNAi) (Table 7, Figure 33). CeCENP-C is upstream of all known kinetochore components except for the centromeric protein CeCENP-A [33, 182]. Depletion of *F55A3.3* and *hcp-4*, both slowed condensation, but did not inhibit it. Also, sister kinetochore resolution was impaired, which normally occurs after condensation is complete. For CeCENP-C, this is consistent with the reported

phenotype [182, 197]. Thus, we speculate a possible involvement of F55A3.3 in the regulation of cell division at the level of CENP-C. Condensation and segregation defects in *lin-53* depleted embryos were similar to the ones observed when the SMC-4 subunit of the condensin I and II is depleted. *C. elegans* possesses two mitotic condensin complexes, I and II. The mitotic Condensin I complex plays a role in chromosome segregation, whereas condensin II has functions in chromosome condensation and segregation [191, 194]. Strikingly, impairment of chromosome condensation appeared to be more severe in *lin-53* depleted embryos than in *smc-4* (RNAi) embryos. In *lin-53* (RNAi) embryos, condensation and distinguishable chromosomes were not visible. In *smc-4* depleted embryos, condensation was delayed but some abnormal compaction was achieved. Before alignment at the metaphase plate, distinct compacted chromosomes were visible (Figure 32, Figure 33, Table 9). This observation is consistent with the condensin phenotype described in the literature and indicates the action of condensing-independent factors that can compact mitotic chromatin [194]. Thus we asked whether LIN-53 might act in an alternative condensation pathway.

3.3.3. *lin-53* might function in assembling centromeric chromatin during condensation and segregation

To address the question whether LIN-53 belongs to the factors that can compact chromatin in the absence of condensin, we analyzed early cell divisions of embryos carrying a GFP fusion of

the Condensin I complex subunit CAPG-1. We found signal for Condensin I delocalized in embryos depleted of each chromatin factor and cell division protein examined. This was likely due to uncompacted chromatin at prophase and lagging chromosomes at anaphase, denoting a secondary defect.

Yet, signal appeared to be dimmer in five out of eight condensin depleted embryos (Figure 36, Table 9) compared to wild-type, *lin-53* and *F55A3.3* (RNAi) embryos. This hints at an impaired loading of Condensin I on chromatin. However, it cannot be entirely ruled out that the lower GFP signal in *smc-4* (RNAi) embryos is caused by variability in expression of the transgene.

Unfortunately, we were not able to confidently test the loading of Condensin II onto chromatin. Condensin II is the actual complex important for condensation. Thus, it might be that *lin-53* is involved in Condensin II dependent compaction of chromatin, but not Condensin I. However, antibody staining of MIX-1 (preliminary data, not shown), a subunit present in both Condensin I and II complexes, showed a wild-type staining pattern in *lin-53* (RNAi) embryos but not in *smc-4* depleted embryos. Thus, it is possible that the condensation defect in *lin-53* (RNAi) embryos is independent of condensin.

Comparison with published data hints at a possible role for *lin-53* in the CENP-A dependent condensation of chromatin. CENP-A is the centromeric histone H3 variant forming the structural base for the kinetochore. It has been shown that after its depletion, condensation is highly aberrant in *C. elegans* embryos. No condensation is observed during primary condensation, yet

coincident with the secondary condensation phase in control embryos, the chromatin is abruptly compacted [197]. Although we did not clearly distinguish between primary and secondary condensation phase due to limited resolution of our time-lapse series, the described CENP-A phenotype appears similar to the one observed in *lin-53* (RNAi) embryos. In *lin-53* depleted embryos, no condensation is observed however, a defined metaphase plate is visible, indicating some kind of abrupt chromosome arrangement.

In the same study [197], the condensation defect due to depletion of CENP-A was reported to be less severe than after depletion of *smc-4*/condensin. This is in contrast to our observations comparing *lin-53* and *smc-4* (RNAi) defects and argues against our hypothesis. Yet, the difference could be explained by different experimental setups leading to different efficiencies in RNAi knockdown. In our study, we performed RNAi by feeding worms bacteria that express the dsRNA, leading to the knockdown of the target gene. Maddox *et al*. [197] depleted genes by injection of dsRNA, which likely gives rise to stronger RNAi phenotypes. Unfortunately, we were not able to analyze CENP-A depleted embryos to compare phenotype severity, as the bacterial clone led to sterility of the worms.

The effect of depleting the kinetochore component *hcp-4*/CeCENP-C on chromosome condensation has been described to be clearly less severe than depleting *hcp-3*/CeCENP-A [197]. It can therefore be assumed that the CeCENP-A function in condensation is independent of its requirement for kinetochore

assembly. We also observed a stronger effect on condensation after *lin-53* depletion than after CeCENP-C depletion. This further hints at a role for LIN-53 in the organization of condensing chromatin at the level of CeCENP-A. Subsequent segregation defects are similarly in hcp-4/ CeCENP-C (RNAi) and *lin-53* (RNAi) embryos (as well as described hcp-3/CeCENP-A (RNAi) [33, 334], indicating a role for LIN-53 in the correct arrangement of kinetochores for segregation.

Indeed, we observed improper localization of KNL-3::GFP in *lin-53* and *hcp-4* (RNAi) embryos. KNL-3 is the kinetochore component directly downstream of CENP-C and CENP-A. The defects in KNL-3::GFP localization point to impaired kinetochore assembly although it remains to be established at which point upstream of KNL-3 the defect is originated. In addition, it cannot be excluded that the defect is caused by impaired compaction of chromosomes, thus being a secondary defect. In *C. elegans*, AIR-2 is necessary for proper kinetochore assembly and attachment to spindle microtubules [196]. As AIR-2::GFP loading appeared to be normal after depletion of *lin-53 and hcp-4*, the observed kinetochore assembly and segregation defects are unlikely due to impaired AIR-2 loading.

Interestingly, it has been reported that human RbAp48 and RbAp46, which are the mammalian *lin-53* homologues, are both required for proper localization of CENP-A. In addition, the fission yeast RbAp46/48 homologues and centromeric proteins, Mis 15 and -16, are also part of the CENP-A recruitment pathway [321].

Thus, it might be that in *C. elegans, lin-5*3 acts in the CENP-A dependent condensation pathway as well.

In follow-up experiments, it has to be examined whether CENP-A recruitment is affected by *lin-53* depletion (e.g. by antibody staining or GFP marker strains). It will be interesting to establish a precise role for LIN-53 in CENP-A-dependent (or related) condensation and segregation. Although CeCENP-A-containing chromatin accounts for only ~5% of total chromatin [197] [195] it has a substantial effect on condensation. This might be due to an organizational function that helps to structure the chromosome and ensure timely compaction. Additionally, it is possible that centromeric chromatin serves to ensure its final placement on opposing surfaces of sister chromatids, necessary for the proper attachment of sister kinetochores to opposite spindle poles. It remains to be established whether its effect on condensation and chromosomal integrity depends on condensin. It would be intriguing to discover the condensin-independent factors capable of compacting mitotic chromatin. LIN-53 might be one of them.

3.3.4. F55A3.3 might have a similar role as CeCENP-C during cell division

As the *F55A.3.3* (RNAi) phenotype was found to be most similar to that of *Hcp*-4/CeCENP-C depleted embryos (Table 7, Figure 31) we examined the behavior of KNL-3::GFP fusion protein after depletion of *F55A3.3*.

Indeed we observed improper localization of KNL-3::GFP signal, in both h*cp*-4/CeCENP-C and *F55A3.3* depleted embryos. This indicates a defect in kinetochore assembly. It remains unclear at which stage upstream of KNL-3 assembly is inhibited. The observed segregation and kinetochore assembly defects are not due to impaired loading of AIR-2. AIR-2::GFP localization appeared normal after depletion of *F55A3.3*. The observed effect of depleting F55A3.3 on chromosome condensation is clearly much less severe than the reported CeCENP-A phenotype, indicating that the action of F55A3.3. downstream of CeCENP-A. Thus, F55A3.3. is likely to be involved in the regulation/recruitment of CeCENP-C, as it is the only component between KNL-3 and CeCENP-A in the kinetochore assembly pathway.

Interestingly, in humans, the F55A3.3 homologue, together with the other subunit of the FACT complex, has been found to biochemically interact with centromeric CENP-A nucleosomes [335, 336]. In yeast, the FACT complex is required for centromeric-heterochromatin integrity and accurate chromosome segregation [328]. These proposed roles for FACT, together with the results obtained in this study, suggest an involvement of F55A3.3 in kinetochore assembly at a similar stage as CeCENP-C.

The fact that depletion of CeCENP-C as well as F55A3.3 slows condensation is interesting as CeCENP-C is also required for proper sister kinetochore resolution, which normally occurs after chromosome compaction is complete [182]. This suggests that successful resolution of sister kinetochores is dependent of the timely completion of condensation. Alternatively, depletion of

CeCENP-C might inhibit an upstream process required for both a normal rate of primary condensation and sister kinetochore resolution. It will be interesting to distinguish between these possibilities in future work as well as to precisely establish the role of F55A3.3 within the pathway.

3.4. Impaired gene expression results in a re-arrangement of chromatin to the nuclear periphery

Apart from the segregation defects discussed in the previous chapter, analysis of time-lapse recordings of embryos depleted of chromatin factors revealed another interesting phenotype: we observed re-arrangement of chromatin to the nuclear periphery, leaving a `hole` in the nuclear centre. Several factors with (proposed) roles in transcription, such as *ama-1* and *F55A3.3*, or in translation, such as l*et-858* and *cir-1*, were found to exhibit this phenotype with a 'ring'-like arrangement of chromosomes.

let-858 encodes nucampholin, a highly conserved protein rich in acidic and basic residues. It is homologous to the human pre-mRNA-splicing factor CWC22 and displays sequence similarities to the eukaryotic translation initiation factor eIF-5 gamma. In yeast, eIF-5 is associated with the spliceosome [312]. Based upon sequence similarity and its nuclear localization it is likely to be involved in general protein expression [337]. CIR-1 is a nuclear protein homologous to mammalian CIR, a component of the co-repressor complex which associates with CBF1 in mammals [313]. Its homologue in yeast is a constituent of 66S pre-ribosomal particles [314]. CIR-1 is known to interact with proteins involved in RNA biogenesis and cell polarity [300].
ama-1 encodes the large subunit of RNA polymerase II required for mRNA transcription. It is essential for proper embryonic development, particularly for early divisions and migration of the

endodermal precursor (E) cells that initiate gastrulation. AMA-1 is expressed ubiquitously in the developing embryo until the 550-cell stage [311, 338-341]. F55A3.3 is a predicted component of the abundant nuclear FACT complex. It is described as a global transcriptional regulator with additional functions in the regulation of cell division [327, 328, 330-332].

Interestingly, the rearrangement of chromatin in the nuclei of embryos did not lead to an enlargement of the nucleolus that fills the central nuclear volume and forms the apparent chromosome-free 'hole' in germ-line nuclei. Antibody staining with anti-NOP-1/Fibrillin, a specific nucleolar marker, revealed staining patterns similar to wild-type (Figure 41). In contrast, germ-line nuclei exhibited the typical staining pattern with anti-NOP-1 signal concentrated in the enlarged nucleolus (Figure 41 top line).

Antibody staining with anti-NST-1/Nucleostemin, showed NST-1 signal absent from the nucleolus and restricted to the nuclear periphery in both, germ-line nuclei and nuclei of embryos depleted of chromatin factors (Figure B). This is different from the staining pattern observed in wild-type nuclei, where NST-1 is concentrated in the (small) nucleolus. NST-1/Nucleostemin is a homologue of the nucleolar GTPase GNL3. It is known to be enriched in the nucleolus but usually absent from regions where rRNA transcription and processing occurs [315]. In *ama-1* and *let-858* (RNAi) embryos, rRNA transcription and processing might be impaired, which could explain the peripherial localization of the anti-NST-1 signal.

This raises the question about the content of the nuclear center. It is possible that sub-organelles, such as Cajal bodies are deposited there as they are no longer needed for RNA biogenesis. Cajal bodies are spherical sub-organelles of 0.3-1.0 µm in diameter. They are nuclear components of proliferative cells such as embryonic or tumor cells as well as of metabolically active cells like neurons [342]. In contrast to cytoplasmic organelles, the content of Cajal bodies is not separated by phospholipid membranes from the surrounding nucleoplasm, and largely consists of concentrated proteins and RNA. Cajal bodies have been implicated in RNA-related metabolic processes such as snRNAPs biogenesis, maturation and recycling, histone mRNA processing and telomere maintenance [343]. Addressing the question whether these sub-organelles occupy the nuclear center in e.g. *ama-1* depleted embryos could be achieved by immuno-staining for p80/Coilin, a specific marker protein for Cajal bodies. In non-dividing cells, Cajal bodies are attached to the nucleolus by Coilin proteins [344].

In addition, it would be interesting to examine the structure of the nuclear ´holes` using electron microscopy.

'Ring' nuclei of embryos depleted of chromatin (and other) factors, were in no case found to divide at later stages. In contrast, 'ring' nuclei in the germ-line are nuclei of proliferating mitotic cells, located at the distal part of the gonad [345]. At later stages in the germ-line, when nuclei enter the meiotic phase, the ring structure is resolved [346]. In embryos depleted of *ama-1* and chromatin-

factors however, the 'ring'- like organization of chromosomes could still be observed after approximately 24 hours.

Taken together, the findings of this study suggest that the rearrangement of chromosomes to the nuclear periphery is a hallmark of impaired gene expression in the *C. elegans* embryo. However, the mechanisms underlying this re-arrangement still remain to be determined.

3.5. Quantitative analysis of chromatin factors exhibiting developmental phenotypes

Using the semi-automatic cell tracking and analysis method established in the course of this study, we could gain new insights into functions of different chromatin factors. Chromatin factors can be grouped into three different classes according to their phenotype. One group exhibits a delay in embryogenesis after depletion by RNAi. Knockdown of a second group leads to more lineage specific defects. Embryos depleted of a third class of chromatin factors show defects most likely attributed to a failure of zygotic gene expression.

Depletion of the majority of chromatin factors analyzed slowed development. The deceleration in developmental speed is observed most severely in embryos depleted of *lin-53* and *F55A3.3*. As described in Chapter 2.3.2., these chromatin factors exhibit segregation defects starting from the first divisions on. The observed cell cycle delay leads to arrest after approximately two hours with only ~30 cells. Cell cycle delay for chromatin factors described in this chapter is also most severe when segregation defects are observed at later stages of development. This is the case for genes encoding putative subunits of the NURD complex such as *rba-1* and *hda-1*, the MLL (mixed lineage leukemia) methyl-transferase *set-16*, as well as the SWI/SNF family members *let-526, swsn-5 and swsn-7* (Figure 42 and Figure 43).

set-16 encodes an H3K4 methyltransferase of the SET1/mixed lineage leukemia (MLL) family [347]. It has been shown to play a

role in attenuating Ras-mediated signaling during vulval development [348]. However, little phenotypic details have previously been reported, making our analysis particularly interesting.

RBA-1 is a homologue of the human retinoblastoma (Rb) – associated protein RbAp46/48, a subunit of various different chromatin remodeling complexes [319]. The human homologues RbAp 46 and RbAp48 are thought to influence chromatin assembly and remodeling and are required for proper localization of CENP-A. In fission yeast, the RBA-1 homologue Mis16 also is part of the CENP-A recruitment pathway, forming the most upstream factors in kinetochore assembly [321]. Its temperature-sensitive-mutant phenotype is described as causing the unequal segregation of chromosomes and generating aneuploid cells that undergo a few rounds of divisions but lose viability. This phenotype is comparable to the segregation defects observed for *rba-1* in this study and implies a similar function in *C. elegans*.

HDA-1 is a histone deacetylase with similarities to the RPD3 histone deacetylases from yeast and fly. RBA-1 and HDA-1 are both members of several distinct NURD (and other related) complexes as discussed in the previous chapter. Depending on the composition of the complex, its role in regulating early genes with mitotic and meiotic functions has been proposed, which is in line with our observations [326].

rba-1 and *hda-1* (RNAi) embryos show a more pronounced effect on developmental speed, compared to *set-16*, and SWI/SNF family members. This indicates a more important function of these

genes in cell division. Alternatively, the differences in observed phenotype might be caused by different efficiencies in gene knockdown. This could be ruled out experimentally by analyzing temperature sensitive knockout strains. However, the severe segregation defects observed after depletion of LIN-53, the other member of the NURD complex analyzed in this study (see Chapter 8.2.), as well as the proposed role of specific NURD complexes in cell division, may indeed point to a specific role of *rba-1* and *hda-1* in segregation.

Depletion of *hda-1* and *rba-1* does not affect cell positioning, in contrast to other gene depletions as discussed below. Cells of all lineages move to their correct positions until development slows down to such an extent that no more movement takes place in general (Figure 49). This indicates that these genes do not have a role in the cellular organization of the embryo.

Another interesting observation was that in case of a less severe (compared to e.g. *rba-1* depletion) deceleration of development, cells of the AB lineage are the ones affected first. In embryos depleted of the three SWI/SNF factors *swsn-5*, *swsn-7*, and *let-526* as well as the MLL factor *set-16*, cell cycle delay started during the fourth round of divisions only in cells of the AB lineage. Only after the fifth round of divisions, other cells exhibited longer cell cycles as well (Figure 42 and Figure 43). This indicates that the defect in cell cycle regulation caused by RNAi depletion of chromatin factors first affects AB lineage descendants. Curiously, active cell movements and thus cell positions do not seem to be more affected in ABa descendants than in other cells. Ingressions of

ABa cells, which starts approximately 90 minutes after the four-cell stage are normal until the arrest of the embryo (and general loss of active cell movements) (Figure 46 and Figure 49).

In contrast, in *egl-27+lin-40* (RNAi) depleted embryos the defects observed in MS descendants seem to be lineage specific. Before any other defect is detectable, MS divisions are delayed, angles are randomly oriented and movements are altered. Yet, by the time when MS descendants have fully internalized, early mis-placements have been compensated and the overall arrangement of the MS lineage appears approximately normal, despite the reduced cell number (Figure 44, Figure 45 and Figure 46 B). Thus, it is likely that lineage-independent factors regulating cell movements compensate defects that are caused early on by the lack of lineage specific factors. It has previously been described that lineage specific fate and polarity factors are necessary for proper internalization and movement, whereas a common cytoskeletal regulation is used by different lineages [92]. Thus, it is likely that common cytoskeletal mechanisms and ingression movements of other cells compensate the lack of MS specific fate and polarity regulators in cell positioning. Alternatively, the control of divisions and angles could be uncoupled from the control movements. At early stages, division angles contribute substantially to positioning of cells while at later stages this influence is less as the cell number increases and relative cell positioning becomes more important. This would explain the observed “correction” of MS positioning as well.

Egl-27 encodes a homologue of human MTA1, a component of the NURD complex. Together with its paralog *lin-40*, it has previously been reported to be required for the proper organization of all parts of the embryo, as well as for proper expression of HLH-8, a protein necessary for muscle development [280]. This is in line with the defects observed in our study. We observe defects in the MS lineage, which gives rise (within others) to muscle tissue. It is possible that the mis-positioning of MS cells leads to further impairment of proper localization of other cells in the embryo. Indeed, the overall cellular morphology of the embryo as observed under the bright-field microscope appeared to be abnormal at later stages. Yet, we did not track single cells to later time-points.

Depletion of the SWI/SNF family members *swsn-5*, *swsn-7*, and *let-526,* leads to failure of active cell movements and ingression, mainly in cells of the C and D lineage (Figure 48). In addition, depletion of *swsn-5* also seems to affect cell cycle timings and positions of the E lineage. Positioning of these lineages is not impaired in general after depletion of chromatin factors, even when cell cycles are severely delayed as observed in *rba-1* and *hda-1* (Figure 49). Thus, SWI/SNF factors might play a specific role in the proper expression of C and D cell fate regulators, and consequently on their movement. The additional effect of *swsn-5* depletion on the E lineage seems to be specific to *swsn-5* and not due to an insufficient knockdown of the other genes. In *swsn-7* and *let -526* depleted embryos, cell cycles of all cells are delayed, not just in cells of the E lineage. Thus, the knockdown seems to be

stronger than for *swsn-5* (RNAi) and lack of E ingression defect is unlikely to be a cause of insufficient gene depletion.

SWI/SNF proteins were first discovered in *Saccharomyces cerevisiae* as components of a 2MDa complex that repositions nucleosomes for vital tasks such as transcriptional control, DNA repair, recombination and chromosome segregation [349, 350]. The SWI/SNF complex consists of at least nine, including both conserved (core) and non-conserved components. Analysis of their role in transcriptional regulation revealed functions as both transcriptional activators and repressors. SWI/SNF was found to switch between these two modes of action at the same gene. In addition, tissue specific complexes have been reported to interact with a variety of transcription factors in different cell types allowing complexes to take on context dependent functions arising from their different interaction partners. *swsn*-5 encodes a homologue of SNF5/Ini1 and its involvement in asymmetric cell division of the T cells has been reported in *C. elegans*. Its yeast homologue is a component of the RSC chromatin remodeling complex and required for cell cycle progression and maintenance of proper ploidy. *let-526* and *swsn*-7 are also predicted subunits of the SWI/SNF complex, yet their precise function is not known. Thus, our observations provide first hints to the role of SWI/SNF proteins in the embryogenesis of the worm and indicate their involvement in the development of the E, C and D lineage. The C lineage gives rise to muscle, hypodermal and neuronal tissue, while D cells are muscle precursors, and E cells precursors of the intestine. The

different phenotypes observed predict the existence of multiple functionally distinct SWI/SNF complexes in the *C. elegans* embryo. Embryos depleted of *cir-1* and *ama-1*, also show defects in E, C and D ingression behavior (Figure 30 - Figure 35). AMA-1 is a subunit of Polymerase II and as such essential for transcription. CIR-1 is the orthologue of a CBF-1 interacting Co-repressor, suggesting its role in translational regulation. The similar lineage phenotypes of *ama-1* and *cir-1* depleted embryos as well as the observed chromosome rearrangement ("ring" phenotype) described in chapter 2.4.3, suggests a role for *cir-1* in zygotic gene expression in the *C. elegans* embryo. Thus, general failure of gene expression likely affects expression of E, C and D cell fate markers, leading to variability in division angles and failure of proper movements in those lineages in *cir-1* and *ama-1* depleted embryos. Alternatively, the observed E ingression defect, hallmark of a lack of gene expression, might cause the mis-positioning of C and D lineages, in order to maintain the correct relative positions and/or due to a lack of proper cell-cell signaling.

In SWI/SNF depleted embryos, the observed defects are similar to the ones observed in *cir-1* and *ama-1* (RNAi) depleted embryos. Thus, one might conclude that SWI/SNF factors do not have a specific role in the proper expression of C and D cell fate regulators, but that defects are due to the general role of SWI/SNF factors in gene expression. Yet, the absence of the "ring" phenotype (section 8.2.3), a hallmark of impaired gene expression, argues against this hypothesis. In contrast to *cir-1* and *ama-1* (RNAi) depleted embryos, we did not observe a rearrangement of

chromosomes to the periphery after depletion of any of the SWI/SNF factors. Also, mis-positioning of C and D lineages cannot be a consequence of an E ingression defect, as *swsn-7* and *let-526* do not show this phenotype.

Taken together, it can be concluded that although *cir-1/ ama-1* depletion and SWI/SNF factor depletion both affect E, C and D lineages, the defects observed have different causes. The phenotype observed for SWI/SNF factors is likely to be lineage specific and implies factor function in E, C and D cell fate. Defects in *cir-1* and *ama-1 (RNAi)* embryos however, seem to be a consequence of general failure of gene expression.

4. Materials and Methods

4.1. *C. elegans* maintenance and strains

All strains were maintained as described previously {Brenner, 1974 #2494} and grown at 20°C. Wild-type is Bristol N2 strain. Most strains were provided by the *Caenorhabditis* Genetics Center (University of Minnesota, Minneapolis) and include RW10029 zuIs178; stIs10029; zuIs178 [his-72::HIS-72::SRPVAT::GFP+ unc-119(+)], stIs10029 [pie-1::H2B::GFP+ unc-119(+)], YL206 unc-119(ed3) III; vrEx6[nst-1p::nst-1::GFP+unc-119(+)], OD1 unc-119(ed3) III; ltIs1[pIC22; pie-1::KNL-3::GFP+ unc-119(+)], OD7 unc-119(ed3) III; ltIs3[pIC31; pie-1::HCP-1::GFP-TEV-STag+unc-119(+)], OD83 ltIs37 [pAA64; pie-1::mCherry::HIS-58+unc-119(+)] IV. qaIs3507 [pie-1::GFP::LEM-2+unc-119(+)], XA3501 unc-119(ed3) ruIs32 III; ojIs1; ruIs32 [pie-1::GFP::H2B+unc-119(+)] III. ojIs1[pie-1::GFP::tbb-2+unc-119(+)]. EKM42 *unc-119*(*ed3*) III; *cldEx4* [*Ppie-1::CAPG-1::GFP unc-119*(+)] was a gift of Gyorgyi Csankovszki. OD224 (GFP: AIR-2 and RFP: H2B) was generously provided by Karen Oegema.

4.2. Imaging for cell tracking

4.2.1. Mounting of embryos

Worms expressing histone-GFP fusion protein (strain RW10029, [158]) were grown on OP50-seeded NGM plates and maintained by daily transferring the worms to maintain a healthy, not-starved population with high-quality eggs. For embryo extraction, young adult worms were picked and placed into a drop of Body's buffer/methyl cellulose in a clean, pre-chilled watch glass as described in [158]. Pre-chilling the watch glass and solutions to 4 °C temporarily slows the rate of development, providing sufficient time for microscope setup. Worms were cut open with syringe needles, placing the cuts at the boundary between the uterus and the gonad, which released embryos of different stages. One up to four-cell embryos were selected from further developed ones and transferred with a 10µl pipette on to a microscope slide with 4µl of 20µm polystyrene beads (Polysciences) in Boyd's buffer/methyl-cellulose (beads diluted 1:30 in buffer to reduce the diameter of the eggs to obtain a more intensive fluorescence signal at the upper planes but without damaging the eggs with the cover slip). 22x22 mm cover slips were gently lowered onto the bead mount to avoid the liquid touching the edge of the cover slip. Edges were sealed with molten paraffin to prevent the mountant from drying out during imaging.

4.2.2. Imaging protocol

Imaging was performed using a Leica TCS SP5 confocal microscope with a 488-nm excitation argon laser. To enhance signal, a relatively large pinhole size (2 Airy units), high detector gain (1,000–1,100), and an amplifier gain of 1.25 were used. To minimize signal loss, we used the RSP 500 filter in the light path. To balance between noise and imaging speed, we used a scan speed of 400Hz and bidirectional scanning. GFP fluorescence signal decreases rapidly towards the bottom of the embryo. Therefore, we used the “auto Z” feature to increase laser power with scanning depth through the embryo. Images were arranged so that the anterior–posterior axis was aligned in parallel to the *x*-axis of the image. This greatly simplified the determination of the embryonic axes during lineage tracing. Each 2D image is 712 × 512 pixels in resolution, resulting in a ≈12-gigabyte series (for 10h time-lapse series). Further details on the microscope setting are shown in the table below (Table 13).

Microscope	Leica TCS SP5
Objective	63x1.4
Zoom	3.4
Excitation laser	30Watt Argon Laser, 488nm laser line, 30% laser power
Emission range	496-567nm
Compensation by AOTF	4-6% (from upper to lower plane)
XY resolution	712x512 (0.13µm per pixel)
Z planes	26-36 (1µm apart)
Scan mode	bidirectional
Pinhole size	2 Airy Units
Amplifier offset	0
Amplifier gain	1.25
Temperature	20°C
Imaging Time	6-10h, one stack per minute

Table 13: Microscope settings for imaging protocol.

4.2.3. Image processing

Previous to cell tracking, time-lapse images were processed with ImageJ (http://rsbweb.nih.gov/ij/). This included cropping of the image to increase the processing speed, image mirroring (as the SP5 microscope is an upright confocal) and noise reduction using a implemented plugin of ImageJ [351].

4.3. The tracking algorithm

The tracking algorithm used in this study was developed by Oleh Dzyubackyk in the lab of Eric Meijering. It is based on a model-evolution approach [352], which performs both segmentation and tracking. The general flow of the algorithm can be divided into four main steps: 1) initial segmentation, 2) division and motion assessment, 3) multi-cell segmentation and tracking, and 4) correction and output.

4.3.1. Initial Segmentation

For initial segmentation of the first image stack, a non-PDE based energy minimization method is used. Further details on the implementation of the described approach can be found in [353]. The output of this step is the starting point for the segmentation and tracking of the subsequent image stacks in the sequence, performed by iterating the steps described in the next subsections.

4.3.2. Division and Motion Assessment

The processing of each next image stack in the sequence starts with the detection and handling of divided cells, and the initial motion estimation of all other cells (adapted from [353]). Both operations rely on measurements obtained from the images. Specifically, markers representing the new positions of nuclei

are extracted by iterating each slice of the image stack with a disk of radius equal to the estimated average radius of the nuclei at the given time point.

4.3.3. Multi-Cell Segmentation and Tracking

The key idea behind multi-cell segmentation and tracking by means of the model-evolution approach is that each cell is represented by a function (the “model”), which is iteratively optimized to fit the true cell region in the image stack at one time point, and then used as initial assumption for the fitting procedure in the next stack of the sequence. Using level sets as a model, the function can be set to the signed distance function of the region, which is positive inside, negative outside, and zero on the boundary of the region. In this algorithm, the function was chosen to be the binary function that is true inside the region and false outside.

The fitting procedure consists of the iterative (and simultaneous for all cells) minimization of an energy functional computed within a narrow band around the current cell boundaries. The resulting trans-formation of each function mimics the displacement and deformation that the corresponding cell carried out between the previous and the present time point.

4.3.4. Correction and Output

The correction of possible errors of the segmentation results consists of a search for false negatives (missed cell nuclei). To this end, the image foreground is estimated by thresholding, where the threshold value is chosen such that the size of the foreground (the number of voxels) is as close as possible to the total segmented volume in the previous time point. This value is obtained from the cumulative histogram of the image intensity distribution. Next, the estimated foreground is divided into regions by applying the marker-controlled watershed algorithm, using the markers extracted. Regions that intersect with at least one of the already known cell regions are excluded. Resulting candidates of false negatives with size exceeding the minimal nucleus size (computed from the previous time point) are added to the list of cell objects, and their corresponding functions are refined by energy minimization as described in the previous section. Newly-found objects whose size after energy minimization falls below the minimal object size threshold are removed from the list. The remaining objects are labeled either as “new" or as division product.

The preparation for segmenting the next image stack in the sequence includes updating several parameters such as, among others, the minimal nucleus size parameter, and detecting mitotic nuclei. The minimal nucleus size is an important parameter that plays a crucial role in distinguishing real nuclei from noise. In this method, an initial value for this

parameter is provided, after which its value is automatically updated after each time step based on the sizes of the segmented nuclei, subject to the physically realistic constraint that it can only decrease, and at most by 5% between two consecutive time points. Detection of mitotic nuclei is based on their pronounced elongated shape and is performed in order to increase the computational efficiency of the algorithm. Specifically, it is taken into account that the majority of the divisions occurs (nearly) in the plane perpendicular to the z-axis: 1) the reference slice of the region currently occupied by the given object is detected as the one having the highest average intensity, 2) the lengths of the minor and the major axes and the orientation of the minor axis are calculated from the shape in the found reference slice, and 3) a cell is labeled as mitotic if the ratio of the lengths of the major to the minor axis is greater than a user-defined threshold. In addition, to simplify the distinction between mitotic nuclei and the newly-born nuclei that did not obtain a spherical shape yet, the natural restriction that a newly-born cell needs more than five minutes before it can divide is taken into account. The software implementation of this method provides several different forms of output: textual, binary, and graphical. The segmentation results are saved in a binary image file format. Also, to facilitate visual inspection, the results per time point can be saved in the form of a 3D rendering, which can be subsequently combined into a movie. Tracking results are exported to a format, readable by the editing programme the “Lineager”, developed in our lab. In addition, information about

important events (cell divisions and deaths) is stored in a readable log file. To further reduce (the propagation of) errors, it is possible to restart the programme at any time-point in the sequence, after manual curation of results (creation of new objects, deletion of existing ones, correction of cell divisions), by using the “Lineager”.

The algorithm was developed in the MATLAB (TheMathWorks, Inc., USA) environment and the most computationally demanding operations were implemented in C. Average processing times of one image stack per time point on a standard PC (Intel(R)Xeon(R) CPU, 2.8 GHz, 6 GB RAM, operating system Windows 7) is 50 minutes until the 100-cell stage, and an additional 100 minutes until the 200-cell-stage.

4.4. Manual lineage curation and analysis

Lineage outputs from the tracking algorithm were analyzed with the ‘Lineager’ programme developed by Rob Jelier. This allows visual evaluation of the output lineages against the recorded images and correcting for errors. Errors were first identified by detecting obvious deviations from the wild-type lineage, such as apparent cell deaths and unusual cell division timing. To ensure that all errors were detected, it was verified systematically that each cell division in the corrected lineage was supported by the images. After editing the lineage, cells were named according to the canonical naming scheme[3].

Corrected lineage data was then used to determine cell cycle timings, division angles and movements using a script developed in our lab. Output graphs were analyzed to detect statistically relevant deviations from wild-type. Further analysis was carried out manually, using the 3D-Viewer function of the 'Lineager': This allows visualization of all cells, highlighting different lineages and overlaying different embryos. Thus, different RNAi embryos can be compared to each other and to wild-type embryos.

4.5. RNAi experiments

RNAi by feeding was performed by an adapted version of the previously described protocol [318]. Briefly, worms were synchronized by bleaching with sodium hydroxide and sodium hypochlorite. Eggs were allowed to hatch and L1-L4 larvae were transferred onto NGM plates (including 4mM isopropyl-beta-D thiogalactopyranoside (IPTG) and 100 µg/ml ampicillin for induction) with a lawn of bacterial clones, expressing the double stranded RNA. RNAi feeding was performed at 20°C. Eggs from young adults on day three and four after hatching were used for imaging and antibody staining experiments.

4.6. Imaging of GFP marker strains

Embryos were imaged on the Leica TCS SP5 confocal microscope and mounted as described above. Images were acquired by using a 60x1.4 N.A. Plan Apo objective lens. To reduce random noise, averaging over eight scans was performed. Images were captured in Z-stacks with planes 1 µm apart from each other and stacks taken in one minute intervals. Each 2D image is 512 × 512 pixels in resolution. Varying Zoom factors were used (4.2 to 14). Images were processed in ImageJ (http://rsb.info.nih.gov/ij/disclaimer.html) using level adjustments.

5. References

1. Hird, S.N., J.E. Paulsen, and S. Strome, *Segregation of germ granules in living Caenorhabditis elegans embryos: cell-type-specific mechanisms for cytoplasmic localisation.* Development, 1996. **122**(4): p. 1303-12.
2. Cowan, C.R. and A.A. Hyman, *Asymmetric cell division in C. elegans: cortical polarity and spindle positioning.* Annu Rev Cell Dev Biol, 2004. **20**: p. 427-53.
3. Sulston, J.E., et al., *The embryonic cell lineage of the nematode Caenorhabditis elegans.* Dev Biol, 1983. **100**(1): p. 64-119.
4. *WormBook*. *WormBook*. WormBook 2005; Available from: http://www.wormbook.org.
5. Rappleye, C.A., et al., *Involvement of fatty acid pathways and cortical interaction of the pronuclear complex in Caenorhabditis elegans embryonic polarity.* BMC Dev Biol, 2003. **3**: p. 8.
6. Rappleye, C.A., et al., *The anaphase-promoting complex and separin are required for embryonic anterior-posterior axis formation.* Dev Cell, 2002. **2**(2): p. 195-206.
7. Cuenca, A.A., et al., *Polarization of the C. elegans zygote proceeds via distinct establishment and maintenance phases.* Development, 2003. **130**(7): p. 1255-65.
8. Munro, E., J. Nance, and J.R. Priess, *Cortical flows powered by asymmetrical contraction transport PAR proteins to establish and maintain anterior-posterior polarity in the early C. elegans embryo.* Dev Cell, 2004. **7**(3): p. 413-24.
9. Kemphues, K.J., M. Kusch, and N. Wolf, *Maternal-effect lethal mutations on linkage group II of Caenorhabditis elegans.* Genetics, 1988. **120**(4): p. 977-86.
10. Kemphues, K.J., et al., *Identification of genes required for cytoplasmic localization in early C. elegans embryos.* Cell, 1988. **52**(3): p. 311-20.
11. Kemphues, K.J. and S. Strome, *Fertilization and Establishment of Polarity in the Embryo.* 1997.

12. Cheeks, R.J., et al., *C. elegans PAR proteins function by mobilizing and stabilizing asymmetrically localized protein complexes.* Curr Biol, 2004. **14**(10): p. 851-62.
13. Albertson, D.G., *Formation of the first cleavage spindle in nematode embryos.* Dev Biol, 1984. **101**(1): p. 61-72.
14. Gotta, M., M.C. Abraham, and J. Ahringer, *CDC-42 controls early cell polarity and spindle orientation in C. elegans.* Curr Biol, 2001. **11**(7): p. 482-8.
15. Kay, A.J. and C.P. Hunter, *CDC-42 regulates PAR protein localization and function to control cellular and embryonic polarity in C. elegans.* Curr Biol, 2001. **11**(7): p. 474-81.
16. Gonczy, P. and L.S. Rose, *Asymmetric cell division and axis formation in the embryo.* WormBook, 2005: p. 1-20.
17. Schubert, C.M., et al., *MEX-5 and MEX-6 function to establish soma/germline asymmetry in early C. elegans embryos.* Mol Cell, 2000. **5**(4): p. 671-82.
18. Guedes, S. and J.R. Priess, *The C. elegans MEX-1 protein is present in germline blastomeres and is a P granule component.* Development, 1997. **124**(3): p. 731-9.
19. Mello, C.C., et al., *The pie-1 and mex-1 genes and maternal control of blastomere identity in early C. elegans embryos.* Cell, 1992. **70**(1): p. 163-76.
20. Tabara, H., et al., *pos-1 encodes a cytoplasmic zinc-finger protein essential for germline specification in C. elegans.* Development, 1999. **126**(1): p. 1-11.
21. Draper, B.W., et al., *MEX-3 is a KH domain protein that regulates blastomere identity in early C. elegans embryos.* Cell, 1996. **87**(2): p. 205-16.
22. Gomes, J.E., et al., *The maternal gene spn-4 encodes a predicted RRM protein required for mitotic spindle orientation and cell fate patterning in early C. elegans embryos.* Development, 2001. **128**(21): p. 4301-14.
23. Hird, S., *Cortical actin movements during the first cell cycle of the Caenorhabditis elegans embryo.* J Cell Sci, 1996. **109 (Pt 2)**: p. 525-33.
24. Strome, S. and W.B. Wood, *Generation of asymmetry and segregation of germ-line granules in early C. elegans embryos.* Cell, 1983. **35**(1): p. 15-25.

25. Hunter, C.P. and C. Kenyon, *Spatial and temporal controls target pal-1 blastomere-specification activity to a single blastomere lineage in C. elegans embryos.* Cell, 1996. **87**(2): p. 217-26.
26. Huang, N.N., et al., *MEX-3 interacting proteins link cell polarity to asymmetric gene expression in Caenorhabditis elegans.* Development, 2002. **129**(3): p. 747-59.
27. Gotta, M. and J. Ahringer, *Distinct roles for Galpha and Gbetagamma in regulating spindle position and orientation in Caenorhabditis elegans embryos.* Nat Cell Biol, 2001. **3**(3): p. 297-300.
28. Tsou, M.F., et al., *LET-99 determines spindle position and is asymmetrically enriched in response to PAR polarity cues in C. elegans embryos.* Development, 2002. **129**(19): p. 4469-81.
29. Grill, S.W., et al., *The distribution of active force generators controls mitotic spindle position.* Science, 2003. **301**(5632): p. 518-21.
30. Colombo, K., et al., *Translation of polarity cues into asymmetric spindle positioning in Caenorhabditis elegans embryos.* Science, 2003. **300**(5627): p. 1957-61.
31. Hyman, A.A. and J.G. White, *Determination of cell division axes in the early embryogenesis of Caenorhabditis elegans.* J Cell Biol, 1987. **105**(5): p. 2123-35.
32. Labbe, J.C., E.K. McCarthy, and B. Goldstein, *The forces that position a mitotic spindle asymmetrically are tethered until after the time of spindle assembly.* J Cell Biol, 2004. **167**(2): p. 245-56.
33. Oegema, K., et al., *Functional analysis of kinetochore assembly in Caenorhabditis elegans.* J Cell Biol, 2001. **153**(6): p. 1209-26.
34. Grill, S.W., et al., *Polarity controls forces governing asymmetric spindle positioning in the Caenorhabditis elegans embryo.* Nature, 2001. **409**(6820): p. 630-3.
35. Cheng, N.N., C.M. Kirby, and K.J. Kemphues, *Control of cleavage spindle orientation in Caenorhabditis elegans: the role of the genes par-2 and par-3.* Genetics, 1995. **139**(2): p. 549-59.

36. Bergmann, D.C., et al., *Embryonic handedness choice in C. elegans involves the Galpha protein GPA-16.* Development, 2003. **130**(23): p. 5731-40.
37. Gotta, M., et al., *Asymmetrically distributed C. elegans homologs of AGS3/PINS control spindle position in the early embryo.* Curr Biol, 2003. **13**(12): p. 1029-37.
38. Rose, L.S. and K. Kemphues, *The let-99 gene is required for proper spindle orientation during cleavage of the C. elegans embryo.* Development, 1998. **125**(7): p. 1337-46.
39. Schmidt, D.J., et al., *Functional analysis of cytoplasmic dynein heavy chain in Caenorhabditis elegans with fast-acting temperature-sensitive mutations.* Mol Biol Cell, 2005. **16**(3): p. 1200-12.
40. Srinivasan, D.G., et al., *A complex of LIN-5 and GPR proteins regulates G protein signaling and spindle function in C elegans.* Genes Dev, 2003. **17**(10): p. 1225-39.
41. Wood, W.B., *Evidence from reversal of handedness in C. elegans embryos for early cell interactions determining cell fates.* Nature, 1991. **349**(6309): p. 536-8.
42. Schnabel, R., *Duels without obvious sense: counteracting inductions involved in body wall muscle development in the Caenorhabditis elegans embryo.* Development, 1995. **121**(7): p. 2219-32.
43. Priess, J.R., *Notch signaling in the C. elegans embryo.* WormBook, 2005: p. 1-16.
44. Bergmann, D.C., et al., *Cuticle chirality and body handedness in Caenorhabditis elegans.* Dev Genet, 1998. **23**(3): p. 164-74.
45. Pohl, C. and Z. Bao, *Chiral forces organize left-right patterning in C. elegans by uncoupling midline and anteroposterior axis.* Dev Cell. **19**(3): p. 402-12.
46. Good, K., et al., *The T-box transcription factors TBX-37 and TBX-38 link GLP-1/Notch signaling to mesoderm induction in C. elegans embryos.* Development, 2004. **131**(9): p. 1967-78.
47. Neves, A. and J.R. Priess, *The REF-1 family of bHLH transcription factors pattern C. elegans embryos through Notch-dependent and Notch-independent pathways.* Dev Cell, 2005. **8**(6): p. 867-79.

48. Maduro, M.F., et al., *Restriction of mesendoderm to a single blastomere by the combined action of SKN-1 and a GSK-3beta homolog is mediated by MED-1 and -2 in C. elegans.* Mol Cell, 2001. **7**(3): p. 475-85.
49. Broitman-Maduro, G., M.F. Maduro, and J.H. Rothman, *The noncanonical binding site of the MED-1 GATA factor defines differentially regulated target genes in the C. elegans mesendoderm.* Dev Cell, 2005. **8**(3): p. 427-33.
50. Schnabel, R., *Autonomy and nonautonomy in cell fate specification of muscle in the Caenorhabditis elegans embryo: a reciprocal induction.* Science, 1994. **263**(5152): p. 1449-52.
51. Mango, S.E., et al., *Two maternal genes, apx-1 and pie-1, are required to distinguish the fates of equivalent blastomeres in the early Caenorhabditis elegans embryo.* Development, 1994. **120**(8): p. 2305-15.
52. Lin, R., S. Thompson, and J.R. Priess, *pop-1 encodes an HMG box protein required for the specification of a mesoderm precursor in early C. elegans embryos.* Cell, 1995. **83**(4): p. 599-609.
53. Bowerman, B., B.A. Eaton, and J.R. Priess, *skn-1, a maternally expressed gene required to specify the fate of ventral blastomeres in the early C. elegans embryo.* Cell, 1992. **68**(6): p. 1061-75.
54. Mango, S.E., E.J. Lambie, and J. Kimble, *The pha-4 gene is required to generate the pharyngeal primordium of Caenorhabditis elegans.* Development, 1994. **120**(10): p. 3019-31.
55. Horner, M.A., et al., *pha-4, an HNF-3 homolog, specifies pharyngeal organ identity in Caenorhabditis elegans.* Genes Dev, 1998. **12**(13): p. 1947-52.
56. Kalb, J.M., et al., *pha-4 is Ce-fkh-1, a fork head/HNF-3alpha,beta,gamma homolog that functions in organogenesis of the C. elegans pharynx.* Development, 1998. **125**(12): p. 2171-80.
57. Priess, J.R., H. Schnabel, and R. Schnabel, *The glp-1 locus and cellular interactions in early C. elegans embryos.* Cell, 1987. **51**(4): p. 601-11.
58. Doyle, T.G., C. Wen, and I. Greenwald, *SEL-8, a nuclear protein required for LIN-12 and GLP-1 signaling in*

Caenorhabditis elegans. Proc Natl Acad Sci U S A, 2000. **97**(14): p. 7877-81.
59. Petcherski, A.G. and J. Kimble, *LAG-3 is a putative transcriptional activator in the C. elegans Notch pathway.* Nature, 2000. **405**(6784): p. 364-8.
60. Lambie, E.J. and J. Kimble, *Two homologous regulatory genes, lin-12 and glp-1, have overlapping functions.* Development, 1991. **112**(1): p. 231-40.
61. Moskowitz, I.P. and J.H. Rothman, *lin-12 and glp-1 are required zygotically for early embryonic cellular interactions and are regulated by maternal GLP-1 signaling in Caenorhabditis elegans.* Development, 1996. **122**(12): p. 4105-17.
62. Alper, S. and C. Kenyon, *REF-1, a protein with two bHLH domains, alters the pattern of cell fusion in C. elegans by regulating Hox protein activity.* Development, 2001. **128**(10): p. 1793-804.
63. Moskowitz, I.P., S.B. Gendreau, and J.H. Rothman, *Combinatorial specification of blastomere identity by glp-1-dependent cellular interactions in the nematode Caenorhabditis elegans.* Development, 1994. **120**(11): p. 3325-38.
64. Way, J.C., et al., *Cell polarity and the mechanism of asymmetric cell division.* Bioessays, 1994. **16**(12): p. 925-31.
65. Kaletta, T., H. Schnabel, and R. Schnabel, *Binary specification of the embryonic lineage in Caenorhabditis elegans.* Nature, 1997. **390**(6657): p. 294-8.
66. Lin, R., R.J. Hill, and J.R. Priess, *POP-1 and anterior-posterior fate decisions in C. elegans embryos.* Cell, 1998. **92**(2): p. 229-39.
67. Rocheleau, C.E., et al., *WRM-1 activates the LIT-1 protein kinase to transduce anterior/posterior polarity signals in C. elegans.* Cell, 1999. **97**(6): p. 717-26.
68. Maduro, M.F., R. Lin, and J.H. Rothman, *Dynamics of a developmental switch: recursive intracellular and intranuclear redistribution of Caenorhabditis elegans POP-1 parallels Wnt-inhibited transcriptional repression.* Dev Biol, 2002. **248**(1): p. 128-42.

69. Lo, M.C., et al., *Phosphorylation by the beta-catenin/MAPK complex promotes 14-3-3-mediated nuclear export of TCF/POP-1 in signal-responsive cells in C. elegans.* Cell, 2004. **117**(1): p. 95-106.
70. Rocheleau, C.E., et al., *Wnt signaling and an APC-related gene specify endoderm in early C. elegans embryos.* Cell, 1997. **90**(4): p. 707-16.
71. Thorpe, C.J., et al., *Wnt signaling polarizes an early C. elegans blastomere to distinguish endoderm from mesoderm.* Cell, 1997. **90**(4): p. 695-705.
72. Park, F.D. and J.R. Priess, *Establishment of POP-1 asymmetry in early C. elegans embryos.* Development, 2003. **130**(15): p. 3547-56.
73. Park, F.D., J.R. Tenlen, and J.R. Priess, *C. elegans MOM-5/frizzled functions in MOM-2/Wnt-independent cell polarity and is localized asymmetrically prior to cell division.* Curr Biol, 2004. **14**(24): p. 2252-8.
74. Gendreau, S.B., et al., *The potential to differentiate epidermis is unequally distributed in the AB lineage during early embryonic development in C. elegans.* Dev Biol, 1994. **166**(2): p. 770-81.
75. Wittmann, C., et al., *The expression of the C. elegans labial-like Hox gene ceh-13 during early embryogenesis relies on cell fate and on anteroposterior cell polarity.* Development, 1997. **124**(21): p. 4193-200.
76. Bischoff, M. and R. Schnabel, *Global cell sorting is mediated by local cell-cell interactions in the C. elegans embryo.* Dev Biol, 2006. **294**(2): p. 432-44.
77. Bei, Y., et al., *SRC-1 and Wnt signaling act together to specify endoderm and to control cleavage orientation in early C. elegans embryos.* Dev Cell, 2002. **3**(1): p. 113-25.
78. Goldstein, B., *Induction of gut in Caenorhabditis elegans embryos.* Nature, 1992. **357**(6375): p. 255-7.
79. Schlesinger, A., et al., *Wnt pathway components orient a mitotic spindle in the early Caenorhabditis elegans embryo without requiring gene transcription in the responding cell.* Genes Dev, 1999. **13**(15): p. 2028-38.
80. Meneghini, M.D., et al., *MAP kinase and Wnt pathways converge to downregulate an HMG-domain repressor in*

Caenorhabditis elegans. Nature, 1999. **399**(6738): p. 793-7.
81. Peters, J.M., et al., *Casein kinase I transduces Wnt signals.* Nature, 1999. **401**(6751): p. 345-50.
82. Shin, T.H., et al., *MOM-4, a MAP kinase kinase kinase-related protein, activates WRM-1/LIT-1 kinase to transduce anterior/posterior polarity signals in C. elegans.* Mol Cell, 1999. **4**(2): p. 275-80.
83. Walston, T., et al., *Multiple Wnt signaling pathways converge to orient the mitotic spindle in early C. elegans embryos.* Dev Cell, 2004. **7**(6): p. 831-41.
84. Smit, L., et al., *Wnt activates the Tak1/Nemo-like kinase pathway.* J Biol Chem, 2004. **279**(17): p. 17232-40.
85. Calvo, D., et al., *A POP-1 repressor complex restricts inappropriate cell type-specific gene transcription during Caenorhabditis elegans embryogenesis.* EMBO J, 2001. **20**(24): p. 7197-208.
86. Gay, F., et al., *Acetylation regulates subcellular localization of the Wnt signaling nuclear effector POP-1.* Genes Dev, 2003. **17**(6): p. 717-22.
87. Hermann, G.J., B. Leung, and J.R. Priess, *Left-right asymmetry in C. elegans intestine organogenesis involves a LIN-12/Notch signaling pathway.* Development, 2000. **127**(16): p. 3429-40.
88. Bowerman, B., et al., *Cell interactions involved in development of the bilaterally symmetrical intestinal valve cells during embryogenesis in Caenorhabditis elegans.* Development, 1992. **116**(4): p. 1113-22.
89. Greenwald, I.S., P.W. Sternberg, and H.R. Horvitz, *The lin-12 locus specifies cell fates in Caenorhabditis elegans.* Cell, 1983. **34**(2): p. 435-44.
90. Edgar, L.G., et al., *Zygotic expression of the caudal homolog pal-1 is required for posterior patterning in Caenorhabditis elegans embryogenesis.* Dev Biol, 2001. **229**(1): p. 71-88.
91. Nance, J. and J.R. Priess, *Cell polarity and gastrulation in C. elegans.* Development, 2002. **129**(2): p. 387-97.
92. Harrell, J.R. and B. Goldstein, *Internalization of multiple cells during C. elegans gastrulation depends on common*

cytoskeletal mechanisms but different cell polarity and cell fate regulators. Dev Biol. **350**(1): p. 1-12.
93. Sawyer, J.M., et al., *Apical constriction: a cell shape change that can drive morphogenesis.* Dev Biol. **341**(1): p. 5-19.
94. Maduro, M.F., et al., *Genetic redundancy in endoderm specification within the genus Caenorhabditis.* Dev Biol, 2005. **284**(2): p. 509-22.
95. Lee, M.H., et al., *LIP-1 phosphatase controls the extent of germline proliferation in Caenorhabditis elegans.* EMBO J, 2006. **25**(1): p. 88-96.
96. Zhu, J., et al., *end-1 encodes an apparent GATA factor that specifies the endoderm precursor in Caenorhabditis elegans embryos.* Genes Dev, 1997. **11**(21): p. 2883-96.
97. Lee, J.Y., et al., *Wnt/Frizzled signaling controls C. elegans gastrulation by activating actomyosin contractility.* Curr Biol, 2006. **16**(20): p. 1986-97.
98. Lee, J.Y. and B. Goldstein, *Mechanisms of cell positioning during C. elegans gastrulation.* Development, 2003. **130**(2): p. 307-20.
99. Etemad-Moghadam, B., S. Guo, and K.J. Kemphues, *Asymmetrically distributed PAR-3 protein contributes to cell polarity and spindle alignment in early C. elegans embryos.* Cell, 1995. **83**(5): p. 743-52.
100. Boyd, L., et al., *PAR-2 is asymmetrically distributed and promotes association of P granules and PAR-1 with the cortex in C. elegans embryos.* Development, 1996. **122**(10): p. 3075-84.
101. Hung, T.J. and K.J. Kemphues, *PAR-6 is a conserved PDZ domain-containing protein that colocalizes with PAR-3 in Caenorhabditis elegans embryos.* Development, 1999. **126**(1): p. 127-35.
102. Roh-Johnson, M., et al., *Triggering a cell shape change by exploiting preexisting actomyosin contractions.* Science, 2012. **335**(6073): p. 1232-5.
103. Roh-Johnson, M. and B. Goldstein, *In vivo roles for Arp2/3 in cortical actin organization during C. elegans gastrulation.* J Cell Sci, 2009. **122**(Pt 21): p. 3983-93.

104. Sawa, M., et al., *Essential role of the C. elegans Arp2/3 complex in cell migration during ventral enclosure.* J Cell Sci, 2003. **116**(Pt 8): p. 1505-18.
105. Severson, A.F. and B. Bowerman, *Cytokinesis: closing in on the central spindle.* Dev Cell, 2002. **2**(1): p. 4-6.
106. Millard, T.H., S.J. Sharp, and L.M. Machesky, *Signalling to actin assembly via the WASP (Wiskott-Aldrich syndrome protein)-family proteins and the Arp2/3 complex.* Biochem J, 2004. **380**(Pt 1): p. 1-17.
107. Schnabel, R., et al., *Assessing normal embryogenesis in Caenorhabditis elegans using a 4D microscope: variability of development and regional specification.* Dev Biol, 1997. **184**(2): p. 234-65.
108. Schnabel, R., et al., *Global cell sorting in the C. elegans embryo defines a new mechanism for pattern formation.* Dev Biol, 2006. **294**(2): p. 418-31.
109. Hench, J., et al., *Spatio-temporal reference model of Caenorhabditis elegans embryogenesis with cell contact maps.* Dev Biol, 2009. **333**(1): p. 1-13.
110. Nance, J., J.Y. Lee, and B. Goldstein, *Gastrulation in C. elegans.* WormBook, 2005: p. 1-13.
111. Page, B.D., et al., *ELT-1, a GATA-like transcription factor, is required for epidermal cell fates in Caenorhabditis elegans embryos.* Genes Dev, 1997. **11**(13): p. 1651-61.
112. Quintin, S., et al., *The Caenorhabditis elegans gene lin-26 can trigger epithelial differentiation without conferring tissue specificity.* Dev Biol, 2001. **235**(2): p. 410-21.
113. McMahon, L., et al., *Assembly of C. elegans apical junctions involves positioning and compaction by LET-413 and protein aggregation by the MAGUK protein DLG-1.* J Cell Sci, 2001. **114**(Pt 12): p. 2265-77.
114. Williams-Masson, E.M., A.N. Malik, and J. Hardin, *An actin-mediated two-step mechanism is required for ventral enclosure of the C. elegans hypodermis.* Development, 1997. **124**(15): p. 2889-901.
115. Chin-Sang, I.D., et al., *The ephrin VAB-2/EFN-1 functions in neuronal signaling to regulate epidermal morphogenesis in C. elegans.* Cell, 1999. **99**(7): p. 781-90.

116. Chin-Sang, I.D., et al., *The divergent C. elegans ephrin EFN-4 functions inembryonic morphogenesis in a pathway independent of the VAB-1 Eph receptor.* Development, 2002. **129**(23): p. 5499-510.
117. George, S.E., et al., *The VAB-1 Eph receptor tyrosine kinase functions in neural and epithelial morphogenesis in C. elegans.* Cell, 1998. **92**(5): p. 633-43.
118. Wang, X., et al., *Multiple ephrins control cell organization in C. elegans using kinase-dependent and -independent functions of the VAB-1 Eph receptor.* Mol Cell, 1999. **4**(6): p. 903-13.
119. Withee, J., et al., *Caenorhabditis elegans WASP and Ena/VASP proteins play compensatory roles in morphogenesis and neuronal cell migration.* Genetics, 2004. **167**(3): p. 1165-76.
120. Heid, P.J., et al., *The zinc finger protein DIE-1 is required for late events during epithelial cell rearrangement in C. elegans.* Dev Biol, 2001. **236**(1): p. 165-80.
121. Williams-Masson, E.M., et al., *The cellular mechanism of epithelial rearrangement during morphogenesis of the Caenorhabditis elegans dorsal hypodermis.* Dev Biol, 1998. **204**(1): p. 263-76.
122. Chisholm, A.D. and J. Hardin, *Epidermal morphogenesis.* WormBook, 2005: p. 1-22.
123. Soto, M.C., et al., *The GEX-2 and GEX-3 proteins are required for tissue morphogenesis and cell migrations in C. elegans.* Genes Dev, 2002. **16**(5): p. 620-32.
124. Lundquist, E.A., et al., *Three C. elegans Rac proteins and several alternative Rac regulators control axon guidance, cell migration and apoptotic cell phagocytosis.* Development, 2001. **128**(22): p. 4475-88.
125. Reddien, P.W. and H.R. Horvitz, *CED-2/CrkII and CED-10/Rac control phagocytosis and cell migration in Caenorhabditis elegans.* Nat Cell Biol, 2000. **2**(3): p. 131-6.
126. Thomas-Virnig, C.L., et al., *The inositol 1,4,5-trisphosphate receptor regulates epidermal cell migration in Caenorhabditis elegans.* Curr Biol, 2004. **14**(20): p. 1882-7.

127. Raich, W.B., C. Agbunag, and J. Hardin, *Rapid epithelial-sheet sealing in the Caenorhabditis elegans embryo requires cadherin-dependent filopodial priming.* Curr Biol, 1999. **9**(20): p. 1139-46.
128. Roy, P.J., et al., *mab-20 encodes Semaphorin-2a and is required to prevent ectopic cell contacts during epidermal morphogenesis in Caenorhabditis elegans.* Development, 2000. **127**(4): p. 755-67.
129. Pasterkamp, R.J. and A.L. Kolodkin, *Semaphorin junction: making tracks toward neural connectivity.* Curr Opin Neurobiol, 2003. **13**(1): p. 79-89.
130. Pettitt, J., et al., *The Caenorhabditis elegans p120 catenin homologue, JAC-1, modulates cadherin-catenin function during epidermal morphogenesis.* J Cell Biol, 2003. **162**(1): p. 15-22.
131. Priess, J.R. and D.I. Hirsh, *Caenorhabditis elegans morphogenesis: the role of the cytoskeleton in elongation of the embryo.* Dev Biol, 1986. **117**(1): p. 156-73.
132. McKeown, C., V. Praitis, and J. Austin, *sma-1 encodes a betaH-spectrin homolog required for Caenorhabditis elegans morphogenesis.* Development, 1998. **125**(11): p. 2087-98.
133. Costa, M., B.W. Draper, and J.R. Priess, *The role of actin filaments in patterning the Caenorhabditis elegans cuticle.* Dev Biol, 1997. **184**(2): p. 373-84.
134. Costa, M., et al., *A putative catenin-cadherin system mediates morphogenesis of the Caenorhabditis elegans embryo.* J Cell Biol, 1998. **141**(1): p. 297-308.
135. Piekny, A.J., A. Wissmann, and P.E. Mains, *Embryonic morphogenesis in Caenorhabditis elegans integrates the activity of LET-502 Rho-binding kinase, MEL-11 myosin phosphatase, DAF-2 insulin receptor and FEM-2 PP2c phosphatase.* Genetics, 2000. **156**(4): p. 1671-89.
136. Simske, J.S., et al., *The cell junction protein VAB-9 regulates adhesion and epidermal morphology in C. elegans.* Nat Cell Biol, 2003. **5**(7): p. 619-25.
137. Norman, K.R. and D.G. Moerman, *Alpha spectrin is essential for morphogenesis and body wall muscle formation in Caenorhabditis elegans.* J Cell Biol, 2002. **157**(4): p. 665-77.

138. Hammarlund, M., W.S. Davis, and E.M. Jorgensen, *Mutations in beta-spectrin disrupt axon outgrowth and sarcomere structure.* J Cell Biol, 2000. **149**(4): p. 931-42.
139. Praitis, V., E. Ciccone, and J. Austin, *SMA-1 spectrin has essential roles in epithelial cell sheet morphogenesis in C. elegans.* Dev Biol, 2005. **283**(1): p. 157-70.
140. Shelton, C.A., et al., *The nonmuscle myosin regulatory light chain gene mlc-4 is required for cytokinesis, anterior-posterior polarity, and body morphology during Caenorhabditis elegans embryogenesis.* J Cell Biol, 1999. **146**(2): p. 439-51.
141. Wissmann, A., et al., *Caenorhabditis elegans LET-502 is related to Rho-binding kinases and human myotonic dystrophy kinase and interacts genetically with a homolog of the regulatory subunit of smooth muscle myosin phosphatase to affect cell shape.* Genes Dev, 1997. **11**(4): p. 409-22.
142. Wissmann, A., J. Ingles, and P.E. Mains, *The Caenorhabditis elegans mel-11 myosin phosphatase regulatory subunit affects tissue contraction in the somatic gonad and the embryonic epidermis and genetically interacts with the Rac signaling pathway.* Dev Biol, 1999. **209**(1): p. 111-27.
143. Piekny, A.J., et al., *The Caenorhabditis elegans nonmuscle myosin genes nmy-1 and nmy-2 function as redundant components of the let-502/Rho-binding kinase and mel-11/myosin phosphatase pathway during embryonic morphogenesis.* Development, 2003. **130**(23): p. 5695-704.
144. Francis, R. and R.H. Waterston, *Muscle cell attachment in Caenorhabditis elegans.* J Cell Biol, 1991. **114**(3): p. 465-79.
145. Hresko, M.C., B.D. Williams, and R.H. Waterston, *Assembly of body wall muscle and muscle cell attachment structures in Caenorhabditis elegans.* J Cell Biol, 1994. **124**(4): p. 491-506.
146. Hresko, M.C., et al., *Myotactin, a novel hypodermal protein involved in muscle-cell adhesion in Caenorhabditis elegans.* J Cell Biol, 1999. **146**(3): p. 659-72.

147. Bosher, J.M., et al., *The Caenorhabditis elegans vab-10 spectraplakin isoforms protect the epidermis against internal and external forces.* J Cell Biol, 2003. **161**(4): p. 757-68.
148. Woo, W.M., et al., *Intermediate filaments are required for C. elegans epidermal elongation.* Dev Biol, 2004. **267**(1): p. 216-29.
149. Gupta, M.C., P.L. Graham, and J.M. Kramer, *Characterization of alpha1(IV) collagen mutations in Caenorhabditis elegans and the effects of alpha1 and alpha2(IV) mutations on type IV collagen distribution.* J Cell Biol, 1997. **137**(5): p. 1185-96.
150. Huang, X., et al., *UNC-71, a disintegrin and metalloprotease (ADAM) protein, regulates motor axon guidance and sex myoblast migration in C. elegans.* Development, 2003. **130**(14): p. 3147-61.
151. Hird, S.N. and J.G. White, *Cortical and cytoplasmic flow polarity in early embryonic cells of Caenorhabditis elegans.* J Cell Biol, 1993. **121**(6): p. 1343-55.
152. Minden, J.S., et al., *Direct cell lineage analysis in Drosophila melanogaster by time-lapse, three-dimensional optical microscopy of living embryos.* J Cell Biol, 1989. **109**(2): p. 505-16.
153. Sanford, B.A., et al., *A dual fluorescence technique for visualization of Staphylococcus epidermidis biofilm using scanning confocal laser microscopy.* J Ind Microbiol, 1996. **16**(1): p. 48-56.
154. Hamahashi, S., S. Onami, and H. Kitano, *Detection of nuclei in 4D Nomarski DIC microscope images of early Caenorhabditis elegans embryos using local image entropy and object tracking.* BMC Bioinformatics, 2005. **6**: p. 125.
155. Bao, Z., et al., *Automated cell lineage tracing in Caenorhabditis elegans.* Proc Natl Acad Sci U S A, 2006. **103**(8): p. 2707-12.
156. Hadjantonakis, A.K. and V.E. Papaioannou, *Dynamic in vivo imaging and cell tracking using a histone fluorescent protein fusion in mice.* BMC Biotechnol, 2004. **4**: p. 33.

157. Boyle, T.J., et al., *AceTree: a tool for visual analysis of Caenorhabditis elegans embryogenesis.* BMC Bioinformatics, 2006. **7**: p. 275.
158. Murray, J.I., et al., *The lineaging of fluorescently-labeled Caenorhabditis elegans embryos with StarryNite and AceTree.* Nat Protoc, 2006. **1**(3): p. 1468-76.
159. Dzyubachyk, O., et al., *Model-based approach for tracking embryogenesis in Caenorhabditis elegans fluorescence microscopy data.* Conf Proc IEEE Eng Med Biol Soc, 2009. **2009**: p. 5356-9.
160. Deppe, U., et al., *Cell lineages of the embryo of the nematode Caenorhabditis elegans.* Proc Natl Acad Sci U S A, 1978. **75**(1): p. 376-80.
161. Schierenberg, E., *Altered cell-division rates after laser-induced cell fusion in nematode embryos.* Dev Biol, 1984. **101**(1): p. 240-5.
162. Edgar, R.S. and W.B. Wood, *The nematode Caenorhabditis elegans: a new organism for intensive biological study.* Science, 1977. **198**(4323): p. 1285-6.
163. Bischoff, M. and R. Schnabel, *A posterior centre establishes and maintains polarity of the Caenorhabditis elegans embryo by a Wnt-dependent relay mechanism.* PLoS Biol, 2006. **4**(12): p. e396.
164. Brauchle, M., K. Baumer, and P. Gonczy, *Differential activation of the DNA replication checkpoint contributes to asynchrony of cell division in C. elegans embryos.* Curr Biol, 2003. **13**(10): p. 819-27.
165. Encalada, S.E., et al., *A spindle checkpoint functions during mitosis in the early Caenorhabditis elegans embryo.* Mol Biol Cell, 2005. **16**(3): p. 1056-70.
166. Fernandez, A.G., et al., *New genes with roles in the C. elegans embryo revealed using RNAi of ovary-enriched ORFeome clones.* Genome Res, 2005. **15**(2): p. 250-9.
167. Fraser, A.G., et al., *Functional genomic analysis of C. elegans chromosome I by systematic RNA interference.* Nature, 2000. **408**(6810): p. 325-30.
168. Kamath, R.S., et al., *Systematic functional analysis of the Caenorhabditis elegans genome using RNAi.* Nature, 2003. **421**(6920): p. 231-7.

169. Simmer, F., et al., *Genome-wide RNAi of C. elegans using the hypersensitive rrf-3 strain reveals novel gene functions.* PLoS Biol, 2003. **1**(1): p. E12.
170. Gonczy, P., et al., *Functional genomic analysis of cell division in C. elegans using RNAi of genes on chromosome III.* Nature, 2000. **408**(6810): p. 331-6.
171. Maeda, I., et al., *Large-scale analysis of gene function in Caenorhabditis elegans by high-throughput RNAi.* Curr Biol, 2001. **11**(3): p. 171-6.
172. Piano, F., et al., *RNAi analysis of genes expressed in the ovary of Caenorhabditis elegans.* Curr Biol, 2000. **10**(24): p. 1619-22.
173. Sonnichsen, B., et al., *Full-genome RNAi profiling of early embryogenesis in Caenorhabditis elegans.* Nature, 2005. **434**(7032): p. 462-9.
174. Rual, J.F., et al., *Toward improving Caenorhabditis elegans phenome mapping with an ORFeome-based RNAi library.* Genome Res, 2004. **14**(10B): p. 2162-8.
175. Zipperlen, P., et al., *Roles for 147 embryonic lethal genes on C.elegans chromosome I identified by RNA interference and video microscopy.* EMBO J, 2001. **20**(15): p. 3984-92.
176. Lee, K.K., et al., *C. elegans nuclear envelope proteins emerin, MAN1, lamin, and nucleoporins reveal unique timing of nuclear envelope breakdown during mitosis.* Mol Biol Cell, 2000. **11**(9): p. 3089-99.
177. Liu, J., et al., *Essential roles for Caenorhabditis elegans lamin gene in nuclear organization, cell cycle progression, and spatial organization of nuclear pore complexes.* Mol Biol Cell, 2000. **11**(11): p. 3937-47.
178. Oegema, K. and A.A. Hyman, *Cell division.* WormBook, 2006: p. 1-40.
179. Hirano, M. and T. Hirano, *Opening closed arms: long-distance activation of SMC ATPase by hinge-DNA interactions.* Mol Cell, 2006. **21**(2): p. 175-86.
180. Chan, R.C., et al., *Chromosome cohesion is regulated by a clock gene paralogue TIM-1.* Nature, 2003. **423**(6943): p. 1002-9.
181. Pasierbek, P., et al., *The Caenorhabditis elegans SCC-3 homologue is required for meiotic synapsis and for*

proper chromosome disjunction in mitosis and meiosis. Exp Cell Res, 2003. **289**(2): p. 245-55.
182. Moore, L.L., et al., *HCP-4/CENP-C promotes the prophase timing of centromere resolution by enabling the centromere association of HCP-6 in Caenorhabditis elegans.* Mol Cell Biol, 2005. **25**(7): p. 2583-92.
183. Mito, Y., A. Sugimoto, and M. Yamamoto, *Distinct developmental function of two Caenorhabditis elegans homologs of the cohesin subunit Scc1/Rad21.* Mol Biol Cell, 2003. **14**(6): p. 2399-409.
184. Haering, C.H. and K. Nasmyth, *Building and breaking bridges between sister chromatids.* Bioessays, 2003. **25**(12): p. 1178-91.
185. Hudson, D.F., K.M. Marshall, and W.C. Earnshaw, *Condensin: Architect of mitotic chromosomes.* Chromosome Res, 2009. **17**(2): p. 131-44.
186. Csankovszki, G., *Condensin function in dosage compensation.* Epigenetics, 2009. **4**(4): p. 212-5.
187. Mets, D.G. and B.J. Meyer, *Condensins regulate meiotic DNA break distribution, thus crossover frequency, by controlling chromosome structure.* Cell, 2009. **139**(1): p. 73-86.
188. Stear, J.H. and M.B. Roth, *Characterization of HCP-6, a C. elegans protein required to prevent chromosome twisting and merotelic attachment.* Genes Dev, 2002. **16**(12): p. 1498-508.
189. Ono, T., et al., *Differential contributions of condensin I and condensin II to mitotic chromosome architecture in vertebrate cells.* Cell, 2003. **115**(1): p. 109-21.
190. Chan, R.C., A.F. Severson, and B.J. Meyer, *Condensin restructures chromosomes in preparation for meiotic divisions.* J Cell Biol, 2004. **167**(4): p. 613-25.
191. Csankovszki, G., et al., *Three distinct condensin complexes control C. elegans chromosome dynamics.* Curr Biol, 2009. **19**(1): p. 9-19.
192. Hirota, T., et al., *Distinct functions of condensin I and II in mitotic chromosome assembly.* J Cell Sci, 2004. **117**(Pt 26): p. 6435-45.

193. Gerlich, D., et al., *Condensin I stabilizes chromosomes mechanically through a dynamic interaction in live cells.* Curr Biol, 2006. **16**(4): p. 333-44.
194. Hagstrom, K.A., et al., *C. elegans condensin promotes mitotic chromosome architecture, centromere organization, and sister chromatid segregation during mitosis and meiosis.* Genes Dev, 2002. **16**(6): p. 729-42.
195. Hudson, D.F., et al., *Condensin is required for nonhistone protein assembly and structural integrity of vertebrate mitotic chromosomes.* Dev Cell, 2003. **5**(2): p. 323-36.
196. Kaitna, S., et al., *The aurora B kinase AIR-2 regulates kinetochores during mitosis and is required for separation of homologous Chromosomes during meiosis.* Curr Biol, 2002. **12**(10): p. 798-812.
197. Maddox, P.S., et al., *Molecular analysis of mitotic chromosome condensation using a quantitative time-resolved fluorescence microscopy assay.* Proc Natl Acad Sci U S A, 2006. **103**(41): p. 15097-102.
198. Schumacher, J.M., et al., *A highly conserved centrosomal kinase, AIR-1, is required for accurate cell cycle progression and segregation of developmental factors in Caenorhabditis elegans embryos.* Development, 1998. **125**(22): p. 4391-402.
199. Severson, A.F., et al., *The aurora-related kinase AIR-2 recruits ZEN-4/CeMKLP1 to the mitotic spindle at metaphase and is required for cytokinesis.* Curr Biol, 2000. **10**(19): p. 1162-71.
200. Kaitna, S., et al., *Incenp and an aurora-like kinase form a complex essential for chromosome segregation and efficient completion of cytokinesis.* Curr Biol, 2000. **10**(19): p. 1172-81.
201. Rogers, E., et al., *The aurora kinase AIR-2 functions in the release of chromosome cohesion in Caenorhabditis elegans meiosis.* J Cell Biol, 2002. **157**(2): p. 219-29.
202. Collette, K.S., et al., *Different roles for Aurora B in condensin targeting during mitosis and meiosis.* J Cell Sci. **124**(Pt 21): p. 3684-94.
203. Schumacher, J.M., A. Golden, and P.J. Donovan, *AIR-2: An Aurora/Ipl1-related protein kinase associated with*

chromosomes and midbody microtubules is required for polar body extrusion and cytokinesis in Caenorhabditis elegans embryos. J Cell Biol, 1998. **143**(6): p. 1635-46.
204. Cohen, M., et al., *Transmission electron microscope studies of the nuclear envelope in Caenorhabditis elegans embryos.* J Struct Biol, 2002. **140**(1-3): p. 232-40.
205. Riemer, D., H. Dodemont, and K. Weber, *A nuclear lamin of the nematode Caenorhabditis elegans with unusual structural features; cDNA cloning and gene organization.* Eur J Cell Biol, 1993. **62**(2): p. 214-23.
206. Gruenbaum, Y., et al., *The expression, lamin-dependent localization and RNAi depletion phenotype for emerin in C. elegans.* J Cell Sci, 2002. **115**(Pt 5): p. 923-9.
207. Liu, J., et al., *MAN1 and emerin have overlapping function(s) essential for chromosome segregation and cell division in Caenorhabditis elegans.* Proc Natl Acad Sci U S A, 2003. **100**(8): p. 4598-603.
208. Lee, K.K. and K.L. Wilson, *All in the family: evidence for four new LEM-domain proteins Lem2 (NET-25), Lem3, Lem4 and Lem5 in the human genome.* Symp Soc Exp Biol, 2004(56): p. 329-39.
209. Segura-Totten, M. and K.L. Wilson, *BAF: roles in chromatin, nuclear structure and retrovirus integration.* Trends Cell Biol, 2004. **14**(5): p. 261-6.
210. Zheng, R., et al., *Barrier-to-autointegration factor (BAF) bridges DNA in a discrete, higher-order nucleoprotein complex.* Proc Natl Acad Sci U S A, 2000. **97**(16): p. 8997-9002.
211. Margalit, A., et al., *Barrier-to-autointegration factor is required to segregate and enclose chromosomes within the nuclear envelope and assemble the nuclear lamina.* Proc Natl Acad Sci U S A, 2005. **102**(9): p. 3290-5.
212. Lee, K.K., et al., *Lamin-dependent localization of UNC-84, a protein required for nuclear migration in Caenorhabditis elegans.* Mol Biol Cell, 2002. **13**(3): p. 892-901.
213. Galy, V., I.W. Mattaj, and P. Askjaer, *Caenorhabditis elegans nucleoporins Nup93 and Nup205 determine the*

limit of nuclear pore complex size exclusion in vivo. Mol Biol Cell, 2003. **14**(12): p. 5104-15.
214. Askjaer, P., et al., *Ran GTPase cycle and importins alpha and beta are essential for spindle formation and nuclear envelope assembly in living Caenorhabditis elegans embryos.* Mol Biol Cell, 2002. **13**(12): p. 4355-70.
215. Bamba, C., et al., *The GTPase Ran regulates chromosome positioning and nuclear envelope assembly in vivo.* Curr Biol, 2002. **12**(6): p. 503-7.
216. Walther, T.C., et al., *RanGTP mediates nuclear pore complex assembly.* Nature, 2003. **424**(6949): p. 689-94.
217. Hamill, D.R., et al., *Centrosome maturation and mitotic spindle assembly in C. elegans require SPD-5, a protein with multiple coiled-coil domains.* Dev Cell, 2002. **3**(5): p. 673-84.
218. Kemp, C.A., et al., *Centrosome maturation and duplication in C. elegans require the coiled-coil protein SPD-2.* Dev Cell, 2004. **6**(4): p. 511-23.
219. Pelletier, L., et al., *The Caenorhabditis elegans centrosomal protein SPD-2 is required for both pericentriolar material recruitment and centriole duplication.* Curr Biol, 2004. **14**(10): p. 863-73.
220. Maddox, P.S., et al., *"Holo"er than thou: chromosome segregation and kinetochore function in C. elegans.* Chromosome Res, 2004. **12**(6): p. 641-53.
221. Blower, M.D. and G.H. Karpen, *The role of Drosophila CID in kinetochore formation, cell-cycle progression and heterochromatin interactions.* Nat Cell Biol, 2001. **3**(8): p. 730-9.
222. Buchwitz, B.J., et al., *A histone-H3-like protein in C. elegans.* Nature, 1999. **401**(6753): p. 547-8.
223. Howman, E.V., et al., *Early disruption of centromeric chromatin organization in centromere protein A (Cenpa) null mice.* Proc Natl Acad Sci U S A, 2000. **97**(3): p. 1148-53.
224. Sullivan, E., et al., *Drosophila stem loop binding protein coordinates accumulation of mature histone mRNA with cell cycle progression.* Genes Dev, 2001. **15**(2): p. 173-87.

225. Moore, L.L. and M.B. Roth, *HCP-4, a CENP-C-like protein in Caenorhabditis elegans, is required for resolution of sister centromeres.* J Cell Biol, 2001. **153**(6): p. 1199-208.
226. Desai, A., et al., *KNL-1 directs assembly of the microtubule-binding interface of the kinetochore in C. elegans.* Genes Dev, 2003. **17**(19): p. 2421-35.
227. Cheeseman, I.M., et al., *A conserved protein network controls assembly of the outer kinetochore and its ability to sustain tension.* Genes Dev, 2004. **18**(18): p. 2255-68.
228. Howe, M., et al., *HIM-10 is required for kinetochore structure and function on Caenorhabditis elegans holocentric chromosomes.* J Cell Biol, 2001. **153**(6): p. 1227-38.
229. Moore, L.L., M. Morrison, and M.B. Roth, *HCP-1, a protein involved in chromosome segregation, is localized to the centromere of mitotic chromosomes in Caenorhabditis elegans.* J Cell Biol, 1999. **147**(3): p. 471-80.
230. Powers, J., et al., *Loss of KLP-19 polar ejection force causes misorientation and missegregation of holocentric chromosomes.* J Cell Biol, 2004. **166**(7): p. 991-1001.
231. Glotzer, M., *The molecular requirements for cytokinesis.* Science, 2005. **307**(5716): p. 1735-9.
232. Jantsch-Plunger, V., et al., *CYK-4: A Rho family gtpase activating protein (GAP) required for central spindle formation and cytokinesis.* J Cell Biol, 2000. **149**(7): p. 1391-404.
233. Dechant, R. and M. Glotzer, *Centrosome separation and central spindle assembly act in redundant pathways that regulate microtubule density and trigger cleavage furrow formation.* Dev Cell, 2003. **4**(3): p. 333-44.
234. Swan, K.A., et al., *cyk-1: a C. elegans FH gene required for a late step in embryonic cytokinesis.* J Cell Sci, 1998. **111 (Pt 14)**: p. 2017-27.
235. Guo, S. and K.J. Kemphues, *A non-muscle myosin required for embryonic polarity in Caenorhabditis elegans.* Nature, 1996. **382**(6590): p. 455-8.

236. Citi, S. and J. Kendrick-Jones, *Regulation of non-muscle myosin structure and function.* Bioessays, 1987. **7**(4): p. 155-9.
237. Piekny, A.J. and P.E. Mains, *Rho-binding kinase (LET-502) and myosin phosphatase (MEL-11) regulate cytokinesis in the early Caenorhabditis elegans embryo.* J Cell Sci, 2002. **115**(Pt 11): p. 2271-82.
238. Mishima, M., S. Kaitna, and M. Glotzer, *Central spindle assembly and cytokinesis require a kinesin-like protein/RhoGAP complex with microtubule bundling activity.* Dev Cell, 2002. **2**(1): p. 41-54.
239. Powers, J., et al., *A nematode kinesin required for cleavage furrow advancement.* Curr Biol, 1998. **8**(20): p. 1133-6.
240. Raich, W.B., et al., *Cytokinesis and midzone microtubule organization in Caenorhabditis elegans require the kinesin-like protein ZEN-4.* Mol Biol Cell, 1998. **9**(8): p. 2037-49.
241. Bishop, J.D. and J.M. Schumacher, *Phosphorylation of the carboxyl terminus of inner centromere protein (INCENP) by the Aurora B Kinase stimulates Aurora B kinase activity.* J Biol Chem, 2002. **277**(31): p. 27577-80.
242. Fraser, A.G., et al., *Caenorhabditis elegans inhibitor of apoptosis protein (IAP) homologue BIR-1 plays a conserved role in cytokinesis.* Curr Biol, 1999. **9**(6): p. 292-301.
243. Romano, A., et al., *CSC-1: a subunit of the Aurora B kinase complex that binds to the survivin-like protein BIR-1 and the incenp-like protein ICP-1.* J Cell Biol, 2003. **161**(2): p. 229-36.
244. Speliotes, E.K., et al., *The survivin-like C. elegans BIR-1 protein acts with the Aurora-like kinase AIR-2 to affect chromosomes and the spindle midzone.* Mol Cell, 2000. **6**(2): p. 211-23.
245. Luger, K., et al., *Characterization of nucleosome core particles containing histone proteins made in bacteria.* J Mol Biol, 1997. **272**(3): p. 301-11.
246. Allard, S., et al., *NuA4, an essential transcription adaptor/histone H4 acetyltransferase complex containing*

Esa1p and the ATM-related cofactor Tra1p. EMBO J, 1999. **18**(18): p. 5108-19.
247. Howe, L., et al., *Histone H3 specific acetyltransferases are essential for cell cycle progression.* Genes Dev, 2001. **15**(23): p. 3144-54.
248. Jenuwein, T. and C.D. Allis, *Translating the histone code.* Science, 2001. **293**(5532): p. 1074-80.
249. Peterson, C.L. and M.A. Laniel, *Histones and histone modifications.* Curr Biol, 2004. **14**(14): p. R546-51.
250. Cairns, B.R., *Chromatin remodeling complexes: strength in diversity, precision through specialization.* Curr Opin Genet Dev, 2005. **15**(2): p. 185-90.
251. Saha, A., J. Wittmeyer, and B.R. Cairns, *Chromatin remodelling: the industrial revolution of DNA around histones.* Nat Rev Mol Cell Biol, 2006. **7**(6): p. 437-47.
252. Kobor, M.S., et al., *A protein complex containing the conserved Swi2/Snf2-related ATPase Swr1p deposits histone variant H2A.Z into euchromatin.* PLoS Biol, 2004. **2**(5): p. E131.
253. Krogan, N.J., et al., *Regulation of chromosome stability by the histone H2A variant Htz1, the Swr1 chromatin remodeling complex, and the histone acetyltransferase NuA4.* Proc Natl Acad Sci U S A, 2004. **101**(37): p. 13513-8.
254. Mizuguchi, G., et al., *ATP-driven exchange of histone H2AZ variant catalyzed by SWR1 chromatin remodeling complex.* Science, 2004. **303**(5656): p. 343-8.
255. Ruhl, D.D., et al., *Purification of a human SRCAP complex that remodels chromatin by incorporating the histone variant H2A.Z into nucleosomes.* Biochemistry, 2006. **45**(17): p. 5671-7.
256. Vanfleteren, J.R., et al., *Multiple forms of histone H2B from the nematode Caenorhabditis elegans.* Biochem J, 1986. **235**(3): p. 769-73.
257. Vanfleteren, J.R., S.M. Van Bun, and J.J. Van Beeumen, *The primary structure of histone H2A from the nematode Caenorhabditis elegans.* Biochem J, 1987. **243**(1): p. 297-300.
258. Vanfleteren, J.R., S.M. Van Bun, and J.J. Van Beeumen, *The primary structure of histone H3 from the nematode*

Caenorhabditis elegans. FEBS Lett, 1987. **211**(1): p. 59-63.
259. Vanfleteren, J.R., S.M. Van Bun, and J.J. Van Beeumen, *The primary structure of histone H4 from the nematode Caenorhabditis elegans.* Comp Biochem Physiol B, 1987. **87**(4): p. 847-9.
260. Vanfleteren, J.R., S.M. Van Bun, and J.J. Van Beeumen, *The histones of Caenorhabditis elegans: no evidence of stage-specific isoforms. An overview.* FEBS Lett, 1989. **257**(2): p. 233-7.
261. Kelly, W.G., et al., *X-chromosome silencing in the germline of C. elegans.* Development, 2002. **129**(2): p. 479-92.
262. Bender, L.B., et al., *The MES-2/MES-3/MES-6 complex and regulation of histone H3 methylation in C. elegans.* Curr Biol, 2004. **14**(18): p. 1639-43.
263. Bender, L.B., et al., *MES-4: an autosome-associated histone methyltransferase that participates in silencing the X chromosomes in the C. elegans germ line.* Development, 2006. **133**(19): p. 3907-17.
264. Ho, L. and G.R. Crabtree, *Chromatin remodelling during development.* Nature, 2010. **463**(7280): p. 474-84.
265. Andersen, E.C., X. Lu, and H.R. Horvitz, *C. elegans ISWI and NURF301 antagonize an Rb-like pathway in the determination of multiple cell fates.* Development, 2006. **133**(14): p. 2695-704.
266. Bender, A.M., O. Wells, and D.S. Fay, *lin-35/Rb and xnp-1/ATR-X function redundantly to control somatic gonad development in C. elegans.* Dev Biol, 2004. **273**(2): p. 335-49.
267. Cardoso, C., et al., *XNP-1/ATR-X acts with RB, HP1 and the NuRD complex during larval development in C. elegans.* Dev Biol, 2005. **278**(1): p. 49-59.
268. Cui, M., et al., *SynMuv genes redundantly inhibit lin-3/EGF expression to prevent inappropriate vulval induction in C. elegans.* Dev Cell, 2006. **10**(5): p. 667-72.
269. Cui, M., D.S. Fay, and M. Han, *lin-35/Rb cooperates with the SWI/SNF complex to control Caenorhabditis elegans larval development.* Genetics, 2004. **167**(3): p. 1177-85.

270. Fong, Y., et al., *Regulation of the different chromatin states of autosomes and X chromosomes in the germ line of C. elegans.* Science, 2002. **296**(5576): p. 2235-8.
271. Kim, J.K., et al., *Functional genomic analysis of RNA interference in C. elegans.* Science, 2005. **308**(5725): p. 1164-7.
272. Robert, V.J., et al., *Chromatin and RNAi factors protect the C. elegans germline against repetitive sequences.* Genes Dev, 2005. **19**(7): p. 782-7.
273. Wang, D., et al., *Somatic misexpression of germline P granules and enhanced RNA interference in retinoblastoma pathway mutants.* Nature, 2005. **436**(7050): p. 593-7.
274. Pothof, J., et al., *Identification of genes that protect the C. elegans genome against mutations by genome-wide RNAi.* Genes Dev, 2003. **17**(4): p. 443-8.
275. Updike, D.L. and S.E. Mango, *Temporal regulation of foregut development by HTZ-1/H2A.Z and PHA-4/FoxA.* PLoS Genet, 2006. **2**(9): p. e161.
276. Ferguson, E.L. and H.R. Horvitz, *The multivulva phenotype of certain Caenorhabditis elegans mutants results from defects in two functionally redundant pathways.* Genetics, 1989. **123**(1): p. 109-21.
277. Horvitz, H.R. and J.E. Sulston, *Isolation and genetic characterization of cell-lineage mutants of the nematode Caenorhabditis elegans.* Genetics, 1980. **96**(2): p. 435-54.
278. Ceol, C.J. and H.R. Horvitz, *A new class of C. elegans synMuv genes implicates a Tip60/NuA4-like HAT complex as a negative regulator of Ras signaling.* Dev Cell, 2004. **6**(4): p. 563-76.
279. Dufourcq, P., et al., *Functional requirement for histone deacetylase 1 in Caenorhabditis elegans gonadogenesis.* Mol Cell Biol, 2002. **22**(9): p. 3024-34.
280. Solari, F. and J. Ahringer, *NURD-complex genes antagonise Ras-induced vulval development in Caenorhabditis elegans.* Curr Biol, 2000. **10**(4): p. 223-6.
281. Nathan, D., et al., *Histone sumoylation is a negative regulator in Saccharomyces cerevisiae and shows*

dynamic interplay with positive-acting histone modifications. Genes Dev, 2006. **20**(8): p. 966-76.
282. Lu, X. and H.R. Horvitz, *lin-35 and lin-53, two genes that antagonize a C. elegans Ras pathway, encode proteins similar to Rb and its binding protein RbAp48.* Cell, 1998. **95**(7): p. 981-91.
283. Unhavaithaya, Y., et al., *MEP-1 and a homolog of the NURD complex component Mi-2 act together to maintain germline-soma distinctions in C. elegans.* Cell, 2002. **111**(7): p. 991-1002.
284. von Zelewsky, T., et al., *The C. elegans Mi-2 chromatin-remodelling proteins function in vulval cell fate determination.* Development, 2000. **127**(24): p. 5277-84.
285. Xue, Y., et al., *NURD, a novel complex with both ATP-dependent chromatin-remodeling and histone deacetylase activities.* Mol Cell, 1998. **2**(6): p. 851-61.
286. Cui, M., E.B. Kim, and M. Han, *Diverse chromatin remodeling genes antagonize the Rb-involved SynMuv pathways in C. elegans.* PLoS Genet, 2006. **2**(5): p. e74.
287. Doyon, Y., et al., *ING tumor suppressor proteins are critical regulators of chromatin acetylation required for genome expression and perpetuation.* Mol Cell, 2006. **21**(1): p. 51-64.
288. Eissenberg, J.C., M. Wong, and J.C. Chrivia, *Human SRCAP and Drosophila melanogaster DOM are homologs that function in the notch signaling pathway.* Mol Cell Biol, 2005. **25**(15): p. 6559-69.
289. Park, J.H. and R.G. Roeder, *GAS41 is required for repression of the p53 tumor suppressor pathway during normal cellular proliferation.* Mol Cell Biol, 2006. **26**(11): p. 4006-16.
290. Betschinger, J. and J.A. Knoblich, *Dare to be different: asymmetric cell division in Drosophila, C. elegans and vertebrates.* Curr Biol, 2004. **14**(16): p. R674-85.
291. Morrison, S.J. and J. Kimble, *Asymmetric and symmetric stem-cell divisions in development and cancer.* Nature, 2006. **441**(7097): p. 1068-74.
292. Herman, M.A., et al., *EGL-27 is similar to a metastasis-associated factor and controls cell polarity and cell*

migration in C. elegans. Development, 1999. **126**(5): p. 1055-64.
293. Sawa, H., H. Kouike, and H. Okano, *Components of the SWI/SNF complex are required for asymmetric cell division in C. elegans.* Mol Cell, 2000. **6**(3): p. 617-24.
294. Sternberg, P.W. and H.R. Horvitz, *lin-17 mutations of Caenorhabditis elegans disrupt certain asymmetric cell divisions.* Dev Biol, 1988. **130**(1): p. 67-73.
295. Herman, M.A., et al., *The C. elegans gene lin-44, which controls the polarity of certain asymmetric cell divisions, encodes a Wnt protein and acts cell nonautonomously.* Cell, 1995. **83**(1): p. 101-10.
296. Sawa, H., L. Lobel, and H.R. Horvitz, *The Caenorhabditis elegans gene lin-17, which is required for certain asymmetric cell divisions, encodes a putative seven-transmembrane protein similar to the Drosophila frizzled protein.* Genes Dev, 1996. **10**(17): p. 2189-97.
297. Murray, J.I., et al., *Automated analysis of embryonic gene expression with cellular resolution in C. elegans.* Nat Methods, 2008. **5**(8): p. 703-9.
298. Bao, Z., et al., *Control of cell cycle timing during C. elegans embryogenesis.* Dev Biol, 2008. **318**(1): p. 65-72.
299. Sulston, J.E., *Neuronal cell lineages in the nematode Caenorhabditis elegans.* Cold Spring Harb Symp Quant Biol, 1983. **48 Pt 2**: p. 443-52.
300. Cui, M. and M. Han, *Roles of chromatin factors in C. elegans development.* WormBook, 2007: p. 1-16.
301. Boulton, S.J., et al., *Combined functional genomic maps of the C. elegans DNA damage response.* Science, 2002. **295**(5552): p. 127-31.
302. Jones, D., et al., *Functional and phylogenetic analysis of the ubiquitylation system in Caenorhabditis elegans: ubiquitin-conjugating enzymes, ubiquitin-activating enzymes, and ubiquitin-like proteins.* Genome Biol, 2002. **3**(1): p. RESEARCH0002.
303. Zhang, H., et al., *The C. elegans Polycomb gene SOP-2 encodes an RNA binding protein.* Mol Cell, 2004. **14**(6): p. 841-7.

304. Solari, F., A. Bateman, and J. Ahringer, *The Caenorhabditis elegans genes egl-27 and egr-1 are similar to MTA1, a member of a chromatin regulatory complex, and are redundantly required for embryonic patterning.* Development, 1999. **126**(11): p. 2483-94.
305. Pettitt, J., et al., *The Caenorhabditis elegans histone hairpin-binding protein is required for core histone gene expression and is essential for embryonic and postembryonic cell division.* J Cell Sci, 2002. **115**(Pt 4): p. 857-66.
306. Michel, F., D. Schumperli, and B. Muller, *Specificities of Caenorhabditis elegans and human hairpin binding proteins for the first nucleotide in the histone mRNA hairpin loop.* RNA, 2000. **6**(11): p. 1539-50.
307. Gunsalus, K.C., et al., *Predictive models of molecular machines involved in Caenorhabditis elegans early embryogenesis.* Nature, 2005. **436**(7052): p. 861-5.
308. Galy, V., et al., *MEL-28, a novel nuclear-envelope and kinetochore protein essential for zygotic nuclear-envelope assembly in C. elegans.* Curr Biol, 2006. **16**(17): p. 1748-56.
309. Kimura, Y., et al., *A CaMK cascade activates CRE-mediated transcription in neurons of Caenorhabditis elegans.* EMBO Rep, 2002. **3**(10): p. 962-6.
310. Hirano, T., *At the heart of the chromosome: SMC proteins in action.* Nat Rev Mol Cell Biol, 2006. **7**(5): p. 311-22.
311. Powell-Coffman, J.A., J. Knight, and W.B. Wood, *Onset of C. elegans gastrulation is blocked by inhibition of embryonic transcription with an RNA polymerase antisense RNA.* Dev Biol, 1996. **178**(2): p. 472-83.
312. Ghaemmaghami, S., et al., *Global analysis of protein expression in yeast.* Nature, 2003. **425**(6959): p. 737-41.
313. Kasturi, P., et al., *The C. elegans sex determination protein MOG-3 functions in meiosis and binds to the CSL co-repressor CIR-1.* Dev Biol. **344**(2): p. 593-602.
314. Horsey, E.W., et al., *Role of the yeast Rrp1 protein in the dynamics of pre-ribosome maturation.* RNA, 2004. **10**(5): p. 813-27.

315. Kudron, M.M. and V. Reinke, *C. elegans nucleostemin is required for larval growth and germline stem cell division.* PLoS Genet, 2008. **4**(8): p. e1000181.
316. Lee, L.W., et al., *The nucleolus of Caenorhabditis elegans.* J Biomed Biotechnol. **2012**: p. 601274.
317. Tsai, R.Y. and R.D. McKay, *A nucleolar mechanism controlling cell proliferation in stem cells and cancer cells.* Genes Dev, 2002. **16**(23): p. 2991-3003.
318. Kamath, R.S. and J. Ahringer, *Genome-wide RNAi screening in Caenorhabditis elegans.* Methods, 2003. **30**(4): p. 313-21.
319. Loyola, A. and G. Almouzni, *Bromodomains in living cells participate in deciphering the histone code.* Trends Cell Biol, 2004. **14**(6): p. 279-81.
320. Marhold, J., et al., *The Drosophila MBD2/3 protein mediates interactions between the MI-2 chromatin complex and CpT/A-methylated DNA.* Development, 2004. **131**(24): p. 6033-9.
321. Hayashi, T., et al., *Mis16 and Mis18 are required for CENP-A loading and histone deacetylation at centromeres.* Cell, 2004. **118**(6): p. 715-29.
322. Zinovyeva, A.Y., et al., *The C. elegans histone deacetylase HDA-1 is required for cell migration and axon pathfinding.* Dev Biol, 2006. **289**(1): p. 229-42.
323. Wade, P.A., et al., *Mi-2 complex couples DNA methylation to chromatin remodelling and histone deacetylation.* Nat Genet, 1999. **23**(1): p. 62-6.
324. Wade, P.A., et al., *A multiple subunit Mi-2 histone deacetylase from Xenopus laevis cofractionates with an associated Snf2 superfamily ATPase.* Curr Biol, 1998. **8**(14): p. 843-6.
325. Tong, J.K., et al., *Chromatin deacetylation by an ATP-dependent nucleosome remodelling complex.* Nature, 1998. **395**(6705): p. 917-21.
326. Passannante, M., et al., *Different Mi-2 complexes for various developmental functions in Caenorhabditis elegans.* PLoS One. **5**(10): p. e13681.
327. Orphanides, G., et al., *FACT, a factor that facilitates transcript elongation through nucleosomes.* Cell, 1998. **92**(1): p. 105-16.

328. Lejeune, E., et al., *The chromatin-remodeling factor FACT contributes to centromeric heterochromatin independently of RNAi.* Curr Biol, 2007. **17**(14): p. 1219-24.
329. Formosa, T., et al., *Spt16-Pob3 and the HMG protein Nhp6 combine to form the nucleosome-binding factor SPN.* EMBO J, 2001. **20**(13): p. 3506-17.
330. Mason, P.B. and K. Struhl, *The FACT complex travels with elongating RNA polymerase II and is important for the fidelity of transcriptional initiation in vivo.* Mol Cell Biol, 2003. **23**(22): p. 8323-33.
331. Rhoades, A.R., S. Ruone, and T. Formosa, *Structural features of nucleosomes reorganized by yeast FACT and its HMG box component, Nhp6.* Mol Cell Biol, 2004. **24**(9): p. 3907-17.
332. Biswas, D., et al., *The yeast FACT complex has a role in transcriptional initiation.* Mol Cell Biol, 2005. **25**(14): p. 5812-22.
333. Smolka, M.B., et al., *Proteome-wide identification of in vivo targets of DNA damage checkpoint kinases.* Proc Natl Acad Sci U S A, 2007. **104**(25): p. 10364-9.
334. Zeitlin, S.G., R.D. Shelby, and K.F. Sullivan, *CENP-A is phosphorylated by Aurora B kinase and plays an unexpected role in completion of cytokinesis.* J Cell Biol, 2001. **155**(7): p. 1147-57.
335. Obuse, C., et al., *A conserved Mis12 centromere complex is linked to heterochromatic HP1 and outer kinetochore protein Zwint-1.* Nat Cell Biol, 2004. **6**(11): p. 1135-41.
336. Foltz, D.R., et al., *The human CENP-A centromeric nucleosome-associated complex.* Nat Cell Biol, 2006. **8**(5): p. 458-69.
337. Kelly, W.G., et al., *Distinct requirements for somatic and germline expression of a generally expressed Caernorhabditis elegans gene.* Genetics, 1997. **146**(1): p. 227-38.
338. Seydoux, G. and M.A. Dunn, *Transcriptionally repressed germ cells lack a subpopulation of phosphorylated RNA polymerase II in early embryos of Caenorhabditis*

elegans and Drosophila melanogaster. Development, 1997. **124**(11): p. 2191-201.
339. Kuroyanagi, H., et al., *SPK-1, a C. elegans SR protein kinase homologue, is essential for embryogenesis and required for germline development.* Mech Dev, 2000. **99**(1-2): p. 51-64.
340. Walker, A.K., et al., *Distinct requirements for C.elegans TAF(II)s in early embryonic transcription.* EMBO J, 2001. **20**(18): p. 5269-79.
341. Barbee, S.A., A.L. Lublin, and T.C. Evans, *A novel function for the Sm proteins in germ granule localization during C. elegans embryogenesis.* Curr Biol, 2002. **12**(17): p. 1502-6.
342. Gall, J.G., et al., *Assembly of the nuclear transcription and processing machinery: Cajal bodies (coiled bodies) and transcriptosomes.* Mol Biol Cell, 1999. **10**(12): p. 4385-402.
343. Wright, W.E. and J.W. Shay, *Telomere-binding factors and general DNA repair.* Nat Genet, 2005. **37**(2): p. 116-8.
344. Andrade, L.E., et al., *Human autoantibody to a novel protein of the nuclear coiled body: immunological characterization and cDNA cloning of p80-coilin.* J Exp Med, 1991. **173**(6): p. 1407-19.
345. Crittenden, S.L., et al., *Cellular analyses of the mitotic region in the Caenorhabditis elegans adult germ line.* Mol Biol Cell, 2006. **17**(7): p. 3051-61.
346. Crittenden, S.L., et al., *GLP-1 is localized to the mitotic region of the C. elegans germ line.* Development, 1994. **120**(10): p. 2901-11.
347. Anderson, G.R., et al., *Expression and localization of RGS9-2/G 5/R7BP complex in vivo is set by dynamic control of its constitutive degradation by cellular cysteine proteases.* J Neurosci, 2007. **27**(51): p. 14117-27.
348. Fisher, K., et al., *Methylation and demethylation activities of a C. elegans MLL-like complex attenuate RAS signalling.* Dev Biol. **341**(1): p. 142-53.
349. Clapier, C.R. and B.R. Cairns, *The biology of chromatin remodeling complexes.* Annu Rev Biochem, 2009. **78**: p. 273-304.

350. de la Serna, I.L., Y. Ohkawa, and A.N. Imbalzano, *Chromatin remodelling in mammalian differentiation: lessons from ATP-dependent remodellers.* Nat Rev Genet, 2006. **7**(6): p. 461-73.
351. Luisier, F., T. Blu, and M. Unser, *Image denoising in mixed Poisson-Gaussian noise.* IEEE Trans Image Process. **20**(3): p. 696-708.
352. Meijering, E., et al., *Tracking in cell and developmental biology.* Semin Cell Dev Biol, 2009. **20**(8): p. 894-902.
353. Dzyubachyk, O., et al., *Advanced level-set-based cell tracking in time-lapse fluorescence microscopy.* IEEE Trans Med Imaging. **29**(3): p. 852-67.